Louisiana State University
LSU Digital Commons

LSU Doctoral Dissertations | Graduate School

2010

Point-of-care immunoassay system using carbon nanotube labels

Adeyabeba Abera
Louisiana State University and Agricultural and Mechanical College, aabera1@tigers.lsu.edu

Follow this and additional works at: https://digitalcommons.lsu.edu/gradschool_dissertations

 Part of the Electrical and Computer Engineering Commons

Recommended Citation
Abera, Adeyabeba, "Point-of-care immunoassay system using carbon nanotube labels" (2010). *LSU Doctoral Dissertations*. 508.
https://digitalcommons.lsu.edu/gradschool_dissertations/508

This Dissertation is brought to you for free and open access by the Graduate School at LSU Digital Commons. It has been accepted for inclusion in LSU Doctoral Dissertations by an authorized graduate school editor of LSU Digital Commons. For more information, please contactgradetd@lsu.edu.

POINT-OF-CARE IMMUNOASSAY SYSTEM USING CARBON NANOTUBE LABELS

A Dissertation

Submitted to the Graduate Faculty of the
Louisiana State University and
Agricultural and Mechanical College
in partial fulfillment of the
requirements for the degree of
Doctor of Philosophy

in

The Department of Electrical and Computer Engineering

by
Adeyabeba Abera
B.S.E.E., Virginia Polytechnic Institute and State University, Blacksburg, VA, 2004
M.S.E.E., Louisiana State University, Baton Rouge, LA, 2007

December 2010

To my mother,

Amsale Eshete Tessema

Your love, values, and wisdom that I will always cherish.

ACKNOWLEDGEMENTS

I would like to express my gratitude to my advisor Dr. Jin-Woo Choi. I am thankful for his guidance, patience, and understanding that made this research possible. I appreciate his dedication and encouragement towards completion of this work. I am grateful to my co-advisor Dr. Dimitris Nikitopoulos for his expertise and support.

I would like to thank my committee members Dr. Ashok Srivastava, Dr. Todd Monroe, and Dr. Seung-Jong Park. I appreciate the thoughtful suggestions I have received from my committee members in moving this research forward. My overall interactions with my committee members has been empowering as a graduate student and as an individual.

I would also like to extend my gratitude to my colleagues and friends. I am thankful to my research colleagues Chao-Xuan, Edward Song, and Fang Liu. I want to thank Dr. Yoonyoung Jin, Fareed Dawan, Dr. Haoyu Tang, and Chukuma Anakwue for their valuable assistance.

Above all, I am grateful for the love and support of my family. My husband Eyassu Woldesenbet, who came into my life and became part of me. I admire his passion, dedication, and his willingness to make a difference. My daughter Zehr Woldesenbet, who made our lives warmer. My brothers and sister, who are always loving and encouraging.

TABLE OF CONTENTS

ACKNOWLEDGEMENTS ..... **iii**
LIST OF TABLES ..... **vii**
LIST OF FIGURES ..... **viii**
ABSTRACT ..... **xiii**

CHAPTER 1
INTRODUCTION **1**
1.1 Motivation 1
1.1.1 Biosensors 1
1.1.2 Carbon Nanotubes 3
1.1.3 Rapid and Quantitative Immunosensing using Carbon Nanotubes 4
1.2 Objectives 5
1.2.1 Chemical Functionalization and Antibody Conjugation of Carbon Nanotubes 5
1.2.2 Lateral Flow Immunosensing Based on Electrical Signal Detection 6
1.2.3 Microfluidic Immunosensing Based on Electrical Signal Detection 6
1.3 Outline of Dissertation 7

CHAPTER 2
BACKGROUND **9**
2.1 Introduction 9
2.2 Surface Modifications of Carbon Nanotubes 9
2.2.1 Aqueous Solubility of Carbon Nanotubes 11
2.2.2 Protein Adsorption on Carbon Nanotubes 13
2.2.3 Electrical Properties of Carbon Nanotubes as a Result of Functionalization 15
2.3 Carbon Nanotubes for Biosensing 19
2.4 Immunoassay 23
2.4.1 Antibody 24
2.4.2 Immunoassay Formats 25
2.4.3 Label-Based Immunoassay 26
2.5 Point-of-Care Immunoassays 27

CHAPTER 3
SOLUBILITY AND ANTIBODY CONJUGATION OF CARBON NANOTUBES **30**
3.1 Introduction 30
3.2 Solubility of Carbon Nanotubes in Aqueous Solutions 31
3.3 Surfactant Assisted Dispersion of Carbon Nanotubes 31
3.4 Conjugation of Antibody on Carbon Nanotube 32
3.5 Experimental Study 33

3.5.1 Functionalization of MWCNTs 33
3.5.2 Materials and Reagents 34
3.5.3 Surfactant-Assisted Dispersion 34
3.5.4 EDC/Sulfo-NHS Chemistry 35
3.5.5 MWCNT-Antibody Conjugation 35
3.6 Results and Discussion 36
3.6.1 MWCNT Solubility 36
3.6.2 Amidation Process 43
3.6.3 MWCNT-Antibody Conjugation 45
3.6.4 CNT-Antibody Conjugation with Reduced PVP 50
3.6.5 Enhanced CNT-Antibody Conjugation with Increased Antibody Concentration 54
3.7 Summary 57

CHAPTER 4
CARBON NANOTUBE-BASED LATERAL FLOW IMMUNOASSAY 59
4.1 Introduction 59
4.1.1 Lateral Flow Immunoassay Protocol 59
4.1.2 CNT as Sensing Label 60
4.2 CNT-Based Lateral Flow Immunoassay 61
4.2.1 Detection Principle 61
4.2.2 Materials and Reagents 62
4.2.3 Modification of MWCNTs 63
4.2.4 Preparation of the LF Strips 64
4.2.5 Preparation of LF System 64
4.3 Electrical Measurement System 66
4.3.1 Integrated Electrodes 66
4.3.2 LF Cartridge System 69
4.4 Results and Discussion 73
4.4.1 Non-specific Binding 73
4.4.2 Calibration of the LF Immunosensor 74
4.4.3 Competitive Immunoassay 75
4.4.4 Sandwich Immunoassay 78
4.5 Summary 82

CHAPTER 5
MICROFLUIDIC IMMUNOASSAY USING CARBON NANOTUBES 83
5.1 Introduction 83
5.2 Microfluidic Immunoassay 84
5.3 Fabrication of Microfluidic Immunosensor 85
5.4 PDMS Microfluidic Device Fabrication 88
5.4.1 Fabricating PDMS SU-8 Mold Master 88
5.4.2 PDMS Casting 89
5.4.3 PDMS Surface Treatment and Bonding 91
5.4.4 On-Chip Immunoassay Detection Mechanism 91

5.5 Binding Test on IDA Microelectrodes 93
5.5.1 Specific and Non-specific Binding 93
5.5.2 Materials and Reagents 94
5.5.3 Results of Binding Test 95
5.5.4 Sealing and Alignment of PDMS Microfluidic Channel 97
5.6 CNT-Based Immunoassay Using PDMS Microfluidic Chip 99
5.6.1 Detection Protocol 99
5.6.2 Materials and Reagents 100
5.6.3 Experimental Procedure 101
5.7 Results and Discussion 101
5.7.1 On-Chip Immunoassay 101
5.7.2 Flow Characterization 107
5. 8 Simulation 110
5.8.1 Fundamental Equations in Microfluidics 110
5.8.2 Microfluidics Simulation 111
5.8.3 Flow Conditions 115
5.8.4 Simulation Results 116
5. 9 Summary 123

CHAPTER 6
CONCLUSIONS AND FUTURE WORK 126
6.1 Conclusions 126
6.1.1 Functionalization of Carbon Nanotubes 126
6.1.2 Carbon Nanotube Labels for LF Immunoassay 128
6.1.3 Microfluidic Immunoassay Using Carbon Nanotube on IDA Microelectrodes 129
6.2 Future Work 130
6.2.1 Carbon Nanotube-Antibody Conjugation and Quantification 130
6.2.2 Pathogen Detection on Lateral Flow System 130
6.2.3 Microfluidic Parameters for On-Chip Immunoassay 131

REFERENCES 132

VITA 145

LIST OF TABLES

Table 4.1 Summary of the measured resistance values for varying anti-IgG concentrations for LF sandwich immunoassay. 81

Table 5.1 Summary of the measured current for varying anti-HSA concentrations for on-chip immunoassay.……..…….104

Table 5.2 Saturation concentration and time for the anti-IgG and IgG complex at the surface of the microelectrode..... 117

LIST OF FIGURES

Figure 2.1 Different structures of nanotubes (a) armchair (b) zigzag (c) chiral (Saito *et al.*,1992 [9]) 10

Figure 2.2 Illustration of protein occupying the surface of a carbon nanotube in helical manner (Balavoine *et al.*,1999 [50]). 13

Figure 2.3 Demonstration of the conjugation process of proteins to carboxylated CNTs using EDC and Sulfo-NHS (Gao and Kyratzis, 2008 [59]). 15

Figure 2.4 Illustration of wave function with induced impurity state as a result of modification of (10,0) SWCNT with functional groups (a) COOH-functionalization (b) F-functionalization and (c) a C vacancy on the side wall, where the yellow and blue colors indicate the polarity of the wave function (Zhao *et al.*, 2004 [62]). 16

Figure 2.5 Conductance microscope image showing minimal conductance drop of the nanotube network with higher interconnectivity measured at varying locations from the electrode. The conductance at point A, B, and C are 700, 200, and 700 nS (Stadermann *et al.*, 2004 [66]). 17

Figure 2.6 Immunoassay detection principle using CNTs to immobilize multiple labels and secondary antibodies for signal amplification. HRP catalyzes H_2O_2 and generates electrons for amperometric based measurement. (A) conventional single HRP labeled secondary antibody (B) multiple HRP and secondary antibody on carbon nanotube for signal amplification (Yu *et al.*, 2006 [85]) 20

Figure 2.7 CNT-based treatment of MCF7 cancer cell using NIR dosing (a) survival of the cells treated with nanotube attached to non-specific antibody complexe (b) destruction of the cells treated with nanotube attached with specific antibody (anti-IGF1-HER2) complex (Shao *et al.*, 2007 [86]) 21

Figure 2.8 Schematic diagram of Immunoglobulin G (IgG) molecule. 24

Figure 2.9 Illustration of sandwich and competitive immunoassay formats. 26

Figure 3.1 Schematic illustration for functionalized MWCNTs with PVP or PEG by surface adsorption and human IgG through covalent amide bonding (not to scale). 33

Figure 3.2 Dispersion of MWCNTs in water (a) before and (b) after sonication with PVP, PEG, and without surfactant (going from left to right). All samples have same concentration of nanotubes (0.1 mg/ml). 36

Figure 3.3 The UV-Vis absorbance spectra of the MWCNT dispersion (a) immediately after sonication (b) one week after sonication and (c) four months after sonication. The different lines indicate MWCNT disperisons with PVP, PEG, DI water (without surfactant), and PEG as control in the absence of MWCNTs (Figure 3.3 con'd). 38

Figure 3.4 Plot of absorbance versus concentration for the PVP dispersed MWCNT solution for peaks at 500 nm. 40

Figure 3.5 SEM image of MWCNTs dispersed with (a) PEG, (b) PVP, (c) only DI water on silicon substrate..... 41

Figure 3.6 TEM images of MWCNTs (a) with surfactant coating and (b) without surfactant coating..... 42

Figure 3.7 The UV-Vis absorbance spectra of the MWCNT solutions after reacting with EDC/Sulfo-NHS for stable amidation process. The inset shows the dispersion state of MWCNTs in water with PVP, PEG, and without surfactant after reacting with the coupling agents. 44

Figure 3.8 FTIR spectra of samples (a) carboxylated MWCNTs (b) neat PVP (c) PVP-modified MWCNTs (d) neat antibodies and (e) antibody-functionalized MWCNTs..... 46

Figure 3.9 TEM images showing (a) surfactant dispersed MWCNTs conjugated with human IgG and a close up image of the MWCNT-antibody conjugation (b) aggregates of conjugated antibodies on MWCNTs. 49

Figure 3.10 TEM images showing surfactant coating on the surface of the MWCNTs with antibody conjugation..... 51

Figure 3.11 TEM images showing (a) human IgG conjugation of MWCNTs dispersed without surfactant (b) a close up image of the MWCNT-antibody conjugation..... 52

Figure 3.12 (a) TEM characterization showing well dispersed MWCNTs with enhanced antibody conjugation using 4 times lower PVP (b) a close up image showing multiple antibodies attached on the surface of the MWCNTs. 53

Figure 3.13 Dispersion state of MWCNT-antibody conjugate solution using original PVP, amount, 4 times lower PVP, and 10 times lower PVP (going left to right) (b) TEM image showing limited antibody conjugation with MWCNTs due to poor dispersion. 54

Figure 3.14 TEM image showing enhanced antibody conjugation with MWCNTs using 500 µg/ml antibody concentration. 56

Figure 3.15 TEM image showing an increase in MWCNT-antibody conjugation and unbound antibodies using 1000 µg/ml antibody concentration. 56

Figure 4.1 Detection principle of the CNT-labeled immunosensor for quantitative lateral flow diagnostics in competitive format. 61

Figure 4.2 Detection principle of the CNT-labeled immunosensor for quantitative lateral flow diagnostics in sandwich format..... 62

Figure 4.3 SEM images of the capture zone (a) before sample application (b) lower CNT coverage due to a smaller number of binding, and (c) higher CNT coverage due to a larger number of binding. 66

Figure 4.4 Design of integrated electrodes (a) 3D view of the top and bottom plates and (b) the top plate with the two holes for inserting the electrodes and bottom plate with a groove to hold the immunostrips..... 67

Figure 4.5 (a) Polymer plates with integrated electrode showing a close up image of the electrodes (b) electrical measurement and data recording setup for the LF immunosensors using the integrated electrodes. 68

Figure 4.6 The developed LF cartridge (a) the 3D model of the cartridge and the top and bottom covers when opened (b) the dimension of the cartridge (c) the fabricated cartridge, and (d) demonstration of simple electrical measurements on the LF cartridge. 70

Figure 4.7 Non-specific adsorption on the nitrocellulose membrane (i) carbon nanotubes partially coated with PVP bound to Protein A by non-specific adsorption which must be addressed to avoid false signal (ii) almost no carbon nanotubes at the capture line showing that the surface of carbon nanotubes were completely covered eliminating non-specific adsorption after the application of crosslinking agent, EDC, and Sulfo-NHS, and (iii) binding between the MWCNT-IgG conjugate and immobilized Protein A. 73

Figure 4.8 Calibration results using conjugate solutions of different concentrations. CNTs as label provided a quantitative electrical detection capability. 75

Figure 4.9 Competitive immunoassay results (a) lateral flow immunostrips tested with target concentrations in μg/ml (i) 25, (ii) 50, (iii) 75, (iv) 100, (v) 150, and (vi) 200 (from left to right) and (b) the measured electrical resistance of the capture lines. 76

Figure 4.10 Plot of the resistance measurements as a function of time obtained for LF sandwich immunoassay with varying anti-IgG concentrations in ng/ml (a) 50, (b) 20, (c) 10, (d) 5, (e) 1, (f) 0.5, (g) 0.1, and (h) 0. 79

Figure 4.11 Calibration curve for anti-human IgG detection using LF sandwich immunoassay. 80

Figure 4.12 Lateral flow immunostrips demonstrating colorimetric detection capability in sandwich format for target concentrations in ng/ml (i) 50, (ii) 20, (iii) 10, (iv) 5, (v) 1, (vi) 0.5, (vii) 0.1, and (viii) 0. 81

Figure 5.1 Fabrication steps of the IDA microelectrodes on glass substrate (a) UV exposure of positive photoresist on Cr/Au deposited glass substrate (b) development of positive PR in UV expose area (c) Au etching (d) Cr etching, and (e) PR etching……87

Figure 5.2 Optical microscope images of the modified IDA microelectrodes (a) with 20 μm electrode width and spacing (b) closer view of the electrode fingers. 88

Figure 5.3 Fabricated PDMS microfluidic structure (a) dimensions of the microchannel with 1 mm (b) SU-8 mold master with 1 mm (top and bottom row) and 2 mm channel width (middle row). 90

Figure 5.4 Design of the capillary-driven microfluidic chip. 92

Figure 5.5 Illustrations of the detection principle using CNT labels on IDA microelectrodes (a) immobilization of capture molecule on gold IDA microelectrode (b) a cross-section of the IDA microelectrode during the application of conjugate solution, and (c) a cross-section of the IDA microelectrode showing the MWCNT network as a result of specific binding. 93

Figure 5.6 Dynamic electrical measurements as a result of specific binding with anti-human IgG and non-specific binding with BSA using MWCNT labels on IDA microelectrode. 95

Figure 5.7 SEM images showing the conducting network formed across the IDA microelectrode by the MWCNT labels (a) specific binding of anti-human IgG and (b) non-specific binding of BSA. 96

Figure 5.8 Results for PDMS surface modification with corona discharge (a) plot of the contact angle measurements as a function of aging time (b) images of water droplets with low and high contact angles. 97

Figure 5.9 Microscopic image of the PDMS microfluidic structure placed on top of the IDA microelectrode on glass substrate. 99

Figure 5.10 Developed PDMS microfluidic chip with integrated IDA microelectrode for immunoassay. 103

Figure 5.11 Plot of the full current reading starting at sample application until signal saturation was reached. 103

Figure 5.12 Plot of the current measurements as a function of time obtained for on-chip immunoassay with varying anti-HSA concentrations in ng/ml (a) 0, (b) 0.5, (c) 1, (d) 5, (e) 10, and (f) 20. 104

Figure 5.13 Calibration curve for anti-HSA detection using PDMS microfluidic chip. 105

Figure 5.14 SEM characterization of MWCNT matrix formation across the IDA microelectrodes as a result of HSA and anti-HSA binding (a) lower density of the MWCNT labels for low anti-HSA concentration and (b) higher density of the MWCNT matrix for larger anti-HSA concentration. 106

Figure 5.15 Characterization of the flow of the sample solution in the PDMS microfluidic channel in the first three seconds of sample application at (a) t = 0 s, (b) t = 1 s, (c) t = 2 s, and (d) t = 3 s. 108

Figure 5.16 Characterization of the flow in the PDMS microfluidic channel before and after the sample solution crossed over the IDA at (a) t = 160 s, (b) t = 170 s, (c) t = 180 s, (d) t = 200 s, and (e) t = 230 s. 109

Figure 5.17 2D model of the sample flow in a microchannel with microelectrode as a binding surface for immunoassay. 114

Figure 5.18 The anti-IgG and IgG complex concentration at the surface of the microelectrode as a function of time for anti-IgG concentrations in mole/m^3 (a) 80 x 10^{-9}, (b) 40 x 10^{-9}, (c) 10 x 10^{-9}, (d) 1 x 10^{-9}, and (e) 0.5 x 10^{-9}. 117

Figure 5.19 The relationship of anti-IgG concentration and the saturation concentration for the anti-IgG and IgG complex. 118

Figure 5.20 Analyte concentration gradient at the microelectrode for 80 x 10^{-9} mole/m^3 anti-IgG concentration after (a) 0 (initial), (b) 100, (c) 500, and (d) 1600 (saturation) seconds. The graphs are plotted with the x and y axes reversed. 120

Figure 5.21 Influence of flow velocity on the rate of reaction or surface concentration of anti-IgG and IgG complex in mm/s are (a) 10, (b) 5, (c) 1, and (d) 0.5. 121

Figure 5.22 Influence of microchannel height on the rate of reaction. The heights used are (a) 300, (b) 150, (c) 75, (d) 37.5, (e) 18.75, (f) 9.375, and (g) 4.6875 μm. 122

Figure 5.23 Influence of microchannel geometry on the rate of reaction. The heights used are (a) 15, (b) 25, (c) 50, (d) 100, and (e) 150 μm from the microelectrode surface. 124

ABSTRACT

The goal of this research was to develop enhanced signal detection mechanisms for immunosensing using carbon nanotubes (CNTs). The utilization of CNT labels for direct electrical measurement was implemented on lateral flow system and microfluidic integrated interdigitated array microelectrodes. These sensing mechanisms in simple and miniaturized system provided higher sensitivity and autonomous flow control for rapid detection aimed at point-of-care diagnostics.

Specific functionalization protocols were carried out to chemically modify the surface of the CNTs for uniform dispersion and antibody conjugation in aqueous solution. Surfactant assisted dispersion of the CNTs was studied using PVP and PEG. Covalent conjugation of antibodies on the carboxyl groups of the CNTs was accomplished using EDC/Sulfo-NHS coupling chemistry. The adsorption of surfactant and antibodies were manipulated in order to optimize immunoassay detection capability based on electrical measurements.

Following surface functionalization methods, CNTs as a sensing label were employed on a lateral flow system. Competitive and sandwich immunoassay formats were demonstrated based on antibody and antigen binding. The lateral flow system was used for immobilization of capture molecules and passive sample transport by capillary action. CNTs conjugated to antibodies formed conductive network at the capture zone providing a visual indication corresponding to the amount of binding. Most importantly, significant change in electrical conductance was measured for varying low antigen concentrations, detecting anti-human Immunoglobulin G concentration below 1 ng/ml.

Research was also conducted to obtain on-chip immunoassay detection using CNT labels. An IDA microelectrode was used as a binding surface and integrated within a PDMS microfluidic system. The sample and reagents were delivered to the sensing area through a microchannel. The capture of target analyte was indicated by the conjugated CNTs that formed a conducting matrix across the IDA. The detection was based on the selective binding between HSA and anti-HSA, where the conductimetric signal of the binding reaction was monitored through the IDA. The developed miniaturized system provided simple and sensitive immunosensing with detection capability below 1 ng/ml concentration using only 5 µl of sample volume. Simulation was performed in order to understand the influence of the parameters in the microfluidic detection system.

CHAPTER 1

INTRODUCTION

1.1 Motivation

Humankind has been performing bioanalysis since the dawn of time relying on the sensing capability of the nervous system such as the tongue to taste food for poisoning, the nose for detecting scents, or the canaries in the coal mine for gas monitoring. These functions of living organisms are the most efficient and complex sensors to ever exist and they have yet to be fully understood. Meanwhile, scientists have continuously sought to mimic the sensing capabilities of living organisms to develop sensitive and efficient biosensors.

1.1.1 Biosensors

Biosensors are analytical devices that consist of biological recognition elements and signal transducers to detect a particular protein, cell, DNA sequence, or gas molecules. The function of a biosensor can be divided into three parts. The first part is affinity based molecular interaction between the target analyte and its biological receptors. This could involve the use of biological elements such as enzymes, cells, nucleic acids, and proteins, where the biological receptors are often immobilized at a particular surface to capture the analyte being detected. The second part provides an indication of the biomolecular interaction based on signals measured by the transducers. Transducers are often based on fluorescence, piezoelectricity, resonant cantilever, surface plasmon resonance, magnetic particles, and electrochemical protocols. The third part deals with the analysis and quantification of the measured signal into understandable output. These signal processes are carried out using advanced hardware and software for data recording and display in a user friendly manner.

Since the first biosensors were reported in the early 1960s [1], biosensors have experienced a tremendous growth in areas such as health and environmental monitoring. The advancements in microfabrication especially have transformed biosensing apparatus into miniaturized devices. These devices with integrated functions provide major advantages, such as reduced sample reagents and rapid analysis. These advancements have facilitated otherwise time consuming and expensive procedures. However, molecular interactions and recognition has to be well established in order to obtain sensitive measurements for samples in ng/ml level or below. Probe molecules also must be able to selectively detect the target analyte that are mixed with other molecules as in the case with most biological samples. Therefore, direct measurement of these specific molecular interactions has been limited. In order to avoid this limitation, a combination of detection techniques is often implemented that involve additional signal amplification steps. In addition to sensitivity, there has also been a continuous demand for simple, low cost, and rapid biosensors for screening various health and environmental threats. These devices hold a great potential for near-patient use, bio-warfare detection, infectious disease diagnosis, as well as in low-resource areas where a cutting-edge laboratory or skilled person would not be available to operate them. The global need for such tools has been emphasized by recent efforts in microfluidic systems and point-of-care diagnostics such as the one sponsored by the Bill & Melinda Gates Foundation for Global Health Initiatives.

Biosensors addressing some of these needs have been developed using nanomaterials as enhanced signal transducers. Currently, the use of nanomaterials in biosensing is mostly based on optical and electrochemical detection principles. These techniques provide highly sensitive signal generation and amplification using materials such as enzymes and fluorescent

nanoparticles [2]. However, these methods suffer from instability, high cost, and requirement of multiple activation steps and complex signal reader device [3]. On the other hand, electrical biosensors relying on current and/or voltage measurements provide a great alternative to these limitations with ease of detection mechanism and miniaturization. In this work, electrical biosensors are investigated utilizing carbon nanotubes as effective nanomaterials for enhanced signal detection. The use of carbon nanotube labels for direct electrical measurements for improved immunosensing was applied on lateral flow system and interdigitated microelectrodes aimed at point-of-care diagnostics for the first time.

1.1.2 Carbon Nanotubes

Since their discovery in 1991 [4] carbon nanotubes (CNTs) have emerged as one of the most promising materials for the development of nanoscale biosensors. Carbon nanotubes are allotropes of carbon with diameters in the order of a few nanometers, while their length extends up to several millimeters. In addition to their large surface area, carbon nanotubes exhibit superior electrical conductivity, mechanical strength, and chemical inertness [5]. Carbon nanotubes have superior electron transport capability in ballistic manner without dissipating energy due to scattering [6]. They are also one of the strongest and stiffest materials, with tensile strength on the order of 63 GPa, and their elastic modulus in the 1 TPa range [7]. Most of these unique properties are due to the bonding structures of the carbon atoms and the perfect alignment of the lattice along the length of the nanotubes. The carbon-carbon sp^2 bond is one of the strongest chemical bonds containing both σ-bonds and π-bonds that contributes to the enhanced mechanical properties of the CNTs [8]. The electronic properties are predicted to depend on the diameter and helicity of the nanotubes. Helicity, which has to do with the way the planar sheets

of graphite are "rolled up" into hollow core tubes determines the different structures of the carbon nanotubes. These structures are classified as *armchair*, *zigzag* and *chiral* [9]. The *armchair* nanotubes are conducting, while *zigzag* and *chiral* nanotubes can be either conducting or semiconducting [10]. In addition, depending on the number of rolled up graphite sheets, carbon nanotubes are divided into single-walled carbon nanotubes (SWCNTs) and multi-walled carbon nanotubes (MWCNTs). SWCNT are made of a single graphite sheet, while MWCNTs consist of multiple layers rolled up to form tubes. MWCNTs consist of tubes of many different diameters and helicity. They exhibit metallic, semiconductor, and semimetallic conductivity, with the majority of the nanotubes being conductive [5, 11].

Carbon nanotubes with their superior electrical properties have provided alternative and effective electronic sensing of molecular interactions among other applications [12-15]. It has been experimentally proven that bioactive species can be adsorbed either in the hollow cavities or on the outer surface of the nanotubes [16], resulting in conductance change corresponding to the adsorptions [17]. Furthermore, CNTs are known to have high surface specificity and allow multiple modifications with functional groups for sensitive protein recognition based on electron transfer reactions [18]. This has led to the development of CNT-based sensor system for biorecognition, diagnostics, and therapeutic purposes. Some of the most common CNT-based sensor systems are DNA sensors [19], chemical sensors [20], and immunosensors [21].

1.1.3 Rapid and Quantitative Immunosensing using Carbon Nanotubes

Immunoassay is a technique that relies on the binding affinity of antibody to quantify the amount of antigen present in a biological sample. The work described in this dissertation deals with improved signal detection using CNTs as a label for rapid and quantitative immunosensing.

The use of CNTs as a sensing label for direct electrical readout has not been used for the type of immunosensing application demonstrated in this work. Lateral flow and microfluidic immunosensing are developed, both providing passive flow control through capillary action. The two different microfluidic formats are also aimed at simple, low-concentration, and disposable detection mechanism suitable for point-of-care diagnostics. For this purpose, MWCNTs are suspended in aqueous solution and modified with functional groups for efficient dispersion and conjugation with antibodies. The solubility and conjugation methods enable the development of highly specific electronic sensors without the need for additional labeling or signal amplification.

1.2 Objectives

1.2.1 Chemical Functionalization and Antibody Conjugation of Carbon Nanotubes

A major concern in practical use of carbon nanotubes (CNTs) in various solution-based applications is their poor solubility due to the hydrophobic nature of carbon nanotubes and strong van deer Waals attractions between the nanotubes. Uniform dispersion of CNTs is essential in exposing the interfacial areas for optimum antibody conjugation. This will enhance the overall detection capability based on conductimetric signals. A main objective of this work is to modify the surface of the CNTs by non-covalent adsorption of surfactant using mild sonication. The surfactants adsorption penetrates between the CNT bundles to exfoliate the individual tubes. The degree of surfactant adsorption, the uniformity and stability of the CNT suspensions were investigated over different time periods. Covalent conjugation of antibodies with the CNTs was carried out using coupling chemistry to establish stable amide reaction. The anybodies occupied sites on the surface of the CNTs not covered by the surfactant. The surfactant molecules provide

partial coverage that is used for insulating the nanotubes from unwanted interactions with other biological materials while enhancing solubility.

1.2.2 Lateral Flow Immunosensing Based on Electrical Signal Detection

The success of the developed CNT surface functionalization methods for solubility and antibody conjugation provides the capability of immunosensing in this work. The immunosensor utilizes the remarkable electrical conduction properties of CNTs coupled with highly specific biorecognition capabilities of antibodies for enhanced detection mechanism based on direct electrical signal measurements. This detection mechanism is demonstrated on a lateral flow immunoassay system in competitive and sandwich formats. Lateral flow immunoassay is the simplest and most commercially available point-of-care (POC) tests with rapidly growing market worldwide [22]. Implementing sensitive and direct signal detection mechanism in lateral flow test could potentially meet the demand for high throughput diagnostic devices. The CNTs are used as a sensing label, where they form a conducting network at the capture line as a result of binding reactions between target and capture molecule. This CNT network provides a visible indication of the binding reaction, and more importantly exhibits conductance changes corresponding to the amount of captured analyte. In addition to signal detection, this lateral immunosensing technique provides a simple, sensitive, low-concentration, and rapid detection mechanism suitable for point-of-care diagnostics.

1.2.3 Microfluidic Immunosensing Based on Electrical Signal Detection

On-chip immunosensing based on conductimetric detection using CNT matrix is demonstrated. PDMS microfluidic system was developed for sample transport to the to the detection surface. The detection surface is composed of an interdigitated array (IDA)

microelectrode that was fabricated on a glass substrate using UV lithography and wet chemical etching process. The IDA was then covered by immobilized antibody and integrated within the microchannel. This was then used as a sensor area for antibody-antigen binding reaction in sandwich format. The antigen and conjugate sample solution was driven by capillary action in the immunoassay system. The binding reaction was continuously monitored using the IDA. CNTs conjugated with antibody formed a conducting matrix across the IDA providing detection signal corresponding to the amount of captured antigen. Simulation is used in order to understand the influence of the different parameters involved in the microfluidic system.

1.3 Outline of Dissertation

This dissertation contains six chapters. Chapter 1 presents the motivation and objectives of this research, and introduces carbon nanotubes. Application of carbon nanotube-based immunosensing for direct and quantitative electrical measurement is proposed. Chapter 2 reviews previous and current research related to the use carbon nanotubes in biotechnology. It describes the electrical conducting properties of CNTs in regards to surface functionalization. The last part of the chapter provides an insight into one of the main goals of this research, developing immunosensing system suitable for high throughput point-of-care applications. Chapter 3 describes the relevant surface functionalization of carbon nanotubes with surfactants to obtain enhanced solubility in aqueous solutions. Covalent antibody conjugation with the CNTs is then investigated using coupling agents for strong amide bonding. Various characterization techniques are implemented to study stability of the suspensions and surface modifications. Chapter 4 demonstrates the application of carbon nanotube-based detection for lateral flow immunosensing. Competitive and sandwich lateral flow formats are demonstrated, where the

lateral flow immunostrips provide passive sample delivery and detection substrate. Chapter 5 discusses another application of carbon nanotube-based immunoassay that uses interdigitated array (IDA) microelectrodes integrated within a polymer microfluidic chip. Details of mask and device fabrication with corresponding characterizations are also presented. Simulation of the microfluidic system with related binding reactions was conducted in order to understand the effect of the microfluidic parameters. Chapter 6 summarizes results and proposes future work.

CHAPTER 2

BACKGROUND

2.1 Introduction

CNTs have stimulated wide range of scientific interest because of their remarkable combination of properties for the development of novel materials and sensing systems. At the same time, advances have also been made in producing high quality CNTs using techniques such as arc discharge, chemical vapor deposition (CVD), laser ablation, flame synthesis, and high-pressure carbon monoxide (HiPCO). These advancements have led to the use of CNTs in various sensor configurations, as individual molecular wire or as a sensing matrix for biosensing. In this chapter, reviews of previous and current research related to the use of CNTs in biotechnology are presented. Surface functionalization of CNTs, their electrical properties pertaining to functionalization, and practical applications based on electrical measurements are discussed. This chapter will establish the motivation behind the proposed research.

2.2 Surface Modifications of Carbon Nanotubes

CNTs could be either metallic or semiconducting in electrical properties depending on their diameter and helicity [23]. The three categories based on the structure of the CNTs are shown in Figure 2.1. Most of the previous work involving CNTs had focused on SWCNTs due to their simpler structure and smaller diameter making it easier to predict their physical properties [12, 24]. Even though most researchers have focused on SWCNTs, MWCNTs have similar merit of properties as SWCNTs. In addition, the stability of MWCNTs for surface functionalization while maintaining high electrical conductivity has been attracting a lot of attention [25-28]. CNTs are chemically inert and insoluble in most solvents mostly because of

van der Waals attractions between their smooth surfaces [29]. This limitation often requires chemical modification of the CNTs surface in order to improve their solubility [30]. Chemical modification roughens their surface and, also creates reactive groups useful for covalent anchoring of biomolecules [31]. Oxidative treatments utilizing mixture of sulfuric and nitric acids are surface modification protocols commonly used to create functional groups such as carboxylic and hydroxyl functionalization [32-33].

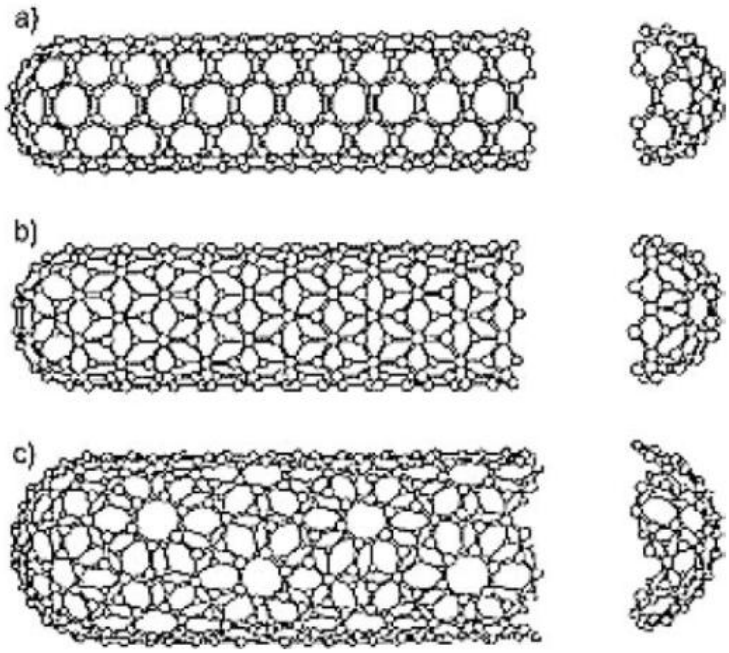

Figure 2.1 Different structures of nanotubes (a) armchair (b) zigzag (c) chiral (Saito *et al.*,1992 [9]).

2.2.1 Aqueous Solubility of Carbon Nanotubes

Uniform dispersion and stability of CNTs suspension is important in order to fully utilize their properties in solution-based processes including biosensing. CNTs in general tend to form clusters. Surface functionalization has been an effective method to enhance their dispersion in aqueous solution. One means of controlling the aggregation of CNTs involves the use of organic solvents and strong acids often involving evaporation steps [34-36]. However, solvents are not desired for biology-related applications due to compatibility issues. Modification of the surface of CNTs in covalent method and the application of high shear force for dispersion would also create defects and introduce shortening of the length of CNTs [37]. Defects destroy the structure of CNTs resulting in alteration of their properties. A preferred method of improving CNTs solubility is the adsorption of surfactants. The interaction of surfactant molecules in non-covalent method minimizes defects to the structure of CNTs while improving their solubility with application low-power sonication [38]. Hydrophobic, electrostatic, and π-π sacking are the main mechanisms suggested for interactions of surfactants with CNTs [39]. In addition, surfactants are non-toxic and low-cost, and require relatively simple experimental procedures for use [40]. Islam *et al.* investigated the solubility of SWCNTs dispersed with various surfactants [41]. The dispersion scheme was carried out by optimizing the ratio of nanotube to surfactants by 1:5 and 1:10 by weight with the application of low-power sonication over extended period of time. Results of the different suspensions showed that commonly used surfactants sodium dodecyl sulfate (SDS) and Triton X-100 had dispersing capability less that 0.1 mg/ml and 0.5 mg/ml, respectively. However, the suspensions were stable only for five days compared to the

SWCNT suspension with sodium dodecylbenzene sulfonate (NaDDBS). NaDDBS suspension was stable over two month time for SWCNT concentration up to 20 mg/ml.

Wrapping of surfactants around the CNTs is another modification mechanism suggested to enhance their solubility in aqueous solutions [42]. O'Connell *et al.* [43] proposed the wrapping of SWCNTs with water soluble polymers such as polyvinylpyrrolidone (PVP) and polystyrene sulfonate (PSS). The uniform wrapping of the polymers were successful in disrupting the hydrophobic interactions between the CNTs and the aqueous medium. The nonionic PVP had a better performance than the ionic PSS in the wrapping process leading to enhanced solubility. It was also reported that the enhanced dispersion of CNTs using charged surfactants such as SDS was due to electrostatic repulsion between the micelles [44].

Moore *et al.* [45] studied the suspension of CNTs with several anionic, cationic, and non-ionic surfactants in water. Results showed that non-ionic surfactants such as PVP wrap around the CNTs, where hydrophobic part of the surfactants interacted with the CNTs and the hydrophilic part extend into the solutions to enhance solubility. The ability to disperse the CNTs also increases with increasing molecular weight due to enhanced steric stabilization. This type of stabilization is not observed for ionic surfactants and charge repulsion is the main mechanism for separating the CNTs. Comparison of the solubility and UV/fluorescence spectra of the CNT suspensions revealed that sodium dodecylbenzene sulfonate was found to be the most effective among the ionic surfactants used. Polyethylene glycol (PEG) and its derivative is another widely used surfactant for minimizing bundling of CNTs in non-covalent method [46]. Lee *et al.* [47] synthesized oligothiophene-terminated PEG (TN-PEG) and examined its ability to stabilize CNT suspensions. The results revealed that TN-PEGs were strongly adsorbed on the CNTs through π-

π interactions. In addition, the application of mild sonication was able to disperse the CNTs into well separated individual tubes.

2.2.2 Protein Adsorption on Carbon Nanotubes

The structure, size, and large surface area of CNTs make them suitable for adsorption of biomolecules. CNTs have inherent affinity for the adsorption of various biomolecules including proteins [48], enzymes [49], and DNA [19]. These biomolecules have been attached to CNTs for the development of sensitive biosensors. Balavoine *et al.* [50] proposed the immobilization of densely packed functional proteins in orderly manner on CNTs as shown in Figure 2.2. This helical crystallization of the proteins was dictated by the structure and properties of the CNTs. The feasibility of this helical arrangement of proteins on CNTs was demonstrated, even though the interactions of the proteins with the CNTs were not fully understood and reproducibility was a challenge. This progress towards the development of new biosensors using CNTs relied on previous work that introduced the encapsulation of proteins in the hollow cavities or on the outer surface of the CNTs without any drastic conformational change [16, 51].

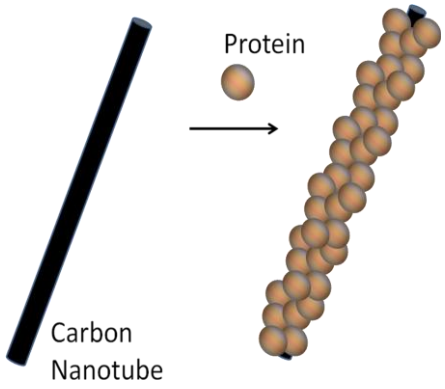

Figure 2.2 Illustration of protein occupying the surface of a carbon nanotube in helical manner (Balavoine *et al.*,1999 [50]).

The natural affinity of CNTs to biomolecules leads to non-specific binding that could be explored for particular applications. However, this phenomenon is often not desired in the development of sensitive biosensors. One strategy of minimizing non-specific binding is the utilization of surfactants such as PEG and PVP [48, 52-53]. PEG has been reported as an effective barrier against unwanted protein adsorption by forming a highly hydrophilic and charge blocking layer at the surface [54]. Chen *et al.* [55] explored nonspecific binding of various proteins on as-grown SWCNTs in solution. Prevention of this nonspecific binding was carried out through non-covalent immobilization of polyethylene oxide chains onto SWCNTs. Specific detection was then carried out by enabling the functionalized SWCNTs to bind with only target analytes. Lin *et al.* [48] also examined the natural affinity of SWCNTs to protein using ferritin in water. Experimental evidence was provided in order to minimize this protein affinity by treating the surface of the SWCNT with PEG.

Conjugation of proteins on the surface of CNTs in more efficient and predictable manner is often conducted through covalent linkage [56]. In this process, covalent bonds are established between the carboxyl groups on the CNTs and the amine groups on the proteins [48]. This amidation reaction is often facilitated by coupling agents such as carbodiimide and succinimidyl ester [57-58]. 1-(3-(dimethylamino)-propyl)-3-ethylcarbodiimide hydrochloride (EDC) is a zero-length cross-linker widely used for covalent conjugation between CNTs and proteins as shown in Figure 2.3 [59]. Low coupling efficiency of EDC due to hydrolysis is often compensated using N-hydroxysulfosuccinimide (Sulfo-NHS) as a stabilizer increasing the coupling efficiency by 10 to 20 fold [58]. Covalent immobilization of proteins with EDC/NHS chemistry has been shown to be more robust compared to non-specific adsorption [60]. Lin *et al.*

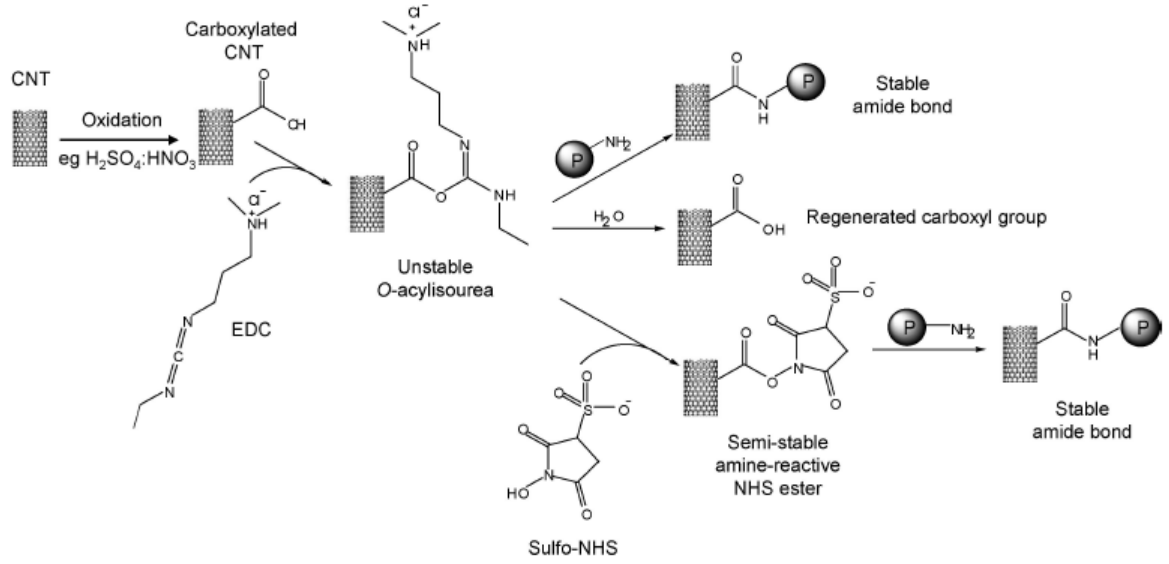

Figure 2.3 Demonstration of the conjugation process of proteins to carboxylated CNTs using EDC and Sulfo-NHS (Gao and Kyratzis, 2008 [59]).

[61] presented comparative work on functionalization of SWCNTs and MWCNTs for potential immunosensing. The CNTs were first functionalized with BSA protein using carbodiimide for amidation reaction between the carboxylate groups on the CNTs and the BSA proteins. The CNTs were further conjugated with *E. Coli* specific antibodies, where the BSA protein also facilitated specific detection of the target analyte.

2.2.3 Electrical Properties of Carbon Nanotubes as a Result of Functionalization

CNTs are highly sensitive to adsorption of molecules and exhibit significant change in their electrical properties. Zhao *et al.* [62] investigated electronic properties of CNTs as a result of covalent sidewall functionalization with functional groups such as COOH and NH_2. Theoretical studies have revealed that sidewall functionalization of CNTs with any type of functional groups disturbs the electronic states near the Fermi level [62]. For metallic CNTs, the

sp^3 hybridization between the CNT and the molecules creates impurity state that affects the ballistic transport properties. The impurity state extends over a large area, even though the defects remain locally around the functionalization. It has also been observed that covalent functionalization changes the conducting properties of the CNT dramatically, hence providing a means to control properties of CNTs for sensing applications. Functional groups have also been shown to behave as electron acceptor or donor facilitating charge transfer between the CNT [63]. Experimental studies showed a drastic reduction in electrical resistance of SWCNTs as a result of functionalization compared to the pristine samples [64-65].

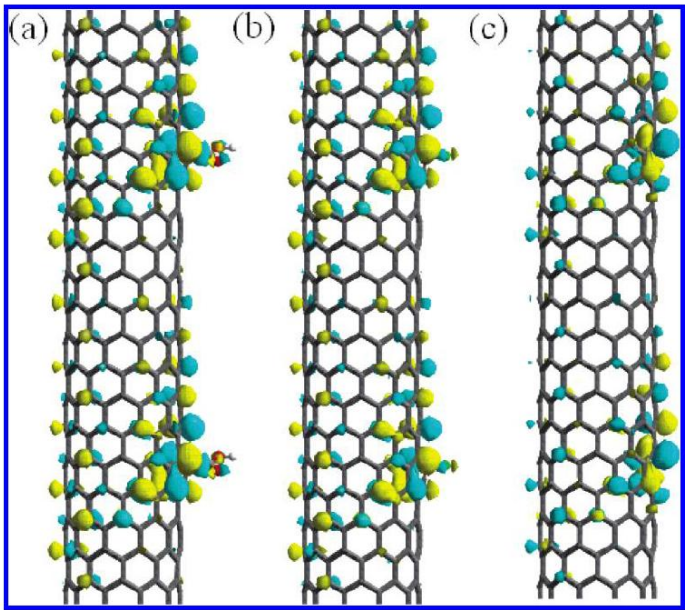

Figure 2.4 Illustration of wave function with induced impurity state as a result of modification of (10,0) SWCNT with functional groups (a) COOH-functionalization (b) F-functionalization and (c) a C vacancy on the side wall, where the yellow and blue colors indicate the polarity of the wave function (Zhao *et al.*, 2004 [62]).

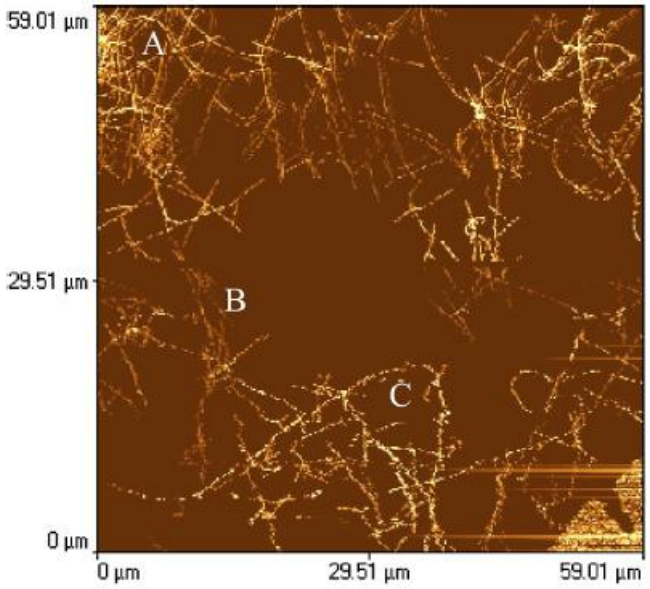

Figure 2.5 Conductance microscope image showing minimal conductance drop of the nanotube network with higher interconnectivity measured at varying locations from the electrode. The conductance at point A, B, and C are 700, 200, and 700 nS (Stadermann *et al.*, 2004 [66]).

Stadermann *et al.* [66] investigated conductance measurement of CNT network. It was observed that conductance did not decrease linearly with the distance from the electrode. Instead, for CNT network with poor interconnection, the conductance dropped due to the formation of Schottky barrier junction by metallic and semiconducting nanotubes. In the case of nanotube network with high interconnection, there could be a chain of metallic nanotubes stretching to the electrode maintaining high conductance as shown in Figure 2.5.

The electronic characteristics of CNTs as molecular wires or interconnect have been studied extensively in various sensing configurations for the detection of biomolecules [6, 18, 66-68]. One of the difficulties in this type of sensing configurations was establishing electrical

contacts between the CNTs and the electrodes. This difficulty was partly overcome by using combination of techniques involving conventional lithography to contact the ends of the CNTs and determine their electrical properties [69]. Subsequently, sensing capabilities based on CNTs was realized by the fabrication of devices such as field-effect transistors that consisted of individual semiconducting or metallic CNTs [67-68, 70]. These devices enabled the electrical transport properties of the CNTs to be manipulated from conducting to insulating state by varying the applied gate voltages. High contact resistance was also observed between the CNT and the electrode interface that required consideration when developing such devices [71]. The detection capability of CNTs between metal contacts was demonstrated for chemical and biological sensing with electron transfer process between the molecules and the CNTs [20, 55, 72-73]. Aligned CNTs were investigated for electron-transfer reactions of proteins with the CNTs acting as molecular wires [74-75]. The CNTs allowed electrical communications between the electrode and redox proteins that were covalently attached to the ends of the SWCNT.

Star *et al.* [76] examined the device characteristics of carbon nanotube field-effect transistors (CNTFETs) for specific and non-specific protein binding. The nonspecific binding caused the device characteristics to shift to negative gate voltage. Nonspecific binding of proteins after blocking the surface with polymer coating caused no change in the device characteristics. Finally, specific binding using biotin-streptavidin resulted in reduced source to drain current. Current model equations have been developed that were useful in analyzing CNTFETs in biosensing applications [77].

Kenzo *et al.* [78] fabricated CNTFET with aptamer modified CNT channel for direct measurement of protein binding. The IgE aptamers were covalently immobilized on the CNT

using 1-pyrenebutanoic acid succinimidyl ester. The capture of target IgE in different concentrations caused a sharp decrease in the source to drain current with gradual saturation at lower concentrations. The performance of the aptamers in capture efficiency was observed to be better than IgE specific antibodies partly due to the smaller size of the aptamers that could pack more densely on the conducting channel.

2.3 Carbon Nanotubes for Biosensing

Electrical measurements provide an alternative to complex and multiple processes involved in optical detection that have been dominating biosensing technique. Electrical biosensors are especially attractive for fast, low cost, and miniaturized devices, since detection of binding reaction could be based on simple current and/or voltage measurements [79]. Especially, electrical biosensors utilizing nanoscale materials and devices offer provide size compatibility and ease of integration [80]. CNTs have been utilized in various electrical based biosensors such as electrochemical impedance spectroscopy (EIS), nanowires [81], and field effect transistors (CNTFETs).

Carbon nanotubes have been used for the detection of DNA. Koehne *et al.* [82] showed low-density nanoelectrodes using aligned MWCNTs embedded within SiO_2 matrix for detecting DNA targets. Enhanced detection of DNA hybridization was previously carried out with glassy carbon electrode using MWCNTs [83]. DNA sensor based on the conductance change of SWCNTs, where DNA hybridization was conducted on gold electrodes, was also demonstrated [84].

Yu *et al.* [85] demonstrated mutli-label strategy using horseradish peroxide (HRP) labels and secondary antibodies attached to MWCNTs for sensitive detection of prostate specific

antigens (PSA) as shown in Figure 2.6. Primary antibodies specific to PSA antigens were attached to SWCNT forests assembled on conductive substrate. Capture of PSA antigens by the primary and secondary antibodies (sandwich immunoassay) were measured by adding a mediator and hydrogen peroxide to activate the peroxidase cycle that resulted in increasing current under a constant voltage. Sensitive detection of PSA was achieved through signal amplification at high HRP/secondary antibody ratio compared to immunosensing based on single-labeled secondary antibodies. This signal amplification was also dependent on controlling nonspecific binding by blocking the immunosensors with BSA and Tween-20. EDC and NHSS were also utilized to attach the primary and secondary antibodies on the CNTs through amide bonding.

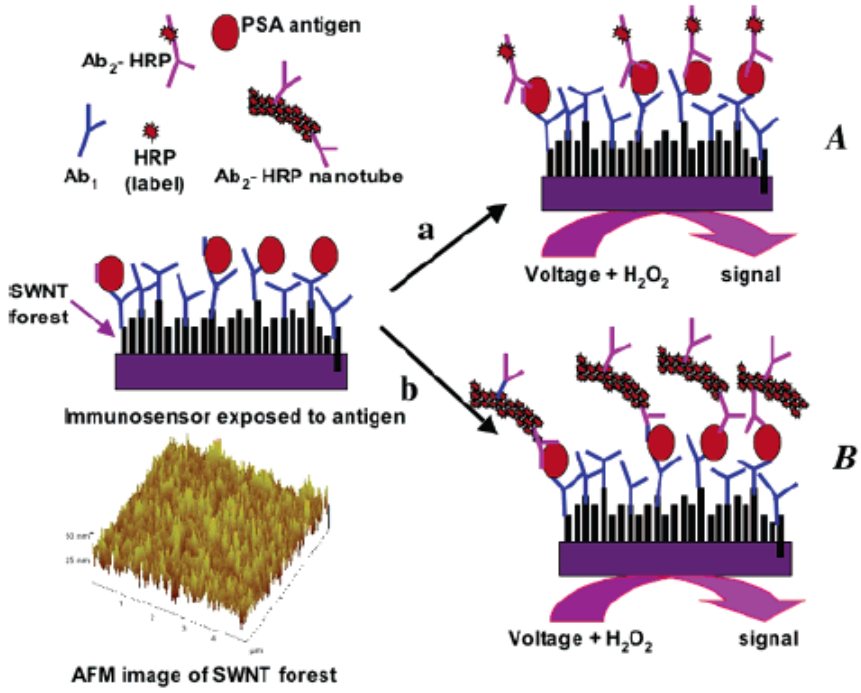

Figure 2.6 Immunoassay detection principle using CNTs to immobilize multiple labels and secondary antibodies for signal amplification. HRP catalyzes H_2O_2 and generates electrons for amperometric based measurement. (A) conventional single HRP labeled secondary antibody (B) multiple HRP and secondary antibody on carbon nanotube for signal amplification (Yu *et al.*, 2006 [85]).

Okuno *et al.* [21] also fabricated SWCNT modified platinum (Pt) wires for the detection of PSA through direct electrical measurements. The performance of the device was tested using nonspecific antigen, BSA and with the Pt electrodes only without the SWCNTs. The application of BSA protein on the SWCNT-Pt microelectrodes treated with PSA specific antibodies resulted in no significant change in the current signal. Application of PSA to the bare Pt microelectrodes also resulted in no signal. This was because the PSA specific antibodies were immobilized covalently using coupling molecule (1-pyrenebutanoic acid succinimidyl ester) on the SWCNTs, and the coupling molecule had no affinity to the Pt electrodes causing non-specific binding.

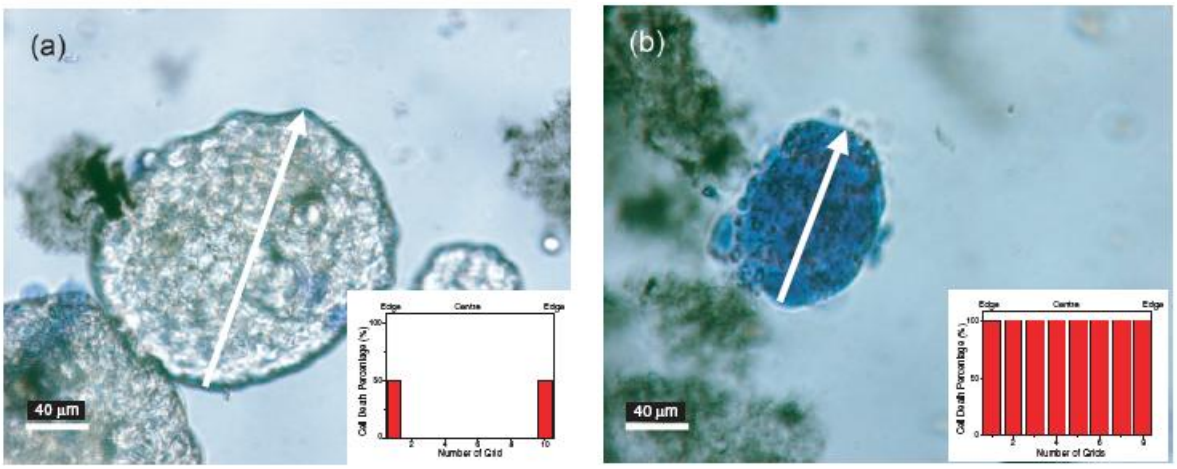

Figure 2.7 CNT-based treatment of MCF7 cancer cell using NIR dosing (a) survival of the cells treated with nanotube attached to non-specific antibody complexe (b) destruction of the cells treated with nanotube attached with specific antibody (anti-IGF1-HER2) complex (Shao *et al.*, 2007 [86]).

Shao *et al.* [86] carried out phototherapy using SWCNT functionalized with antibodies specific to breast cancer cells as shown in Figure 2.7. The application of infrared photons at ~ 808 nm wavelength led to the destruction of the cancer cells due to the concentration of theSWCNTs through selective binding of antibodies specific to the cancer cells. In the case of non-specific antibodies treated with SWCNTs, 80% of the cells remained alive. The SWCNT and antibody conjugation was achieved through amide bonding using 1-pyrenebutanoyl succinimide. Polyethylene glycol was then used to insulate the surface of the SWCNTs from nonspecific interactions.

Liu *et al.* [87] introduced functionalization of SWCNT by chemically partitioning the surface of nanotubes to attach various species non-covalently for potential drug delivery applications. SWCNTs were first functionalized with PEG derivatives to obtain aqueous solubility. The unoccupied sites on the prefunctionalized SWCNTs were used to bind with cancer chemotherapy drug, doxoyrubicin (DOX). Release of DOX drug was also studied by varying the pH for controlled delivery of molecules bound on CNTs.

Chen *et al.* [88] investigated the adsorption of various proteins using SWCNT micromat devices. PEG derivatives and PEG containing surfactants were utilized to block certain parts of the device, and the conductance change due to protein adsorption was observed before and after blocking treatments. It was concluded that protein adsorption on the metal-nanotube contact has a significant contribution to the electronic signal obtained, in addition to the adsorption on the sensing part of the CNTs.

Li *et al.* [89] investigated complementary detection of PSA using In_2O_3 nanowires and SWCNTs as a conducting channel between source and drain electrodes. Both the nanowires and

the nanotubes were modified with PSA specific antibodies. The application of PSA on the indium oxide nanowires resulted in increased conductance, opposite to the decrease in conductance for the SWCNTs. This change in conductance was explained by the nanowires being n-type and the SWCNTs being p-type semiconductors. For both the indium oxide nanowires and SWCNTs, antibody conjugation was achieved using succinimidyl ester.

Panchapakesan *et al.* [90] used SWCNTs interconnects between patterned metal electrodes for the detection of live breast cancer cells. When the capture cells were captured by the specific antibodies on the SWCNTs, a conductance increase was observed corresponding to the amount of captured cancer cells. Prior to constructing the device, the SWCNT bundles were dispersed using NaDBBS, where the surfactant was non-covalently adsorbed on the surface of the CNTs enhancing the aqueous solubility.

2.4 Immunoassay

Immunoassay is an analytical test that uses the selectivity and affinity of an antibody binding to target analyte in a sample. The performance of immunoassay relies on the efficiency of the antibody and analyte (antigen) complex formation and the ability to quantify the binding reaction. The work conducted in this dissertation deals with quantification of the binding reaction based on simple and reliable electrical signals providing quantitative measurements through simple detection mechanisms. In addition to sensitivity, detection time and cost are important factors considered for immunosensing system targeted at high throughput point-of-care tests.

2.4.1 Antibody

Immunoassays take advantage of the extreme specificity of antibodies to recognize structurally distinct epitopes on analytes for binding, making them the most critical reagents [91]. Antibodies also known as immunoglobulin G (IgG) are glycoproteins generated by the immune system to fight against disease and foreign substances present in the body. Immunoglobulin G (IgG) is the most abundant class of antibodies found in the blood and tissue liquids, and also used extensively in immunoassays for ease of production. The "Y" shaped structure of IgG is composed of four polypeptide chains: two heavy chains and two light chains linked by disulfide bond as shown in Figure 2.8. The arms of the "Y" shaped structure are called the Fab region for antigen binding fragment. This region contains the two antigen binding sites and it is composed of one constant and one variable domain from each (heavy and light) chain of the antibody. The base of the "Y" is called the Fc region for crystallizable fragment and contains two heavy chains.

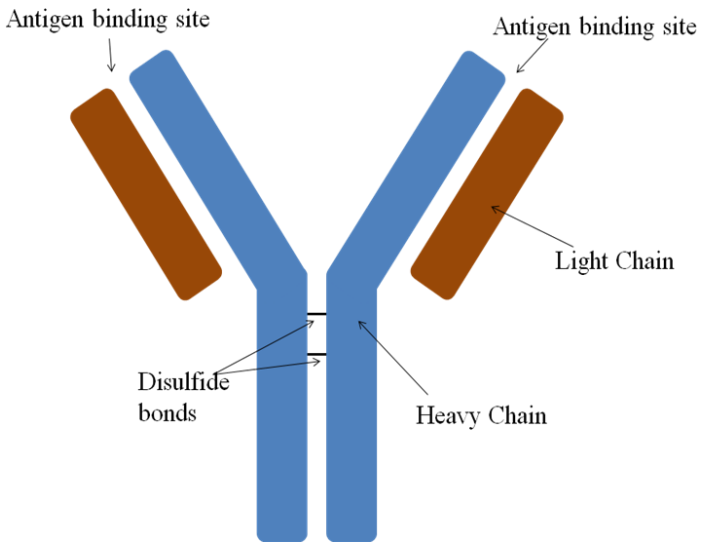

Figure 2.8 Schematic diagram of Immunoglobulin G (IgG) molecule.

Antibodies are mostly monoclonal and polyclonal types, each with their own advantages and disadvantages [92]. Monoclonal antibodies are produced from one type of B-cells and bind to the same epitope of their specific antigen, making them highly specific. The sensitivity of monoclonal antibodies can be affected if there is a slight variation in the epitope structure of their specific antigens. Unlike monoclonal antibodies, polyclonal antibodies are produced from multiple cells. Polyclonal antibodies are sensitive, but less specific since, they can recognize different epitope on their target antigens, subjecting them to cross-reactivity.

2.4.2 Immunoassay Formats

Two of the most common immunoassay formats are competitive and sandwich immunoassays. In competitive assay format, even though there could be different configurations of the test, the target analyte competes for limited binding site with a known labeled sample. In this format, the amount of captured analyte is indirectly proportional to the detected signal by the labels. In non-competitive or sandwich immunoassay, primary and secondary antibodies are utilized. Primary antibodies are often immobilized on a solid substrate to capture the target analyte. The primary function of secondary antibodies is to attach labels that provide indication of a binding reaction between target analyte and primary antibodies. In this case, the amount of captured analyte is directly proportional to the signal detected through the labels

Competitive immunoassay is often used when utilizing smaller molecules with fewer binding sites. They are also simpler with less number of steps and often used for purification of assays. Sandwich immunoassay is considered more sensitive, and therefore is commonly used. A possible configuration of sandwich and competitive immunoassay is shown in Figure 2.9.

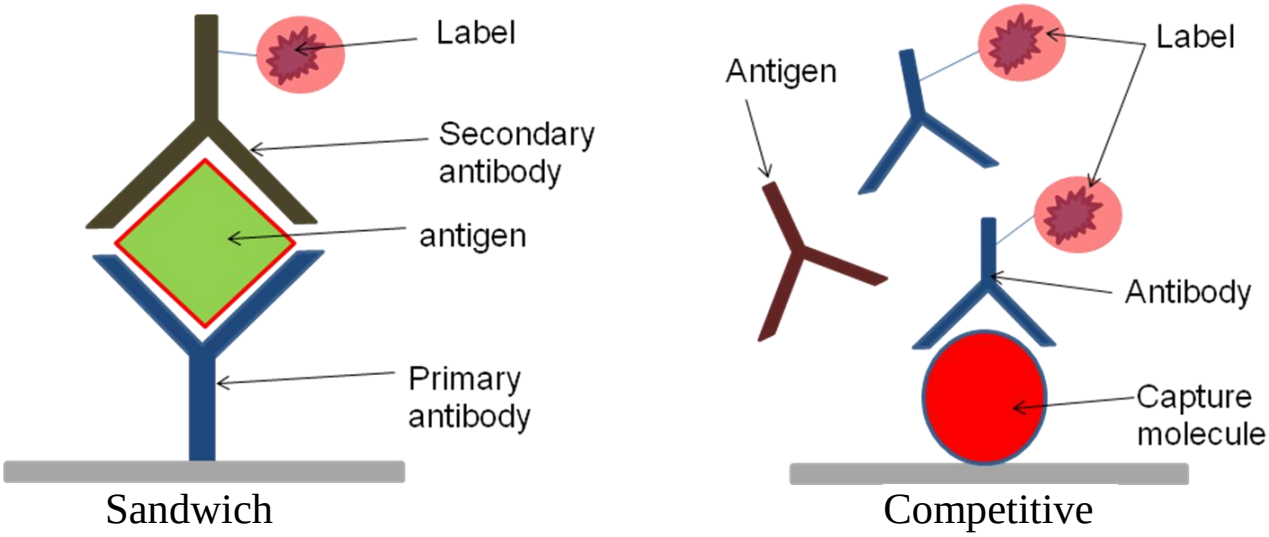

Figure 2.9 Illustration of sandwich and competitive immunoassay formats.

2.4.3 Label-Based Immunoassay

Label is another other important reagent of an immunoassay that is used for the detection of antibody binding reaction. The amount of label detected corresponds to the number of captured targets. One of the earlier immunoassay methods was based on radioisotope labels. Radioimmunoassay (RIA) is highly sensitive, specific, and relatively cheap to perform [93]. However, the use of radioactive materials is hazardous and the cost of their disposal has put constrain on the technique. Since then, various types of labels have been developed including fluorophor, enzymes, magnetic beads, colloidal gold, and chemiluminescent materials [94]. The flexibility and availability of labels have increased the applicability of immunoassays with high degree of stability depending on the sought detection result. However, the labeling step has been considered a shortcoming, since some labels modify the properties of the biomolecules being

detected. In addition, the use of labels and secondary antibodies is considered as additional process and cost. Therefore, label-free methods have emerged as an alternative, eliminating labels by direct monitoring of binding reaction. While direct detection sounds attractive and could possibly save time and cost related to the labeling procedure, label-free methods have their own shortcomings mainly due to the lack of selectivity [95]. Label-free detections are also subjected to background interference and cross-reactivity influencing the sensitivity. In addition, most label-free techniques such as surface plasmon resonance, cantilever, quartz crystal microbalance, and piezoelectric crystals are expensive and complex to fabricate [96]. Therefore, label-free methods have had minimal commercial success as high-throughput techniques [97].

While the search continues for the best label with detection capability down to a single molecule, label-based immunoassay detection remains to be the most reliable and the most widely used. Especially, nanomaterials such as CNTs could provide solutions, while minimizing the existing limitations of labeling techniques. Immunoassay detection based on carbon nanotubes labels for direct electrical measurements is investigated in this work. This technique will eliminate the shortcomings that plague conventional labeling methods.

2.5 Point-of-Care Immunoassays

The ability to produce quality antibodies and various types of labels has advanced the capability and applicability of immunoassays. However, currently technologies related to immunoassay are not only evaluated in terms of low detection limit, but also speed, ease of operation, and continuous monitoring. These requirements are being driven by the demand for point-of-care (POC) diagnostics to be performed near the patient rather than the time consuming

processes involving centralized laboratories. In addition, POC devices should be low-cost and should not require complex procedures or skilled person to operate. These POC devices have applications for use at the doctor's office, home care, the military, and developing countries. POC devices could strongly benefit from advanced materials and fabrication methods to improve their efficiency and sensitivity. Biosensors based on electrical signal detection have been attracting a lot of attention for the development of rapid, miniaturized, and low cost devises. However, high detection sensitivity have not been a critical factor [97]. In this work, CNT-based electrical detection is investigated for sensitive immunosensing, while maintaining the simplicity of the test that is ideal for POC tests.

One of the important factors for POC immunoassay is the label. Labels should be stable, low-cost, sensitive, and easy to conjugate and integrate [94]. For example, in electrochemical-based detection, enzyme labels are often instable and the concentration of the substrate used by the label for signal detection is difficult to optimize [98]. Fluorescence labels suffer from photobleaching [3] and magnetic particles are difficult to detect [99]. In addition, methods for detecting and displaying the signal generated by the labels in a POC devices should be simple to operate and should not be bulky in size.

Multiple reagent handling with external or integrated active components for flow control could complicate POC immunoassay system. In addition, fabrication of such components could be cumbersome with short lifespan of the devices. Rather, passive flow control is desired for POC immunoassays. Lateral flow system, where fiber matrix with microscale pores provide sample transport by capillary action, has been very successful for POC application [22]. Another

platform that provides passive flow control involves the use of microchannels and microchambers in order to manipulate small sample volume and integrate multiple functions for rapid and portable devices [100]. Both miniaturized platforms, lateral flow and microchannel based immunoassay for high detection sensitivity and passive flow control capability have been investigated in Chapter 4 and Chapter 5 of this dissertation, respectively.

CHAPTER 3

SOLUBILITY AND ANTIBODY CONJUGATION OF CARBON NANOTUBES

3.1 Introduction

The remarkable one-dimensional electric conduction properties of CNTs coupled with the ability to adsorb biomolecules on their surface have paved the way for the development of advanced biosensing materials and techniques. The large surface area of CNTs allow chemical modifications for proper anchoring and detection of biomolecules based on electron transfer reactions [17, 38]. These techniques have been explored for protein detection and clinical diagnostics purposes [85, 101-102]. CNT-based detection mechanism holds a potential for simple and quantitative immunosensing without additional labeling or amplification step.

For the pursuit of immunoassay applications, it is important to select functionalization protocols in order to obtain highly soluble and antibody conjugated CNTs [61, 73]. The functionalization protocols should be compatible with biomolecules and should be carried out in a less destructive manner to preserve the electrical properties of the CNTs. The functionalized CNTs will be implemented as label in a matrix format for highly sensitive antibody detection in this research. This chapter describes the development of chemically functionalized MWCNTs for uniform dispersion in aqueous solution and antibody conjugation through covalent bond. The functionalized MWCNTs will be studied as a label for immunosensing based on electrical signal detection.

3.2 Solubility of Carbon Nanotubes in Aqueous Solutions

A major concern in practical use of CNTs is their poor solubility in most common solvents and especially in water due to their hydrophobic nature and the strong van deer attraction between the tubes [46, 103-104]. Surface functionalization of CNTs is therefore necessary in order to enhance their solubility and create reactive groups for efficient anchoring of antibodies. The adsorption of surfactants on the surface of CNTs has been an effective approach to disperse CNTs in aqueous solution [105-107]. The adsorption mechanism of the surfactant molecules on the surface of CNTs is mainly based on electrostatic, hydrophobic, and π-π stacking [37, 108]. These non-covalent functionalization methods are mostly preferred because of their minimal effects on the π networks of the CNTs that determine the inherent structures influencing the electrical conductivity among other properties [109-110]. The surfactant coating with the application of sonication penetrates in between the sidewalls of the CNTs and separates them into individual tubes [111-112]. In addition, surfactants are water soluble and non-toxic, and they do not require evaporation steps as in the case with organic solvents or strong acids.

3.3 Surfactant Assisted Dispersion of Carbon Nanotubes

The adsorption of surfactants is an effective strategy for improving the solubility of CNTs in aqueous solution. The hydrophobic part of the surfactant molecules adsorb on the surface of the CNTs while the hydrophilic parts interact with the aqueous medium to untangle the nanotube bundles [46, 107]. Surfactants such as polyvinylpyrrolidone (PVP) [113], polyethylene glycol (PEG) [111], sodium dodecyl sulfate (SDS) [41], and sodium dodecylbenzene sulfonate (NaDDBS) [45] have been widely investigated for this purpose. In the case of PEG, aromatic molecules are attached on the surface of the CNTs (PEGylation) through

π–π stacking to eliminate the hydrophobic interaction between the CNTs in aqueous medium [38]. In the case of PVP, it is known to provide nearly monolayer coating by wrapping around portion of the CNT surface [43, 107]. The partial coverage of the CNTs surface leaves unoccupied sites to attach multiple molecules on the surface of the CNTs [87]. It has also been reported that thin layer of surfactant coating on CNTs do not reduce the electrical conducting properties [111].

3.4 Conjugation of Antibody on Carbon Nanotube

For a potential immunosensing application, the surface of the CNTs needs to be functionalized with functional groups for the immobilization of antibodies through stable covalent bonding [55]. Functional groups like carboxyl group provide reactive sites for the covalent attachment of proteins through amidation process [31, 114]. Amidation process between the amino group on the antibodies and the carboxyl groups on the CNTs is often facilitated by coupling agents such as carbodiimide chemistry [38, 86]. 1-(3-(dimethylamino)-propyl)-3-ethylcarbodiimide hydrochloride EDC is a widely used cross-linker that reacts with carboxyl groups to form amine reactive intermediate. EDC then reacts with an amine group to produce a stable amide bond [59]. However, EDC is not stable and suffers from low coupling efficiency due to hydrolysis of the intermediate in aqueous environment [115]. Therefore, this process is supplemented with N-hydroxysulfosuccinimide (Sulfo-NHS) to suppress hydrolysis, and increase the efficiency of the cross-linking [58].

CNTs also have inherent affinity to antibodies and other proteins requiring a surface modification protocol to limit non-specific binding [48, 88]. Non-specific attachment of proteins is not desired in immunosensing and could compromise detection capability. A typical method

of addressing these unwanted nanotube-antibody interactions is by insulating the surface of the CNTs with protein repellent molecules. Molecules such as PEG and PVP are commonly used to cover the surface of CNTs in order to prevent non-specific adsorption of proteins [53-54].

3.5 Experimental Study

3.5.1 Functionalization of MWCNTs

The modification of carboxylic acid treated MWCNT with surfactant and antibodies was carried out as illustrated in Figure 3.1. Two different MWCNT samples were prepared. In one sample, the MWCNTs were treated with PVP in aqueous solutions. In the other sample the MWCNTs were treated with PEG in aqueous solutions. These surfactants, when adsorbed on the surface of the MWCNTs, provided partial coverage. The MWCNTs in both samples were then reacted with EDC and Sulfo-NHS to activate covalent bonding between the carboxyl (–COOH) groups of the MWCNTs and primary amines ($–NH_2$) of the antibodies. Finally, human IgG was

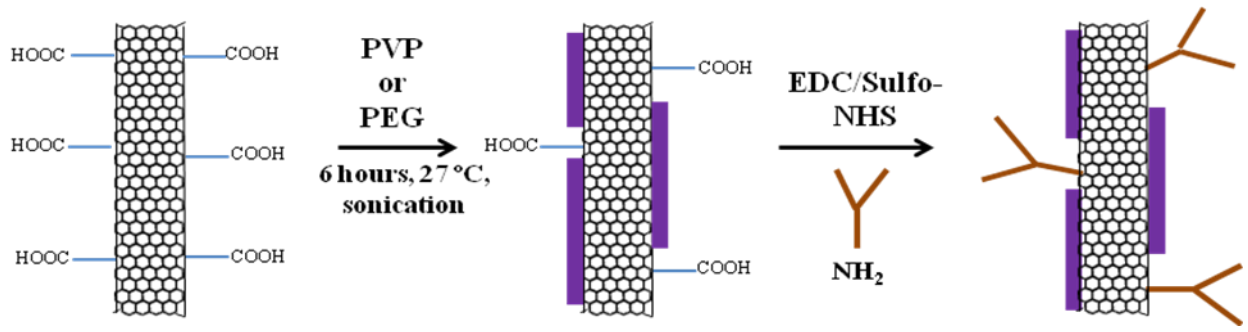

Figure 3.1 Schematic illustration for functionalized MWCNTs with PVP or PEG by surface adsorption and human IgG through covalent amide bonding (not to scale).

added to the MWCNT solutions that resulted in the immobilization of the antibodies on the binding sites not covered by the surfactant. The partial coating of the surfactants was essential in both dispersion as well as blockage of the surface of the MWCNTs from unwanted interactions with proteins.

3.5.2 Materials and Reagents

MWCNTs treated with carboxylic acid groups (MWCNT-COOH) suitable for functionalization chemistry (outer diameter = 8-15 nm, length =10-15 μm, purity > 95 wt %) were obtained from Cheaptubes, Inc., (Brattleboro, VT). Polyvinylpyrrolidone (PVP, MW 10,000) was obtained from Sigma-Aldrich (St. Louis, MO). Polyethylene glycol (PEG, M.W. 8,000) was obtained from Acros Organics (Morris Plains, NJ). EDC and Sulfo-NHS were obtained from Thermo Fisher Scientific, Inc. (Rockford, IL). All immunoreagents were diluted in pH 7.4 phosphate saline buffer (PBS) unless otherwise stated.

3.5.3 Surfactant-Assisted Dispersion

Non-covalent functionalization and dispersion of MWCNTs with surfactants was prepared as follows. COOH-MWCNTs were first dispersed in two separate solutions. In one solution, 0.5 mg of MWCNTs was mixed with 0.6 mg of PVP in 5 ml deionized (DI) water. In another solution, 0.5 mg of MWCNTs was mixed with 5 mg of PEG in 5 ml DI water. Each mixture was then sonicated using a mild bath for 6 hours at room temperature yielding a dark uniformly dispersed MWCNT suspension. Characterization of the dispersion was carried out by optical analysis using UV-Vis spectroscopy. The stability of dispersions was also investigated by allowing the MWCNT solutions remain at room temperature and measure the UV absorbance one week and four months after initial dispersion.

3.5.4 EDC/Sulfo-NHS Chemistry

In order to accomplish stable amidation between the nanotubes and the antibodies, 2 ml of the PVP dispersed MWCNT solutions were centrifuged for 3 minutes to separate the dark supernatant and then the bottom 1/3 of the solution with nanotube aggregates was discarded. Coupling agents, EDC (0.4 M) and Sulfo-NHS (0.1 M) in 1 ml of MES (buffer pH ~ 6.0), were mixed with the remaining modified MWCNT solution. The EDC/Sulfo-NHS chemistry was used to facilitate the covalent bonding between the carboxyl groups (–COOH) on the surface of the carbon nanotubes and the primary amine groups ($–NH_2$) of antibodies through stable amidation process. The mixture was left to incubate for 30 minutes at room temperature. Furthermore, excess surfactants and coupling reagents in the solutions were removed by washing and suspending the MWCNTs in PBS buffer using centrifugation at 13,000 rpm for 3 minutes.

3.5.5 MWCNT-Antibody Conjugation

Purified human IgG (6.2 mg/ml) suspended in 0.01 M sodium phosphate (0.15 M NaCl, pH 7.4) containing 15 mM sodium azide as a preservative was obtained from Sigma-Aldrich (St. Louis, MO). For the MWCNT-antibody conjugation, the human IgG solution was diluted to 200 µg/ml in PBS buffer. Then, 200 µl of the human IgG solution was mixed with the MWCNT solution and the mixture was incubated overnight at room temperature. The washing and suspending process was repeated by centrifugation in PBS buffer to remove unbound antibodies that resulted with antibodies immobilized on MWCNTs. The suspended solutions were kept at 4 ^{o}C until use.

3.6 Results and Discussion

The demonstrated functionalization scheme allowed the partitioning of the surface of the MWCNTs with surfactants and antibodies. The adsorption of surfactants has improved MWCNTs solubility in aqueous solution. The surface of the nanotubes not covered by the surfactants provided potential binding sites for antibodies with MWCNTs through covalent bonding. The surfactant adsorption also served a dual purpose of insulating the nanotubes from unwanted interactions with other biological materials while enhancing solubility.

3.6.1 MWCNT Solubility

The dispersion of MWCNTs with PVP, PEG, and DI water, individually, was investigated. Prior to sonication, the solubility of MWCNTs in all three solutions was poor with almost all the nanotube clusters settling at the bottom of the solutions as shown in Figure 3.2(a). After sonication, the dispersion improved dramatically for all three solutions resulting in dark supernatant with dye-like homogeneity as shown in Figure 3.2(b). A slight intensity variation in

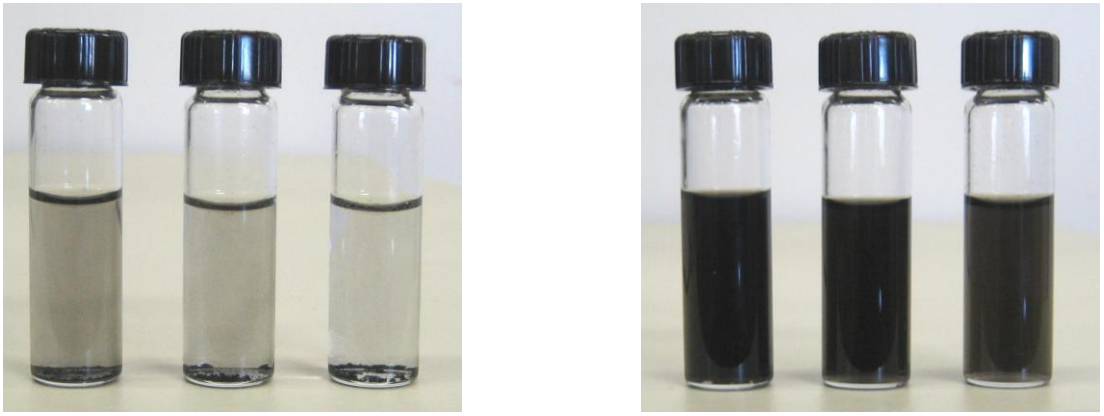

(a) (b)

Figure 3.2 Dispersion of MWCNTs in water (a) before and (b) after sonication with PVP, PEG, and without surfactant (going from left to right). All samples have same concentration of nanotubes (0.1 mg/ml).

the color of the solutions was observed indicating the degree of dispersion. The MWCNT-PVP solution had the darkest color with almost all the MWCNTs suspended in the solution. The MWCNT-PEG solution was the second darkest in intensity and good in dispersion. The MWCNT solution with DI water only and no surfactants had the lightest intensity and the least dispersion, and clusters were easily observed in the suspension. For quantitative investigation of the state of dispersions after sonication, the MWCNT solutions were subjected to optical analysis using UV-Vis-NIR scanning spectrophotometer (Shimadzu UV-3101PC). The UV spectroscopy was used to demonstrate a linear relationship between the absorbance and the dissolved nanotubes in the different suspensions. Figure 3.3(a) shows the absorption spectra of the MWCNTs suspended in the three different solutions. As predicted by the visual intensity of the solutions, MWCNT-PVP had the highest absorbance values followed by MWCNT-PEG and MWCNT-DI water. The absorbance of PVP and PEG solutions without MWCNTs were optically transparent throughout the UV-Vis-NIR spectrum. The stability of the dispersions was also examined by placing the solutions in ambient conditions for longer durations. After one week from their equivalent initial suspensions, the absorbance values of the surfactant dispersed MWCNT solutions remained higher compared to the MWCNT solutions without surfactant as shown in Figure 3.3(b). After a period of four months, the absorbance values of the surfactant dispersed solutions experienced relatively small reduction compared to the MWCNT solutions without surfactant as shown in Figure 3.3(c). The results indicate that the use of surfactants was important in obtaining initial dispersion of the MWCNTs as well as maintaining the stability of suspension. Specifically, it was observed that the performance of PVP in improving MWCNT solubility was better than PEG. The surfactant-assisted dispersion also suggests an equilibrium

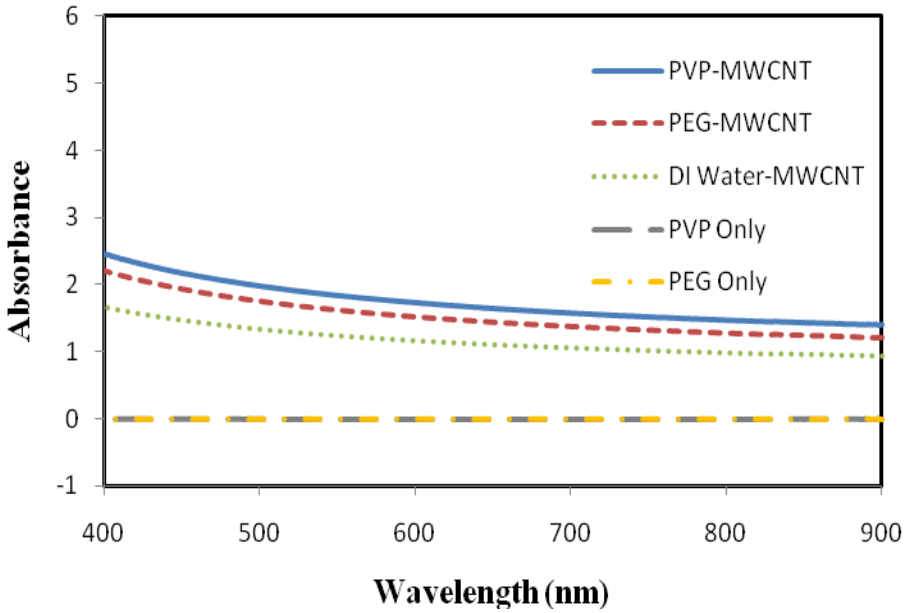

(a)

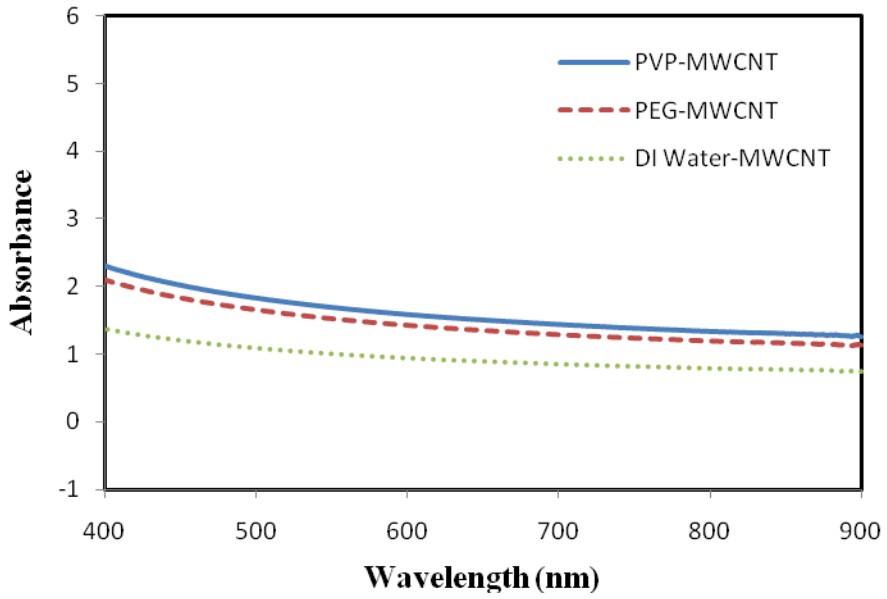

(b)

Figure 3.3 The UV-Vis absorbance spectra of the MWCNT dispersion (a) immediately after sonication (b) one week after sonication and (c) four months after sonication. The different lines indicate MWCNT disperisons with PVP, PEG, DI water (without surfactant), and PEG as control in the absence of MWCNTs (Figure 3.3 con'd).

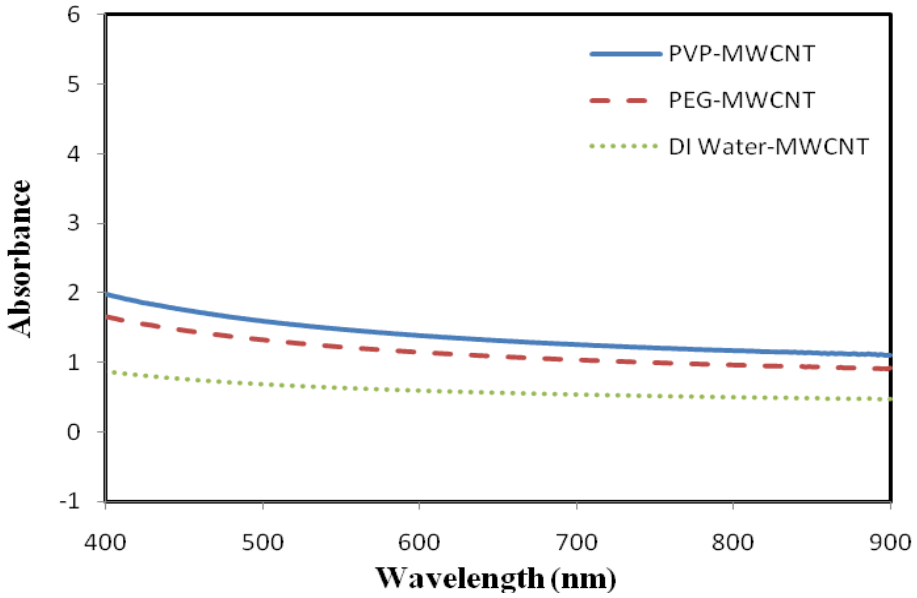

(c)

process between the nanotubes and the surfactants. The slight reduction in solubility observed for the surfactant dispersed MWCNT solutions could be due to the ratio of nanotubes to surfactants, where the surfactant concentration could be below the critical micelle concentration (CMC) [112]. Furthermore, the application of low power sonication facilitated the adsorption of the surfactants on the surface of the CNTs without shortening the length of the nanotubes. In order to establish a benchmark of the relationship between absorbance and concentration, absorbance MWCNT solutions (0.01, 0.02, 0.06, 0.07, 0.08, and 0.1 mg/ml) dispersed with PVP

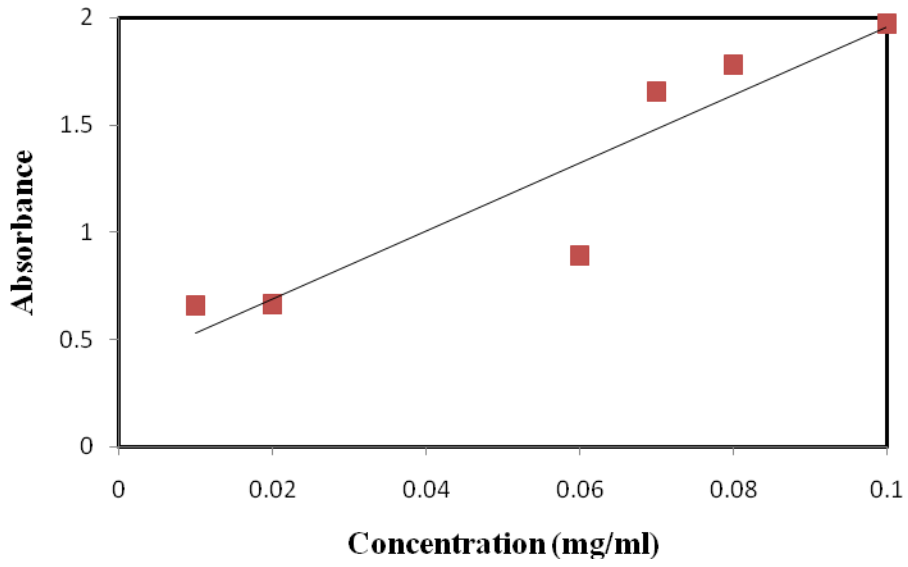

Figure 3.4 Plot of absorbance versus concentration for the PVP dispersed MWCNT solution for peaks at 500 nm.

was obtained after sonication (Figure 3.4). A linear relationship of absorbance values with increasing concentration was observed. This result was in agreement with the Beer-Lambert's law that has been known to establish the linear relationship between absorbance of light and concentration of an absorber [111].

In order to closely examine the dispersion of the MWCNTs, different parts of the solutions were dispensed and dried on a silicon substrate for SEM analysis as shown in Figure 3.5. The MWCNT-PVP solution had the best dispersion with well separated individual nanotubes (Figure 3.5(a)). The MWCNT-PEG solution had dispersed nanotubes but showed a number of small bundles spaced throughout over the substrate (Figure 3.5(b)). The MWCNT

dispersed in DI water without surfactants had the least uniform dispersion showing the nanotubes clustered together at isolated areas of the substrate (Figure 3.5(c)). The influence of the surfactant coverage in separating the bundles was evident in the level of solubility of the MWCNTs. In addition, the adsorption of PVP has resulted in morphological changes observed on the MWCNTs. A rough organic layer with around 1-2 nm in thickness (estimated from TEM

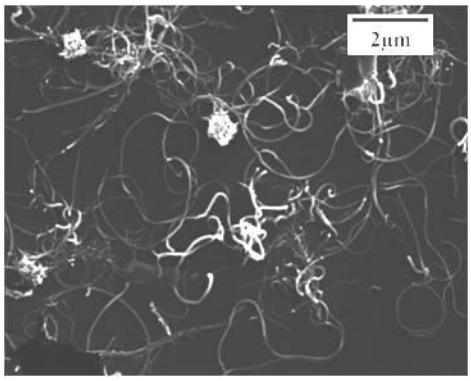

(a)

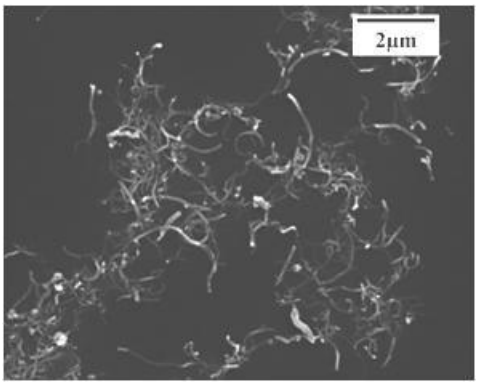

(b)

Figure 3.5 SEM image of MWCNTs dispersed with (a) PEG, (b) PVP, (c) only DI water on silicon substrate (Figure 3.5 con'd).

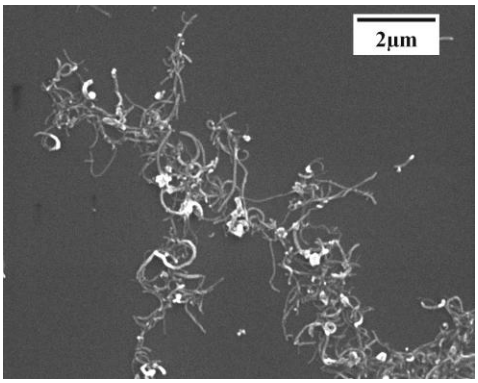

(c)

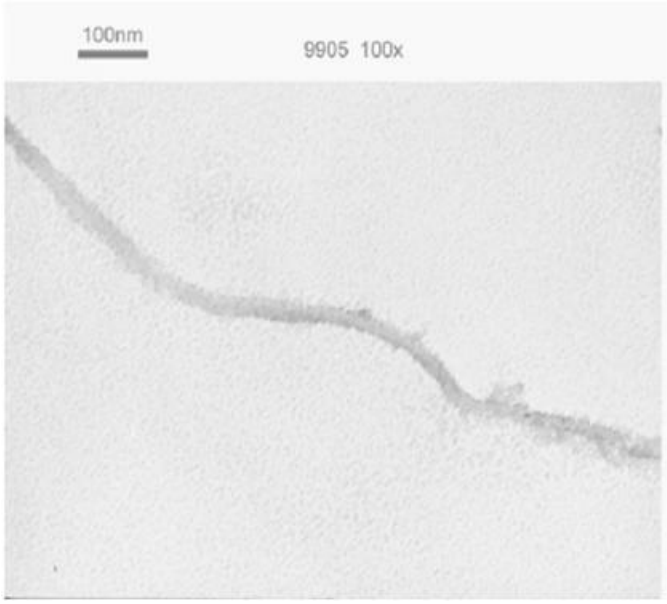

(a)

Figure 3.6 TEM images of MWCNTs (a) with surfactant coating and (b) without surfactant coating (Figure 3.6 con'd).

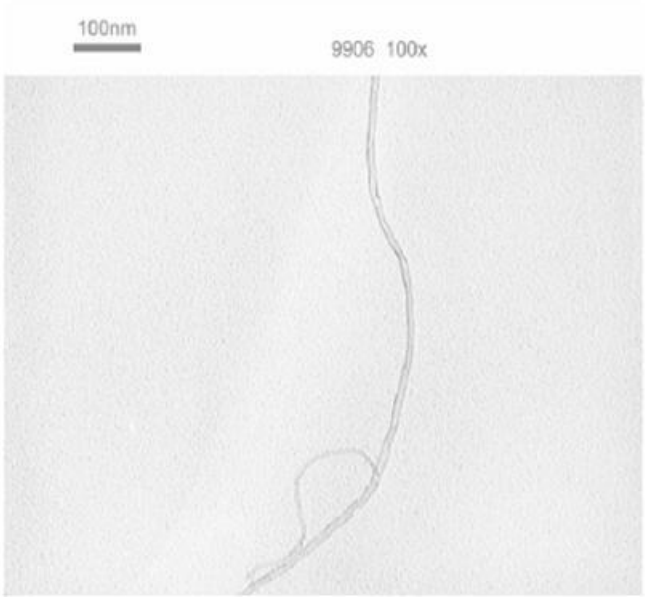

(b)

image) was observed on the MWCNTs treated with PVP compared to the smooth surface of unmodified MWCNTs as shown in Figure 3.6(a) and 3.6(b). This result was also in agreement with striation patterns observed on the surface of the nanotubes treated with surfactant molecules in dry form [116]. Dispersion of the MWCNTs as discussed in section 3.6.1 could be related to the surfactant coverage.

3.6.2 Amidation Process

The coupling agents, EDC/Sulfo-NHS, with primary function of establishing strong amide bonding between the MWCNTs and antibodies had also influenced the solubility of the suspensions. Varying solubility states were observed for the MWCNTs in the three solutions (with PVP, PEG, DI water dispersants) after incubation with the coupling agents as shown in

Figure 3.7. It was observed that the amidation process affects the solubility of the MWCNT, especially in the absence of surfactant. The MWCNT-PVP solution had the highest absorbance value with the least reduction in dispersion. The MWCNT-PEG solution had the second highest absorbance value. In both cases, limited agglomeration of the tubes into bundles was observed due to the addition of the coupling agents. For the MWCNT solution dispersed with only DI water, there was a significant phase separation between the nanotubes and the solution. The solubility reversed dramatically resulting in relatively low absorbance value. The reduction in homogeneity of the dispersion could be due to the short-life span of EDC before hydrolyzing in aqueous solution if not interacted with amine group even with the use of Sulfo-NHS to suppress the hydrolysis [115]. In order to minimize this effect, the reaction time between the MWCNTs and the coupling agents was limited to 30 minutes to maximize the coupling efficiency without a

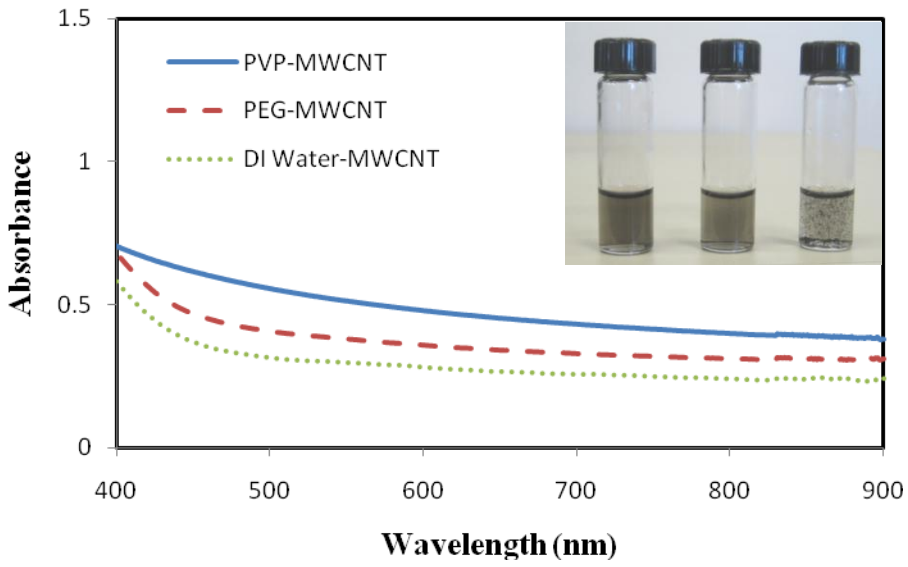

Figure 3.7 The UV-Vis absorbance spectra of the MWCNT solutions after reacting with EDC/Sulfo-NHS for stable amidation process. The inset shows the dispersion state of MWCNTs in water with PVP, PEG, and without surfactant after reacting with the coupling agents.

significant decrease in dispersion. The MWCNT suspension dispersed with surfactant remained stable when interacting with functional groups. However, the poor dispersion of the MWCNTs without the presence of surfactants could escalate during the conjugation process and limit detection performance.

3.6.3 MWCNT-Antibody Conjugation

PVP modified MWCNT solution provided the best dispersion, and therefore, it was used for the conjugation study. The covalent attachment of antibodies on the -COOH groups of the MWCNTs was facilitated by EDC/Sulfo-NHS chemistry in a two-step process. First, the MWCNT-COOH was mixed with EDC/Sulfo-NHS to produce a semistable amine-reactive NHS ester. After washing excess EDC, the activated MWCNTs were then incubated with human IgG. This process was important to reduce aggregation of antibodies and bundles of MWCNT-human IgG conjugate. The reaction time between the MWCNTs and the coupling agents was limited to 30 minutes in order to minimize hydrolysis while optimizing conjugation efficiency. The antibodies occupied binding sites that were not covered by the surfactant. This process produced complete functionalization of the MWCNTs. Analysis of the functional groups on the surface of the MWCNTs was conducted using FTIR. FTIR spectra were recorded for the functionalized MWCNTs using Bruker FTIR spectrometer (Tensor 27) as shown in Figure 3.8. For the MWCNT-COOH sample, the FTIR spectrum showed characteristic peak at ~1714 cm^{-1} that corresponds to the C=O stretch of the carboxylic group (Figure 3.8(a)). The band at ~ 3479 cm^{-1} is related to O-H groups due to the presence of moisture on the surface of the MWCNTs. However, the peaks were weak for the MWCNT-COOH sample that could be attributed to the limited number of COOH groups on the surface of the MWCNTs. Another reason could be that

the black MWCNTs absorbing the entire infrared ray from the FTIR detection [28]. For the neat PVP sample, characteristics peak at 1650 cm^{-1} is assigned to the C=O stretching in the PVP amide unit (Figure 3.8(c)). Characteristics peaks at 1415 and 1286 cm^{-1} are associated with absorption bands of the PVP. The covalent conjugation of antibodies on the MWCNT was observed with distinct characteristic peaks at 1645 and 1538 cm^{-1} corresponding to primary and secondary amides (Figure 3.8(e)). Similar characteristic peaks were shown for neat antibody sample at 1635 and 1538 cm^{-1} that were associated with primary and secondary amines (Figure 3.8(d)). In addition the characteristic peak at 1714 cm^{-1} that belongs to the COOH group on the MWCNTs disappeared during antibody conjugation. The displacement of the peak could be due to the covalent attachment of antibodies on the COOH group of the MWCNT that results in the new amide peaks. The FTIR results confirm the successful conjugation of antibodies on the MWCNTs.

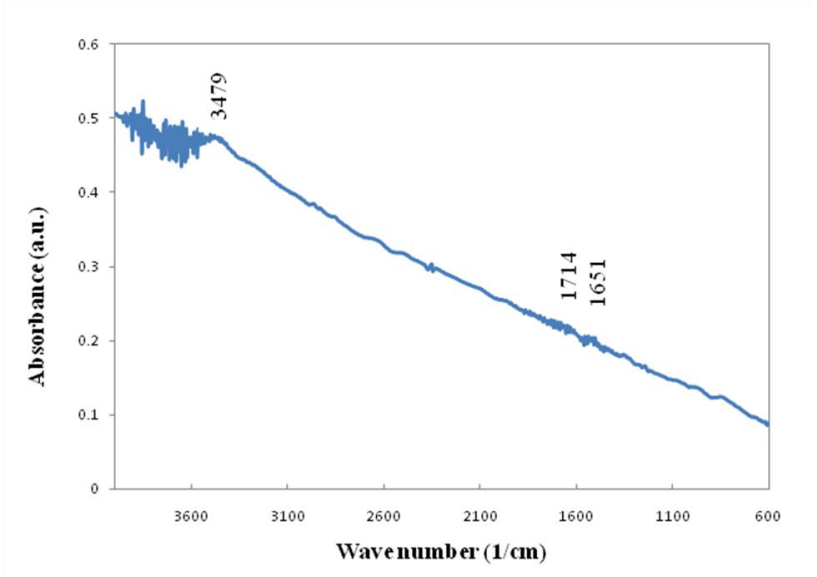

(a)

Figure 3.8 FTIR spectra of samples (a) carboxylated MWCNTs (b) neat PVP (c) PVP-modified MWCNTs (d) neat antibodies and (e) antibody-functionalized MWCNTs (Figure 3.8 con'd).

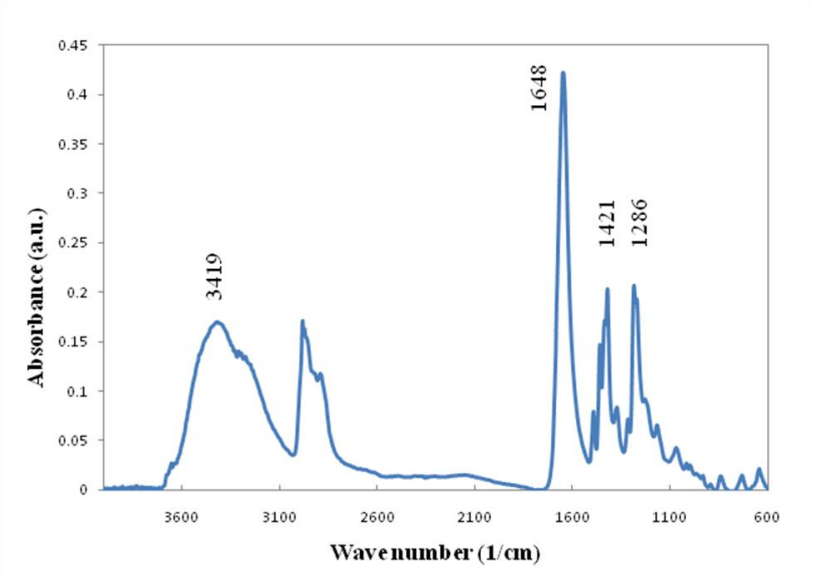
0.45
0.4
0.35
0.3
0.25
0.2
0.15
0.1
0.05
0
Absorbance (a.u.)
3419
1648
1421
1286
3600
3100
2600
2100
1600
1100
600
Wavenumber (1/cm)

(b)

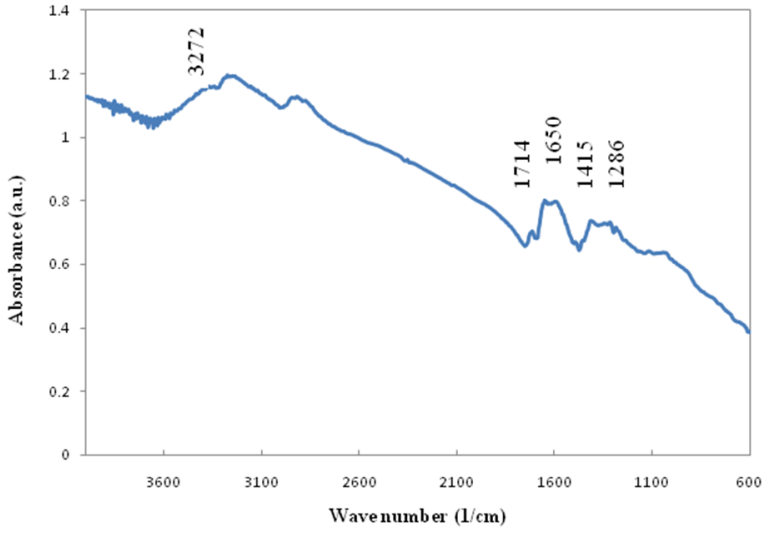
1.4
1.2
1
0.8
0.6
0.4
0.2
0
Absorbance (a.u.)
3272
1714
1650
1415
1286
3600
3100
2600
2100
1600
1100
600
Wavenumber (1/cm)

(c)

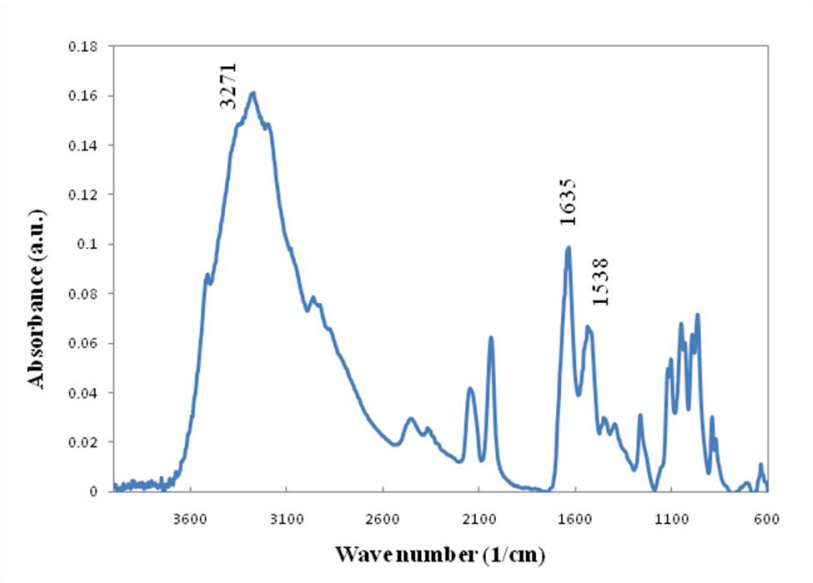
0.18
0.16
0.14
0.12
0.1
0.08
0.06
0.04
0.02
0
Absorbance (a.u.)
3271
1635
1538
3600
3100
2600
2100
1600
1100
600
Wavenumber (1/cm)

(d)

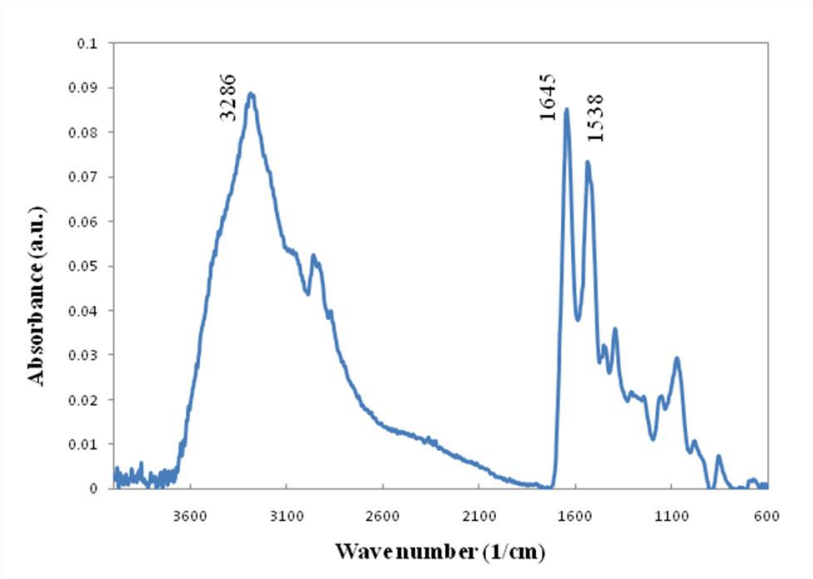
0.1
0.09
0.08
0.07
0.06
0.05
0.04
0.03
0.02
0.01
0
Absorbance (a.u.)
3286
1645
1538
3600
3100
2600
2100
1600
1100
600
Wavenumber (1/cm)

(e)

Dispersion, antibody immobilization, and surfactant coverage were further characterized using TEM by dispensing 1 µl of solution on gold coated carbon TEM grid. It was observed that the MWCNT-PVP sample maintained good dispersion after conjugation process as shown in Figure 3.9(a). The MWCNT-antibody conjugation efficiency was also examined. A close-up image of the MWCNT-antibody conjugate in Figure 3.9(a) shows that antibodies protruded on the surface of the MWCNTs. Unbound antibodies were not observed indicating that unbound antibodies were successfully removed by the multiple rinses without affecting the covalently attached antibodies to the surface of the MWCNTs. Immobilization of antibodies occurred at various sections of the MWCNTs, since the carboxylic groups were located randomly at different

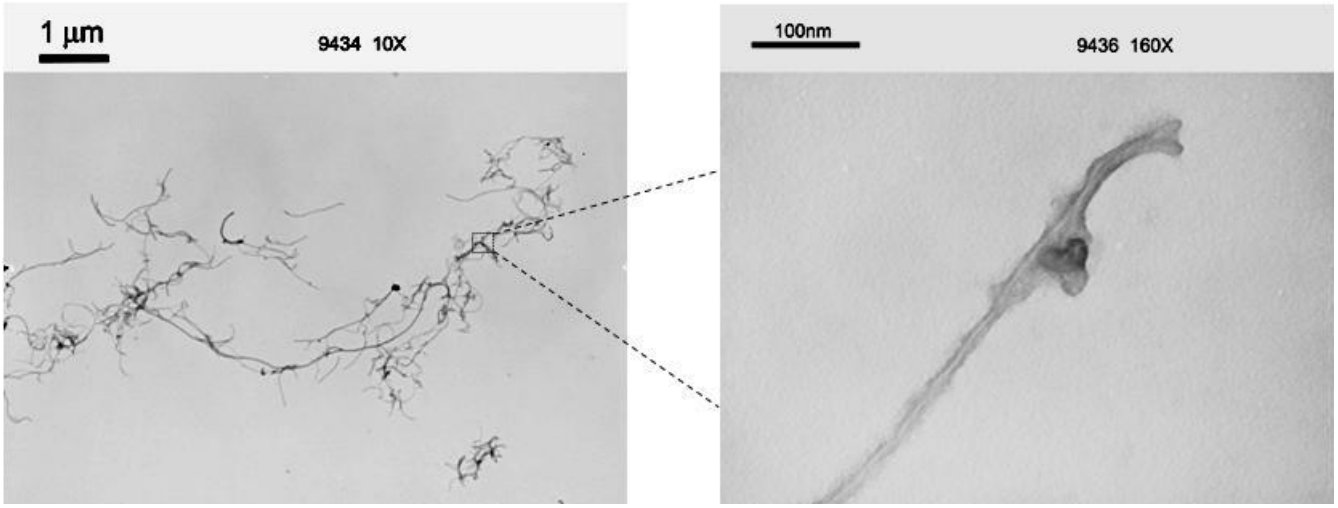

(a)

Figure 3.9 TEM images showing (a) surfactant dispersed MWCNTs conjugated with human IgG and a close up image of the MWCNT-antibody conjugation (b) aggregates of conjugated antibodies on MWCNTs (Figure 3.9 con'd).

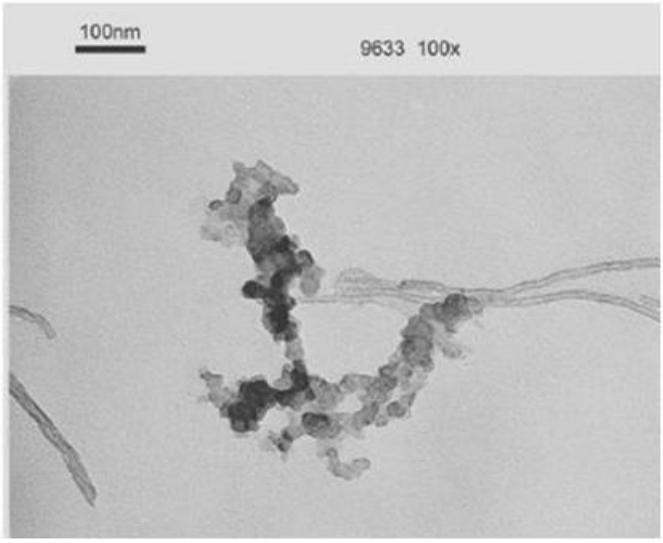

(b)

parts of the CNT in addition to the PVP coverage influence. Aggregates of conjugated antibodies were however observed in spite of the two-step process for coupling chemistry limiting interaction between the antibodies. This was especially evident in the case that the MWCNTs bent or folded during conjugation as shown in Figure 3.9(b).

3.6.4 CNT-Antibody Conjugation with Reduced PVP

Increasing the number of conjugated antibodies per each MWCNT could result in better detection capability. One factor influencing the amount of antibodies conjugated on the MWCNTs could be the degree of the PVP coating limiting binding sites for antibody attachment on the surface of the nanotubes as shown in Figure 3.10. In order to investigate the influence of surfactant coverage in the amount of attached antibodies, the same conjugation procedure was

carried out with the MWCNTs dispersed in DI water only (without PVP). Characterization of the conjugate solution revealed that the MWCNTs had relatively poor dispersion compared to the conjugate solution in the presence of PVP as shown in Figure 3.11(a). In addition, an increase in the number of conjugated antibodies was not observed. This could be due to the poor dispersion of the nanotubes in solution that might have placed a restriction on the interaction of the antibodies with individual MWCNTs. For the limited conjugation observed, the antibodies were mostly buried within the bundles compared to the more distributed antibodies in the presence of PVP as shown in Figure 3.11. Therefore, conjugation process with only DI water was not very useful in studying the influence of PVP coverage in conjugation efficiency since poor dispersion was a dominating factor. However, the process confirmed the importance of surfactants in enhancing the solubility of MWCNTs for efficient conjugation with antibodies and overall detection performance.

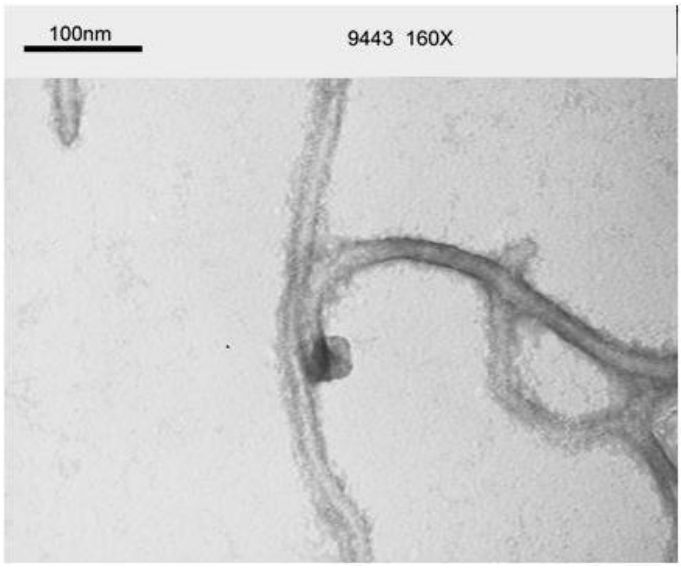

Figure 3.10 TEM images showing surfactant coating on the surface of the MWCNTs with antibody conjugation.

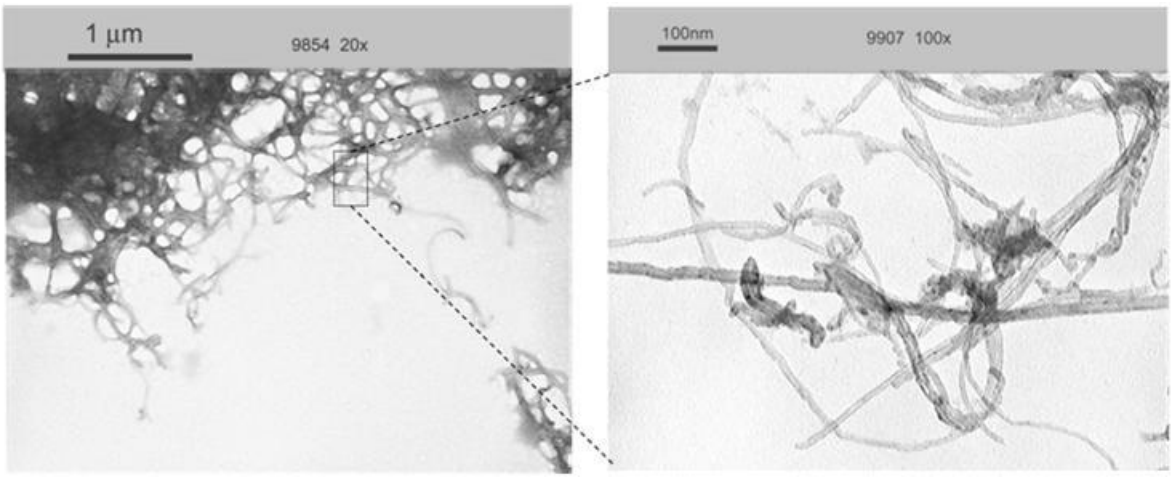

(a) (b)

Figure 3.11 TEM images showing (a) human IgG conjugation of MWCNTs dispersed without surfactant (b) a close up image of the MWCNT-antibody conjugation.

The second step taken in understanding the role of surfactant in antibody conjugation was using lower amounts of PVP to expose more binding sites. For this reason, the amount of PVP was reduced to 25% and 10% from the original amount (0.5 mg of MWCNTs was mixed with0.6 mg of PVP in 5 ml DI water). Characterization of the conjugation solutions revealed that number of conjugated antibodies was increased significantly with 25% reduction of PVP as shown in Figure 3.12. The larger view of the TEM image (Figure 3.12(a)) shows that MWCNT were very well dispersed throughout the solution. A close up images shows multiple antibodies attached on the MWCNTs ((Figure 3.12(b)). For the conjugate solution with 10 times lower PVP, limited antibody conjugation with the MWCNT was obtained compared to the solution with 4 times lower PVP. A reduction in the dispersion of the conjugation solution was observed, since the amount of PVP was too low to carry out a proper conjugation. Comparison of the conjugate

solutions confirms that there was not much difference in the solubility state of the MWCNT with 0.6 mg (original amount) and 4 times lower PVP but there was a reduction in the uniformity of the dispersion for the 10 times solution as shown in Figure 3.13(a). TEM characterization of the conjugate solution with 10 times lower PVP shows the agglomeration of the MWCNTs that limits the surface area for antibody conjugation (Figure 3.13(b)). This result was similar to the conjugate solution obtained with only DI water (Figure 3.11) except more MWCNT-antibody conjugates were obtained in this case. Therefore, varying the amount of PVP used to disperse the MWCNTs could lead to the change in coverage of the MWCNTs and amount of conjugated antibodies. However, the amount of PVP has to be optimized in order to maintain sufficient dispersion of the MWCNTs.

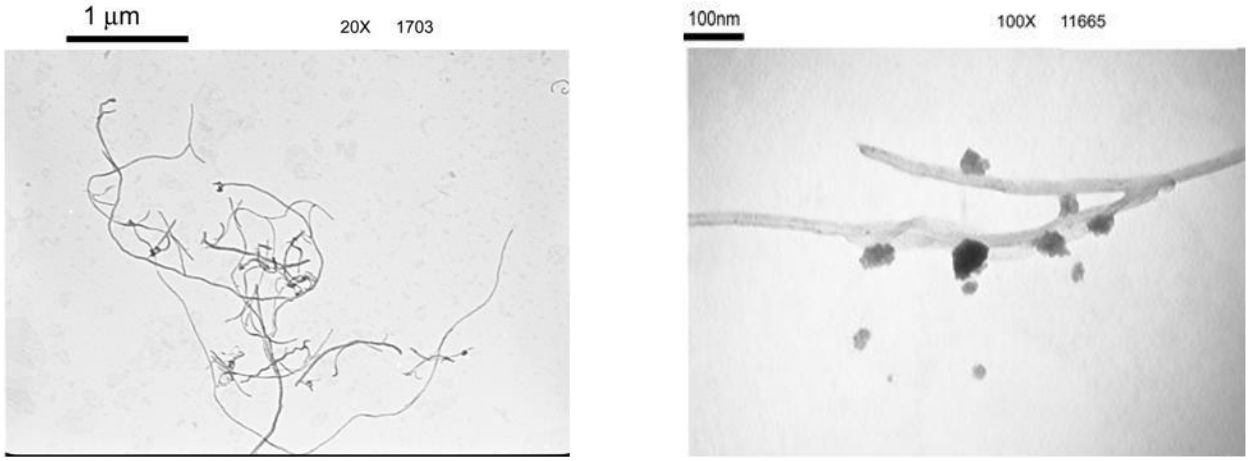

(a) (b)

Figure 3.12 (a) TEM characterization showing well dispersed MWCNTs with enhanced antibody conjugation using 4 times lower PVP (b) a close up image showing multiple antibodies attached on the surface of the MWCNTs.

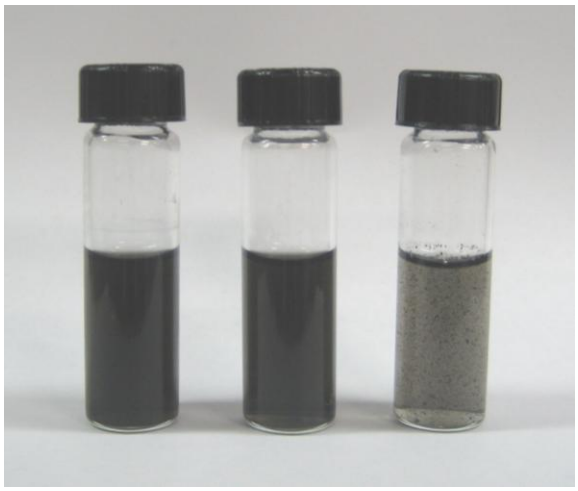

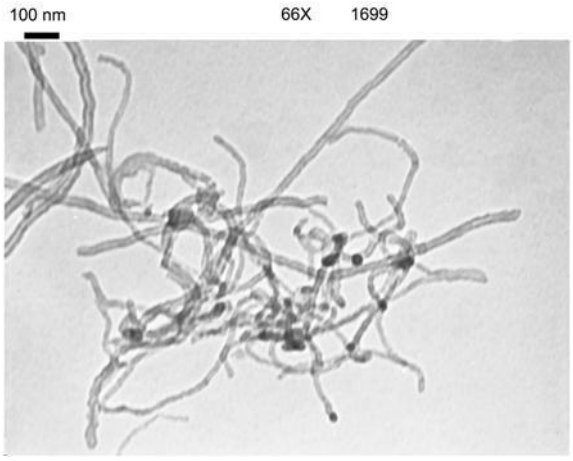

(a) (b)

Figure 3.13 Dispersion state of MWCNT-antibody conjugate solution using original PVP, amount, 4 times lower PVP, and 10 times lower PVP (going left to right) (b) TEM image showing limited antibody conjugation with MWCNTs due to poor dispersion.

3.6.5 Enhanced CNT-Antibody Conjugation with Increased Antibody Concentration

Another parameter considered to enhance the number of antibodies attached on the MWCNTs was the amount of antibodies used for conjugation. This was due to the possibility that concentration of antibodies for conjugation considered in this work (200 µg/ml) could be small compared to the amount of MWCNTs. Lower antibody concentration for conjugation was carefully chosen through experimental optimization in order to provide suitable/sufficient detection capability while eliminating the possibility for unbound (free) antibodies. Unbound (free) antibodies have to be controlled in order to optimize the conjugation efficiency and detection parameters. In addition, unbound antibodies could compete with the conjugate for binding site on the immobilized antibodies (sandwich format) and compromise detection performance. In order to investigate the influence of high antibody concentration on conjugation

efficiency, MWCNT-antibody conjugation was carried out with higher antibody concentrations 250, 500, 1000 µg/ml, under the same experimental procedures. For conjugate solution with 250 µg/ml antibody concentration, a significant difference in the number of antibodies attached to the nanotubes was not observed compared to results obtained with lower concentration of antibodies (200 µg/ml). For the conjugate solution with 500 µg/ml antibody concentration, a dramatic increase in the number of antibodies on the MWCNT was observed as shown in Figure 3.14. Unbound antibodies from the solution not attached to surface of the MWCNTs were also observed. As the concentration of antibody was further increased (1000 µg/ml), the amount of conjugated of antibodies also increased. However, with increased antibody concentration for conjugation, the presence of unbound antibodies also increased dramatically as shown in Figure 3.15.

The results show that enhancing MWCNT-antibody conjugation was successfully conducted by varying the antibody concentrations. The conjugation process with higher amount of antibodies was conducted based on fully optimized protocol that has been developed for lower antibody concentration (200 µg/ml). Results also suggest that the conjugation protocol could be different when varying the antibody concentration in order to get the optimum detection capability. Parameters such as longer incubation time and increasing the number of washing step could lead to further attachment of the antibodies on the CNTs. In addition, quantification of unbound antibodies in the conjugate solution could be useful in choosing proper antibody concentration for conjugation based on the desired detection performance.

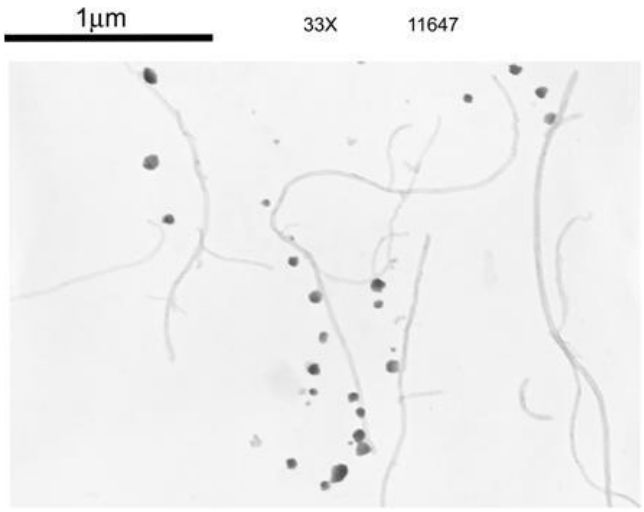

Figure 3.14 TEM image showing enhanced antibody conjugation with MWCNTs using 500 µg/ml antibody concentration.

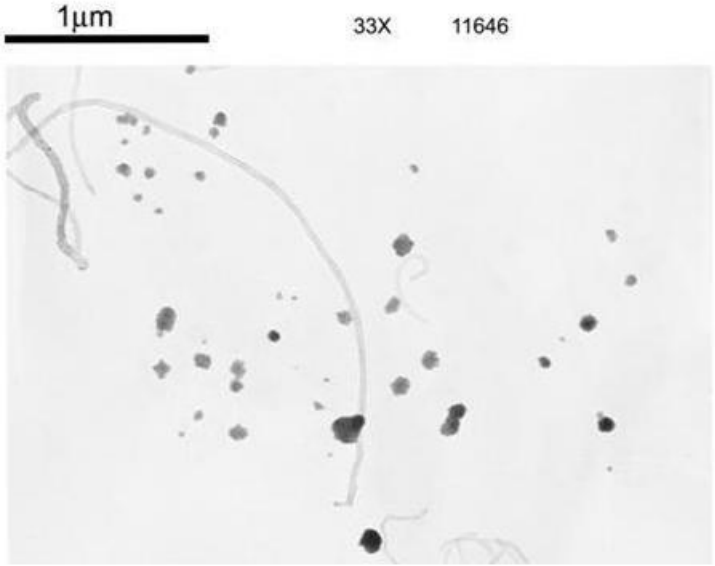

Figure 3.15 TEM image showing an increase in MWCNT-antibody conjugation and unbound antibodies using 1000 µg/ml antibody concentration.

3.7 Summary

The functionalization of multi-walled carbon nanotubes (MWCNTs) with surfactants and antibodies for immunosensing based on electrical measurements was conducted. A comparative study was conducted in uniform dispersion of MWCNTs using PVP, PEG, and DI water. The stability of the suspension was also investigated throughout the conjugation process using UV-Vis spectroscopy. Results show that the partial adsorption of PVP and PEG on the MWCNTs in non-covalent method was effective in improving the dispersion and stabilizing the suspension ((PVP was more effective than PEG) over different time periods. Conjugation of antibodies was also successfully obtained on the carboxylic group of the MWCNTs that were not covered by the surfactant. Human IgG was attached on the MWCNTs covalently through stable amide linkage. FTIR was implemented to successfully identify the modification of the MWCNT surface with PVP and human IgG.

Optimization of the MWCNT-antibody conjugation was carried out in order to maximize detection capability. The amount of PVP was reduced while maintaining the solubility exposing more binding site for the antibodies. The amount of antibodies used for conjugation was also increased ensuring that most binding sites on the CNT are occupied. Both optimization parameters were successful in enhancing the amount of conjugated antibodies. However, the conjugation protocol has to be modified or quantification of unbound antibodies has to be implemented in order to apply the parameters without limitations. Looking ahead, the

chemically functionalized MWCNT network provides quantitative immunosensing capability based on simple and direct electrical measurements.

CHAPTER 4

CARBON NANOTUBE-BASED LATERAL FLOW IMMUNOASSAY

4.1 Introduction

This chapter describes an immunoassay technique using CNTs as a sensing label for enhanced signal detection. The immunoassay technique is applied on lateral flow (LF) system for the first time, where the CNT labels provide conductimetric and colorimetric detection for quantitative and qualitative analysis of binding reactions. The remarkable electrical conducting properties of CNTs coupled with high affinity and selectivity of antibodies provides sensitive immunosensing capability. The developed CNT functionalization protocols for aqueous solubility and antibody conjugation, as discussed in Chapter 3, provides the capability of immunosensing in this chapter.

The LF system is composed of porous membranes for immobilization of capture molecules and sample transport by capillary action. As a result of specific binding reaction, the conjugated MWCNTs form a conducting network at the capture zone and allow conductance measurement corresponding to the captured analyte. Competitive and sandwich immunoassay formats are demonstrated. This detection mechanism combined with the LF system is simple, rapid, and inexpensive immunosensing suitable for point-of-care diagnostics.

4.1.1 Lateral Flow Immunoassay Protocol

Lateral flow (LF) immunoassay is one of the most successful point-of-care diagnostic tools commercially available for detecting various health and environmental agents [117-122]. A LF immunosensor is composed of a porous membrane for both immobilizing biological receptors and transporting sample reagents. The porous membrane drives the sample flow by

capillary action without external flow control. Sample reagents are transported in the lateral direction through the membrane and are captured by the biological receptors immobilized at the capture zone. LF immunosensors are simple to use, low-cost, rapid, and portable with relatively long shelf life. Examples of LF diagnostics include home pregnancy tests, detection of drugs of abuse, and diagnosis of infectious diseases. A LF immunoassay system has also been explored extensively for cardiac and cancer markers in the blood that require periodic monitoring and rapid diagnosis in timely treatment [123-124].

4.1.2 CNT as Sensing Label

Generally, LF immunosensors are based on optical detection where tagged particles or enzymes provide visible signal generation or amplification [125-127]. Several efforts have been made towards signal quantification using enhanced colorimetric labels or conducting materials such as phosphorescent nanoparticles [125], polyaniline [126], and polyaniline with colloidal gold [127]. Colorimetric techniques are often limited by low sensitivity while fluorescent techniques suffer from instability, photobleaching, activation step, and requirement for a complicated reader device. This chapter addresses such limitations by utilizing carbon nanotubes (CNTs) as a labeling material for direct electrical signal measurement. Compared to CNTs, other conducting materials such as colloidal gold and polymer nanowires do not possess the unique material properties suitable for surface functionalization or maintain high electrical conduction after binding reaction [72, 127].

4.2 CNT-Based Lateral Flow Immunoassay

4.2.1 Detection Principle

The LF immunoassay detection protocol for quantitative determination of binding reaction using CNT labeled antibody in competitive format is illustrated in Figure 4.1. MWCNTs are conjugated with human immunoglobulins G (IgG) to bind with Protein A immobilized on the immunostrip at the capture zone. The immunoassay system is composed of nitrocellulose membranes with sample application and absorption pads for transporting sample reagents in lateral direction by capillary force. The binding reaction between human IgG and Protein A is traced by a visible colorimetric signal generated by the MWCNT labels trapped at the capture line. The MWCNT network along the capture line also exhibits conductance difference corresponding to the amount of binding in aqueous environment.

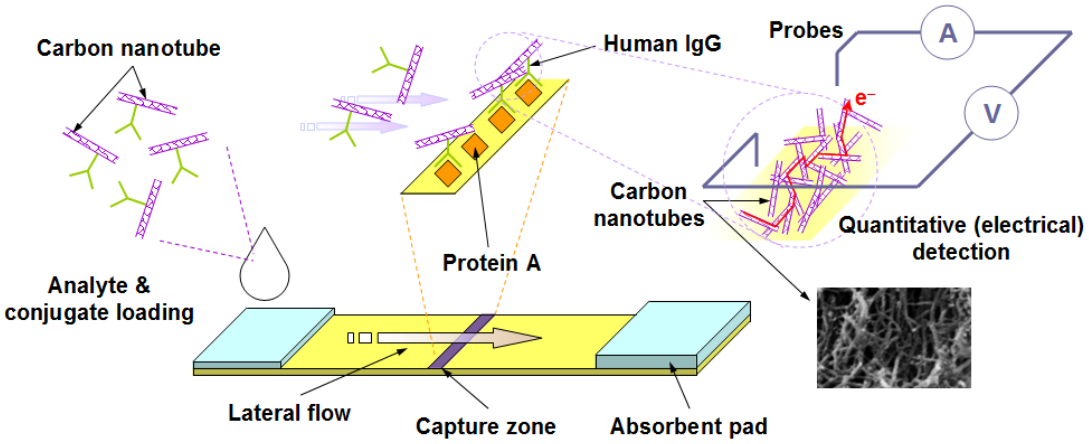

Figure 4.1 Detection principle of the CNT-labeled immunosensor for quantitative lateral flow diagnostics in competitive format.

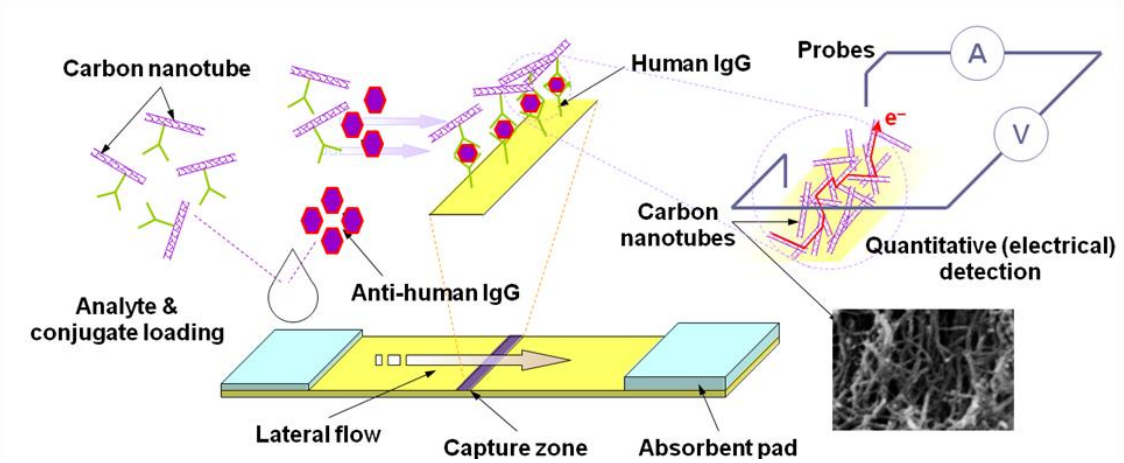

Figure 4.2 Detection principle of the CNT-labeled immunosensor for quantitative lateral flow diagnostics in sandwich format.

For sandwich immunoassay, human IgG is first immobilized at the capture zone to bind with the anti-human IgG that is applied to the LF immunostrips. The binding reaction is indicated by MWCNT labels that are attached to secondary human IgG providing colorimetric and electrical signals. The CNT-based detection principle for sandwich LF immunoassay is illustrated in Figure 4.2. In both immunoassay formats, blocking schemes are implemented to insulate the surface of the CNTs and the LF immunostrips from unwanted binding.

4.2.2 Materials and Reagents

Carboxylated MWCNTs (Purity > 95 wt%) were obtained from Cheaptubes, Inc., (Brattleboro, VT). Hi-flow Plus nitrocellulose membranes (HF13502), glass fiber pads, cellulose membranes, and a supporting card for lateral flow assay were obtained from Millipore (Bedford, MA). Protein A suspended in solution was obtained from BioVision, Inc., (Mountain View, CA). Purified human immunoglobulin G (IgG, 6.2 mg/ml) suspended in 0.01 M sodium

phosphate (0.15 M NaCl, pH 7.4) was obtained from Sigma-Aldrich (St. Louis, MO). Polyvinylpyrrolidone (PVP, MW 10,000), bovine serum albumin (BSA), Tween-20, glutaraldehyde, and 2-(*N*-morpholino)ethanesulfonic acid (MES) were from Sigma-Aldrich. 1-(3-(dimethylamino)-propyl)-3-ethylcarbodiimide hydrochloride (EDC) and N-hydroxysulfosuccinimide (Sulfo-NHS) were obtained from Thermo Fisher Scientific, Inc. (Rockford, IL). All immunoreagents were diluted in pH 7.4 phosphate saline buffer (1X PBS) unless otherwise noted.

4.2.3 Modification of MWCNTs

Uniform dispersion of the MWCNTs was critical to achieve proper surface functionalization with antibodies as discussed in Chapter 3 and also to efficiently flow the samples through the porous membrane. In order to prepare the carbon nanotubes and accelerate the dispersion 1.5 mg of carboxylated MWCNTs were sonicated in 2 ml of deionized (DI) water with 0.6 mg of PVP. Following the dispersion procedure, the MWCNTs were reacted with coupling agents to attach antibodies through stable amide linkage. The coupling agents adsorbed on the surface of the MWCNTs not occupied by the PVP. This was carried out by mixing the MWCNT solution with 1 ml of EDC (0.4 M) and Sulfo-NHS (0.1 M) in pH ~ 6.0 MES buffer. The solution was left to react for 30 minutes at room temperature. The mixture was centrifuged at 13,000 rpm for 3 minutes with PBS buffer and the supernatant was discarded. The washing and re-suspending process was repeated several times to remove excess reagents. Then, 100 µl of the human IgG solution at 200 µg/ml concentration in PBS buffer was added to the MWCNT suspension. The mixture was washed and several times to remove unbound human IgG, and the resulting MWCNT-antibody conjugate solution was kept at 4ºC until use.

4.2.4 Preparation of the LF Strips

A nitrocellulose membrane was utilized as a detection pad with designated capture site for immobilizing capture molecules. Fiberglass for a sample application pad and cellulose membranes for absorbing excess reagents were placed over the nitrocellulose membrane at the two ends of the immunostrip. The LF immunosensor was prepared using the following procedure. First, a nitrocellulose membrane was saturated in 10% (v/v) methanol in deionized (DI) water for 30 minutes to remove any residues and dried in air at room temperature. The membrane was then treated with 0.5% (v/v) glutaraldehyde solution to strengthen the binding of Protein A or human IgG on the nitrocellulose membrane and rinsed several times with DI water. After drying, the membrane was ready for antibody immobilization. For competitive assay, Protein A was diluted in phosphate buffered saline (PBS) to 1 mg/ml and dispensed on the nitrocellulose membrane to form the capture line by dragging a dispenser across the capture line with manual control. The membrane was dried at room temperature before being incubated with 2% BSA and 0.05% (v/v) Tween-20 in PBS for 1 hour to block the membrane from making unwanted binding. The membrane was rinsed several times with PBS containing 0.05% (v/v) Tween-20 to remove the excess blocking reagent and left to dry at room temperature. For sandwich assay format, similar procedures were followed to immobilize human IgG in 1 mg/ml concentration at the capture zone.

4.2.5 Preparation of LF System

The LF immunosensor was constructed by assembling the sample application pad, the lateral flow membrane, and the absorbent pad on a support card that was cut into 7 mm width strips. In the lateral flow immunosensor, sample solutions were delivered to the capture line and

excess solutions flowed to the absorption pad along the lateral direction at the end of the membrane. For the competitive assay configuration, when the sample solution containing the MWCNT-IgG conjugate was applied to the sample application pad, the sample moved across the capture line where the immobilized Protein A made binding with the MWCNT conjugated human IgG. For the sandwich immunoassay, the anti-human IgG was caught between immobilized primary human IgG and MWCNT labeled secondary human IgG. As a result of binding, the human IgG bound MWCNTs formed a visible line with random agglomeration across the capture zone in both cases.

The binding between the immobilized Protein A and MWCNT labeled human IgG was examined using scanning electron microscopy (SEM). Figure 4.3 shows SEM pictures of the nitrocellulose membrane with lower and higher carbon nanotube coverage corresponding to the amount of binding at the capture line. The visible capture line formed by the MWCNT network was subjected to electrical measurements for quantitative analysis. Measurements were taken in the form of resistance, where conductance is the reciprocal of resistance. Prior to conjugate sample application, the resistance across the capture line with immobilized Protein A was measured to be infinite. After full signal development, the resistance across the conducting networks of the MWCNTs varied corresponding to the amount of antibody binding indicated by the MWCNT labels.

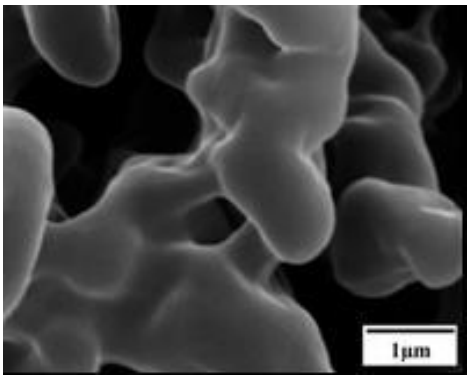

(a)

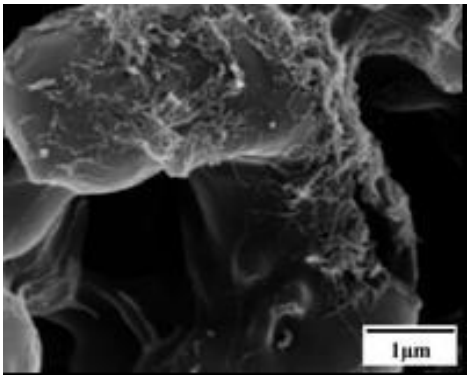

(b)

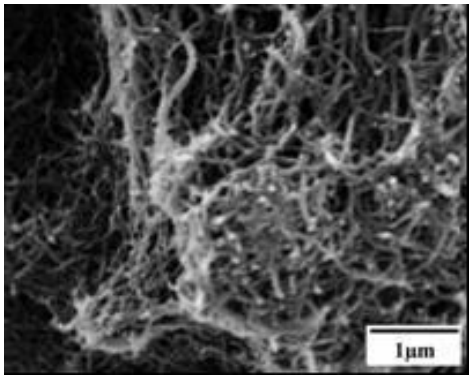

(c)

Figure 4.3 SEM images of the capture zone (a) before sample application (b) lower CNT coverage due to a smaller number of binding, and (c) higher CNT coverage due to a larger number of binding.

4.3 Electrical Measurement System

4.3.1 Integrated Electrodes

A soft electrode system was developed to measure the electrical signal on the immunosensors. The electrode system is important in order to obtain stable and repeatable measurements with minimized contact resistance. The electrode contact force was controlled by the displacement of compression springs applying uniform pressure to the strips. This electrode

system was especially useful to make electrical contact on soft materials such as the nitrocellulose membrane used for the LF strips. The first design of electrical measurement setup that was used in this experiment is shown in Figure 4.4. Top and bottom poly(methyl methacrylate) (PMMA) plates were drilled using a micromilling machine to create holes for stainless steel probes with 0.5 mm in diameter as shown in Figure 4.5(a). Two pieces of metals were attached directly on top of the electrodes using silver conductive epoxy for electrical contact. On the bottom plate, a groove was made to hold the immunostrips. The electrodes were aligned on top of the capture zone, where the CNT network forms in order to obtain electrical measurements as shown in Figure 4.5(b).

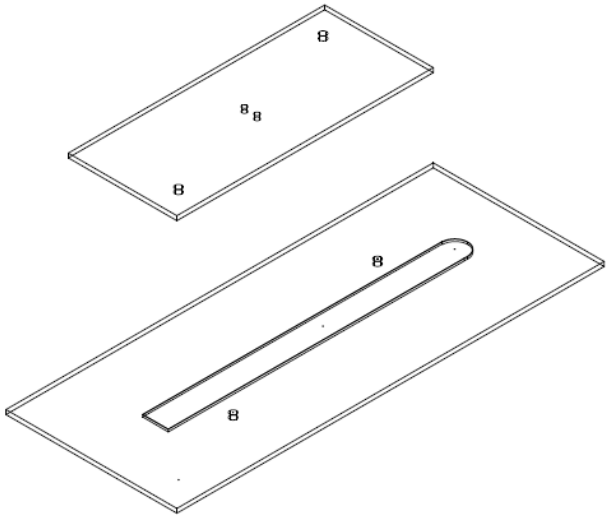

(a)

Figure 4.4 Design of integrated electrodes (a) 3D view of the top and bottom plates and (b) the top plate with the two holes for inserting the electrodes and bottom plate with a groove to hold the immunostrips (Figure 4.4 con'd).

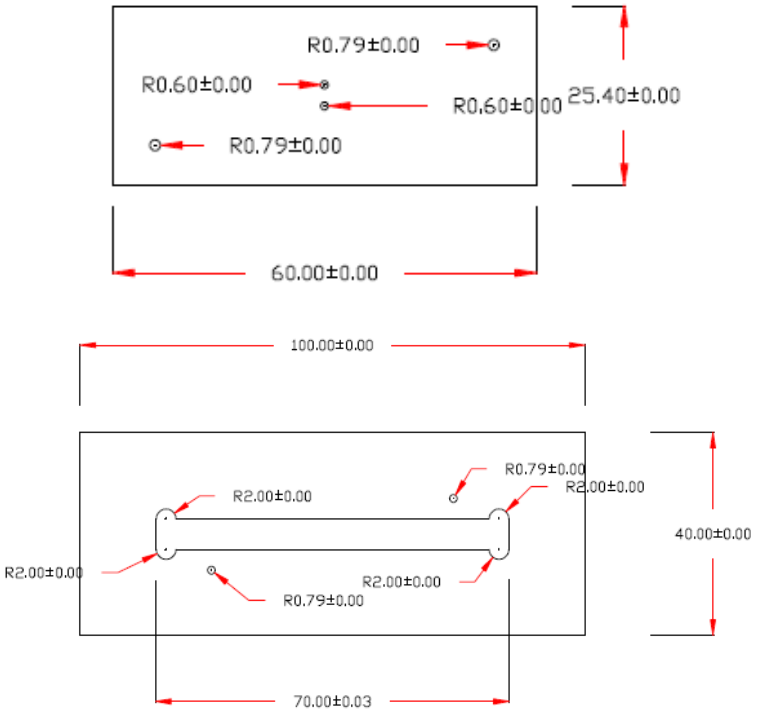

(b)

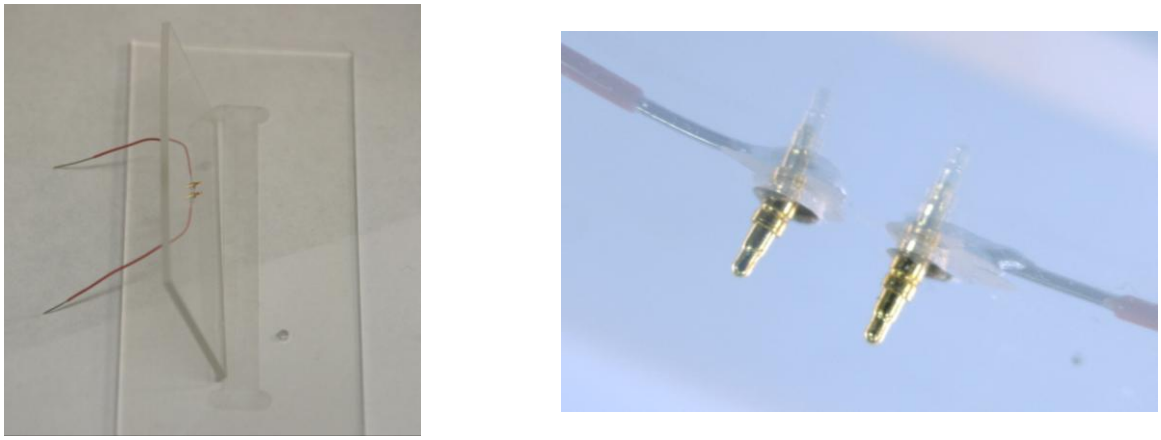

(a)

Figure 4.5 (a) Polymer plates with integrated electrode showing a close up image of the electrodes (b) electrical measurement and data recording setup for the LF immunosensors using the integrated electrodes (Figure 4.5 con'd).

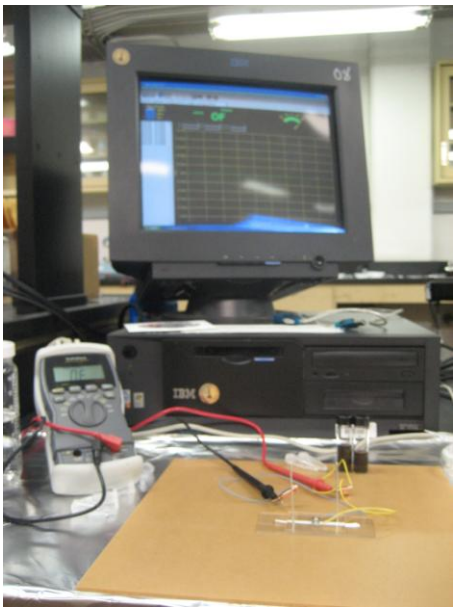

(b)

4.3.2 LF Cartridge System

A second LF cartridge was developed in order to provide improved packaging of the immunostrips for portable and convenient testing setup. The cartridge was fabricated using 3D printing/molding machine (Dimension 3-D/stratasys). The 3D model of the cartridge is shown in Figure 4.6(a). The top cover holds the sample inlet and space for the insertion of the electrodes while the bottom cover holds the immunostrip. The alignment marks on both covers provide proper placement of the electrodes at the capture zone when the cartridge closes. Dimensions of the LF cartridge system in millimeters are shown in Figure 4.6(b). Electrical contacts were made on the cartridge using silver conductive epoxy as shown in Figure 4.6(c). For signal measurements, a multimeter could simply be attached to the cartridge as shown in Figure 4.6(d).

In addition, the cartridge is inexpensive and simple to fabricate making it suitable for mass production of point-of-care test and affordable to the developing world.

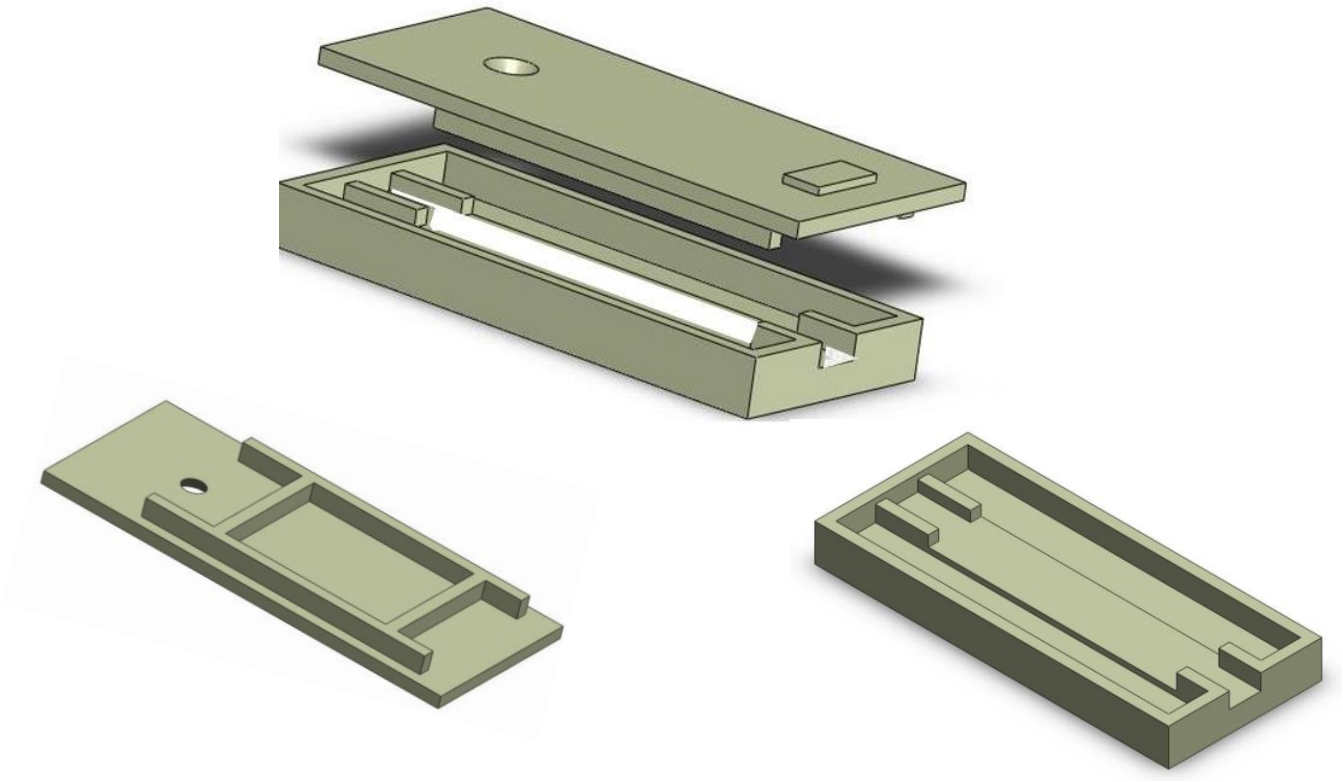

(a)

Figure 4.6 The developed LF cartridge (a) the 3D model of the cartridge and the top and bottom covers when opened (b) the dimension of the cartridge (c) the fabricated cartridge, and (d) demonstration of simple electrical measurements on the LF cartridge (Figure 4.6 con'd).

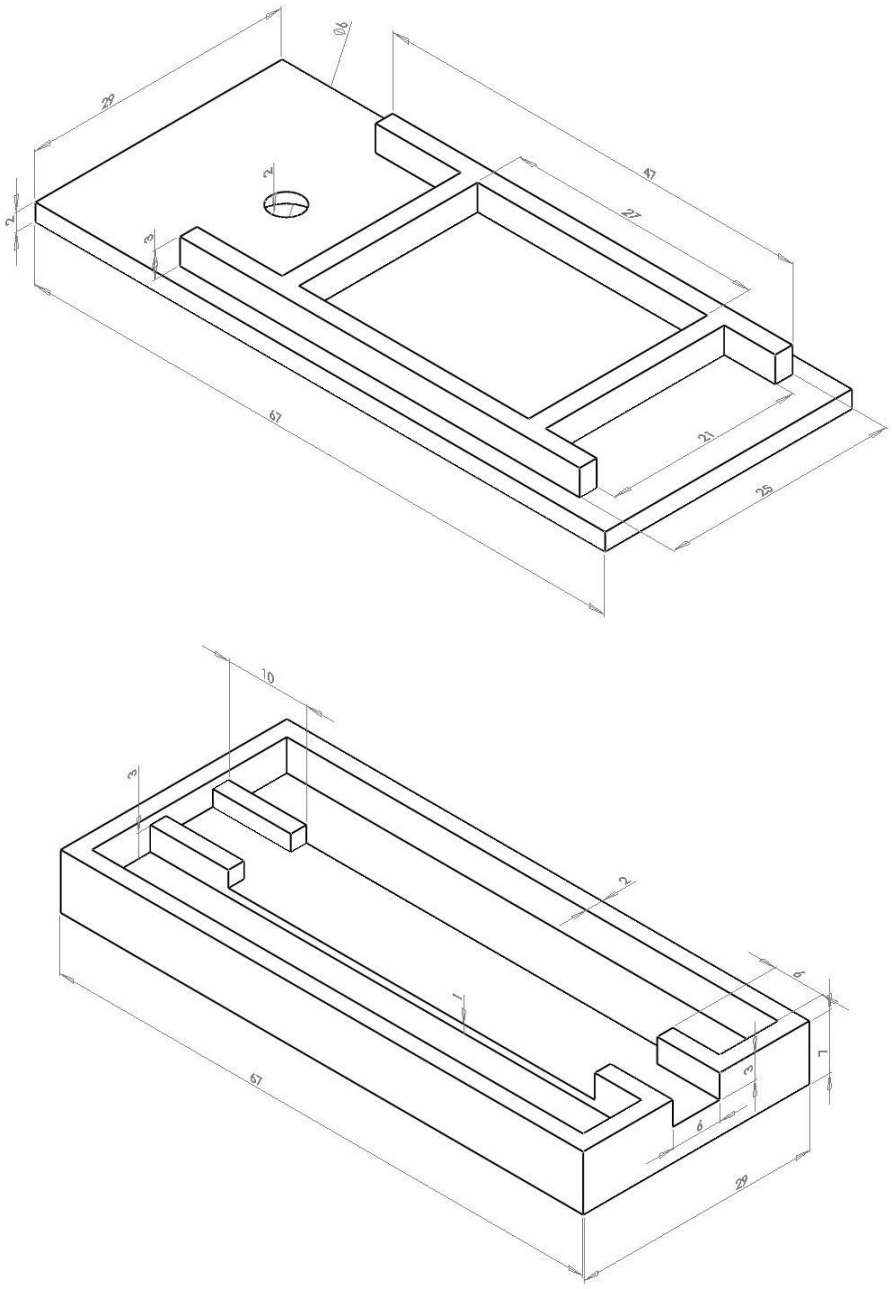

(b)

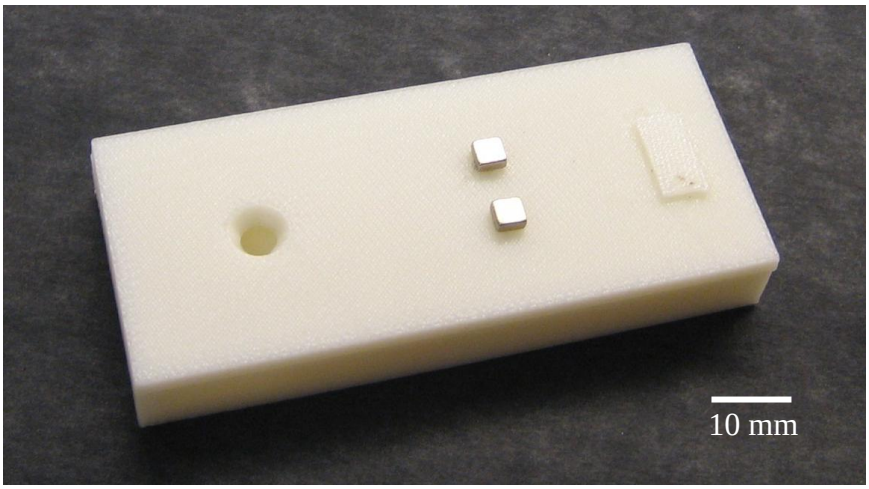

(c)

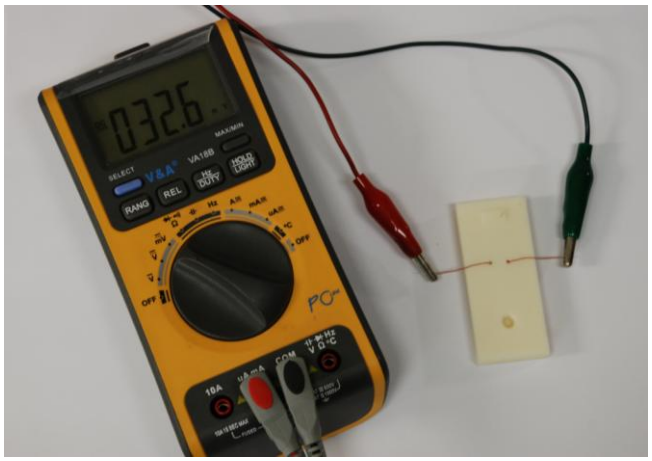

(d)

4.4 Results and Discussion

4.4.1 Non-specific Binding

CNTs have natural affinity to biomolecules that is not desired in immunoassay since it could lead to false signaling [48]. Blocking schemes are required to prevent the non-specific interaction. In this experiment, non-specific binding was investigated by running control tests with partially and fully functionalized MWCNTs in a competitive immunoassay format. First, a sample solution containing MWCNTs treated with PVP only was applied to the Protein A immobilized lateral flow immunostrip. In this situation, unwanted binding was evident between the carbon nanotubes and the immobilized Protein A as shown in Figure 4.7(i). This unwanted binding could have been caused by the interaction between the exposed surface of the MWCNTs

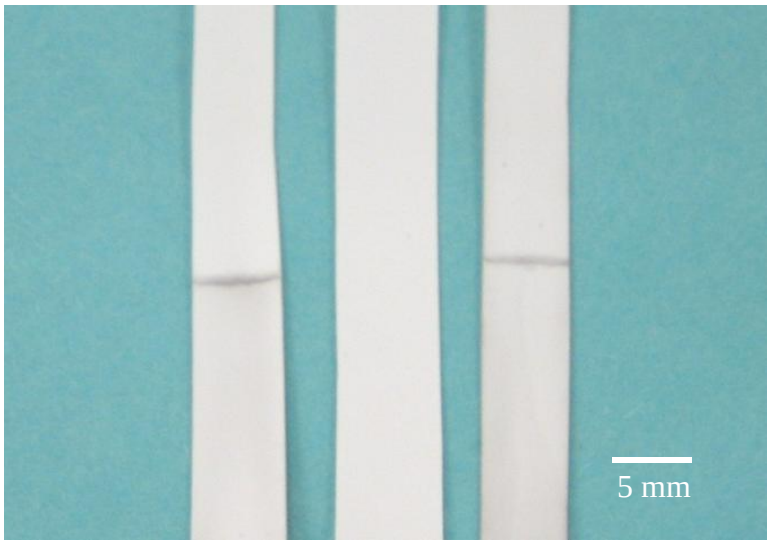

Figure 4.7 Non-specific adsorption on the nitrocellulose membrane (i) carbon nanotubes partially coated with PVP bound to Protein A by non-specific adsorption which must be addressed to avoid false signal (ii) almost no carbon nanotubes at the capture line showing that the surface of carbon nanotubes were completely covered eliminating non-specific adsorption after the application of crosslinking agent, EDC, and Sulfo-NHS, and (iii) binding between the MWCNT-IgG conjugate and immobilized Protein A.

and the immobilized Protein A. Next, the crosslinking agents, EDC and Sulfo-NHS, were added to the PVP treated CNTs. When this solution was applied to the immunostrips, no binding reaction was observed between the MWCNTs and the immobilized Protein A as shown in Figure 4.7(ii). This could be due to the fact that the surfaces of the MWCNTs were completely covered by the PVP and the amide coupling agents leaving no unoccupied sites for non-specific binding. For comparison, the binding between IgG and Protein A was tested by applying the MWCNT-IgG conjugate solution to the immobilized Protein A on the LF immunostrip. The capture line as shown in Figure 4.7(iii) indicates likelihood of specific binding between human IgG and Protein A.

4.4.2 Calibration of the LF Immunosensor

Conjugate solutions were prepared ranging from 0 to 200 µg/ml, and 50 µl of each solution was applied to the lateral flow immunostrips on which Protein A was immobilized at the capture line. The amount of binding between the applied conjugates and the Protein A was indicated by the corresponding intensity of the signal at the capture line as shown in Figure 4.8. The calibration curve was useful in determining the detection limit and linearity for the conjugate solution. For quantitative analysis of the binding reaction, the resistance (or conductance) across the capture line was measured for the immunostrips after the complete development of the visible signal at the capture line. As the concentration of the MWCNT-human IgG increased, the measured resistance decreased due to the electron transfer established by the carbon nanotubenetwork. Multiple replications of the immunostrips of same concentrations were tested and the measured electrical signals were found to be within range.

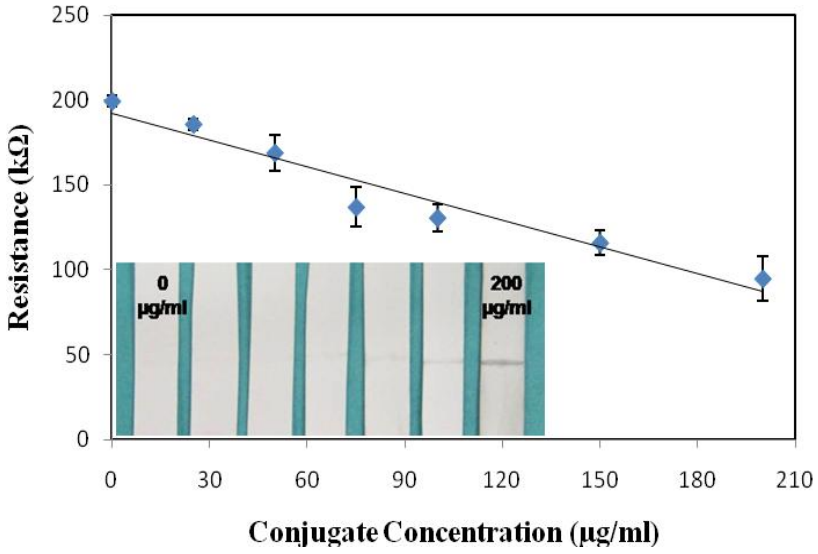

Figure 4.8 Calibration results using conjugate solutions of different concentrations. CNTs as label provided a quantitative electrical detection capability.

4.4.3 Competitive Immunoassay

Human IgG solutions of varying concentration ranging from 25 to 200 µg/ml as a target analyte were added to the MWCNT-IgG conjugate solution to demonstrate the performance of the immunosensor. The concentration of the conjugate solution was 200 µg/ml and 50 µl of the mixed sample solution was applied to each device. When the solution was applied to the immunostrip, the target human IgG competed with the conjugate for binding site at the capture line. As the concentration of the target analyte increased, it occupied more binding sites limiting the binding reaction between the conjugated human IgG and the Protein A. This produced a detection signal across the capture line varying in color intensity as depicted in Figure 4.9(a).

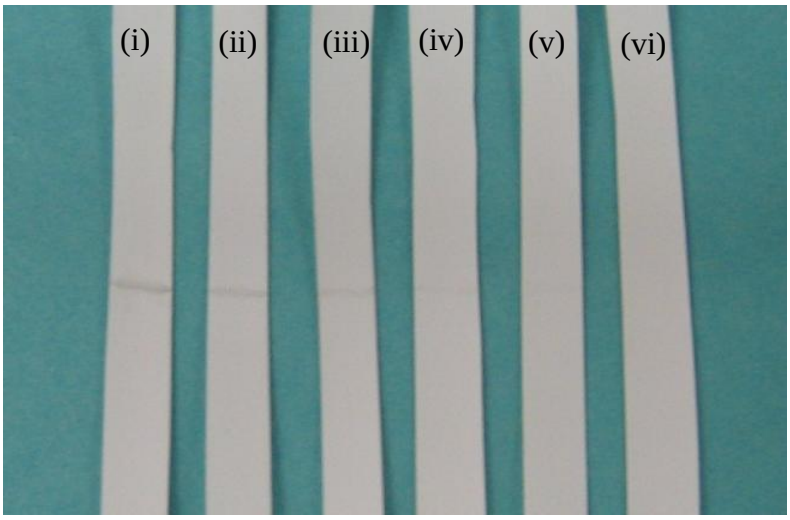

(a)

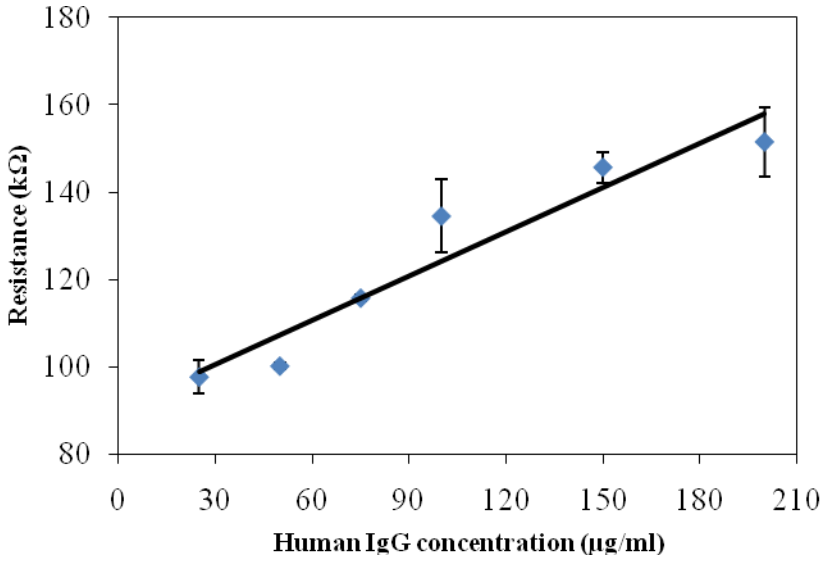

(b)

Figure 4.9 Competitive immunoassay results (a) lateral flow immunostrips tested with target concentrations in µg/ml (i) 25, (ii) 50, (iii) 75, (iv) 100, (v) 150, and (vi) 200 (from left to right) and (b) the measured electrical resistance of the capture lines.

The capture lines became lighter in color intensity with increasing target human IgG captured by the Protein A. This could be explained by the binding of the free target human IgG with Protein A limiting the amount of CNT network at the capture line. This detection signal was also subjected to electrical measurement corresponding to the amount of binding between the target human IgG and Protein A as shown in Figure 4.9(b). For quantitative analysis, the conductance was measured across the capture line where the resistance increased or the conductance decreased with increasing concentration of the target human IgG. The graph in Figure 4.9(b) shows the measured results at specific concentrations. Although the capture lines became visually indistinguishable with increasing concentration of target human IgG (100, 150, and 200 μg/ml), the measured electrical conductance clearly showed variation providing quantitative detection. Since the capture zone was placed at a predetermined location, visibility of the signal was not an issue for positioning the electrodes. The contacting force was kept uniform throughout the experiments to maintain constant contact resistance. However, fluctuation of the signals upon contact was often observed and signals had to stabilize before conductance measurement was obtained.

Overall sensitivity of the demonstrated detection techniques could be varied by changing the sample volume and detection time. In this experiment, the detection signals at the capture zone were saturated in 15 minutes after applying 50 μl of sample solution for all concentrations. For the calibration and competitive results, the conductance measurements were obtained within a fixed time interval of 3 minutes corresponding to signal stabilization. Consequently, the mean values with relative standard deviation were calculated and plotted for the measured resistance

signals. The results and discussion above proves the viability of the detection mechanism as depicted in Figure 4.1.

4.4.4 Sandwich Immunoassay

For sandwich immunoassay, a MWCNT-human IgG conjugate solution of 200 µg/ml concentration was used. Preparation of the conjugate solution was slightly modified from the competitive format. The PVP amount used to disperse the MWCNTs was reduced to 25% to obtain less PVP coverage and more conjugated antibodies. Anti-human IgG was used as a target analyte to be captured between the immobilized human IgG (primary antibody) and the conjugated human IgG (secondary antibody). Prior to sample application, no signal through the immunosensor was measured due to infinite resistance between the electrodes. The immunosensors were also calibrated with buffer solution used to dilute the samples. Following calibration, varying concentration of the anti-human IgG solutions were prepared and applied to the immunosensors as illustrated on Figure 4.2. A total volume of 50 µl was applied to each immunosensor with 1:4 ratio of anti-human IgG solution to conjugate solution. 30 µl of washing buffer was also used to push the samples to the capture line, where unbound and excess reagents were transported to the absorbent pad. Detection of 0, 0.1, 0.5, 1, 5, 10, 20, 50 ng/ml of anti-human IgG was made successfully, where the 0 ng/ml was used as a blank solution. As the concentration of the anti-human IgG varied, different amount of CNT network was formed at the capture line. The conductance across the capture line was directly monitored in real-time producing signals corresponding to the amount of captured antigen. Figure 4.10 shows the measured resistance as a function of time. This figure includes the data points where the signal has stabilized indicating the saturation levels. One of the limitations experienced in the setup was

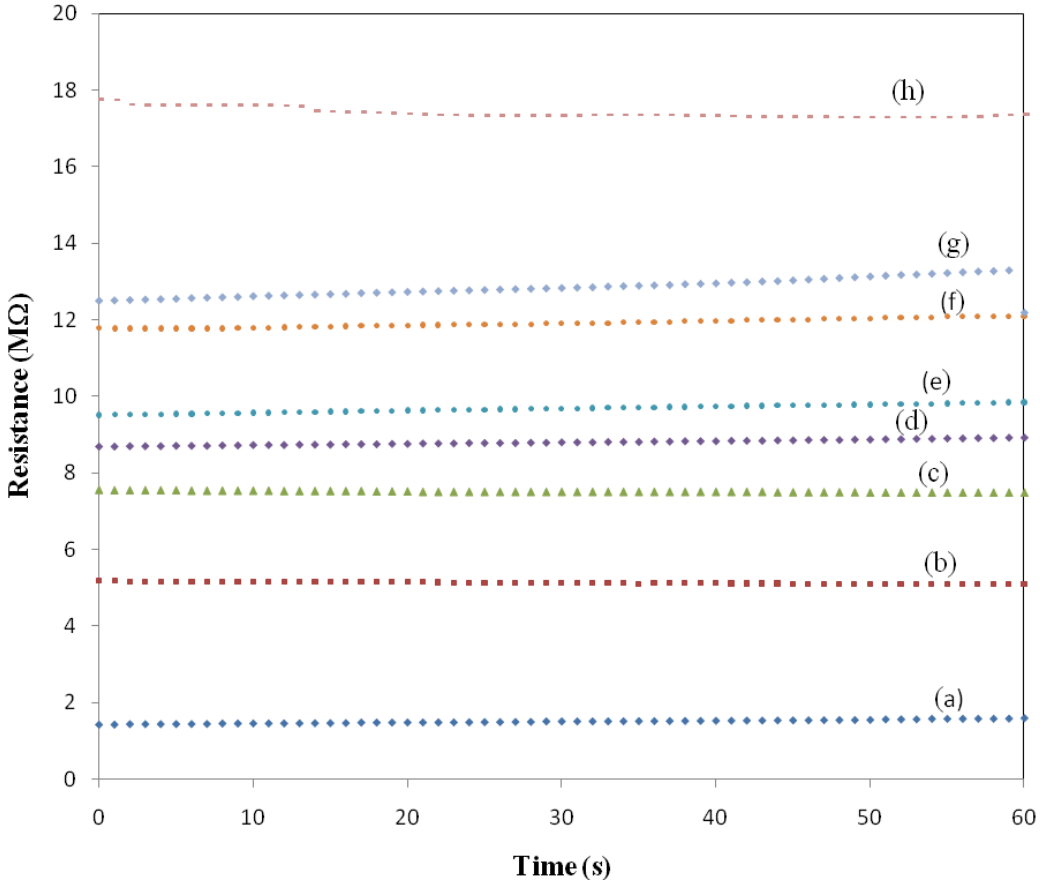

Figure 4.10 Plot of the resistance measurements as a function of time obtained for LF sandwich immunoassay with varying anti-IgG concentrations in ng/ml (a) 50, (b) 20, (c) 10, (d) 5, (e) 1, (f) 0.5, (g) 0.1, and (h) 0.

the saturation time that varied between different tests. This difference was due to the flow velocity that was difficult to control through the immunostrips, even though all parameters were kept consistent. In addition, fluctuation of the signal was observed, especially at the beginning of the measurements, even though the contacting force of the immunosensor device was kept constant.

The measured resistance values during one minute of signal saturation were taken to plot the calibration curve with the mean resistance values including error bars based on standard deviation as shown in Figure 4.11 and Table 4.1. The one minute duration was chosen in order to establish a relevant relationship among all the tests when comparing the conductance results. The measured resistance values increased with decreased analyte concentration. The tested immunostrips corresponding to the above target concentrations and signals are shown in Figure 4.12. The intensity of the lines at the capture zone corroborated the description aforementioned and demonstrates the practicality of CNT as sensing label for sandwich immunoassay on LF system.

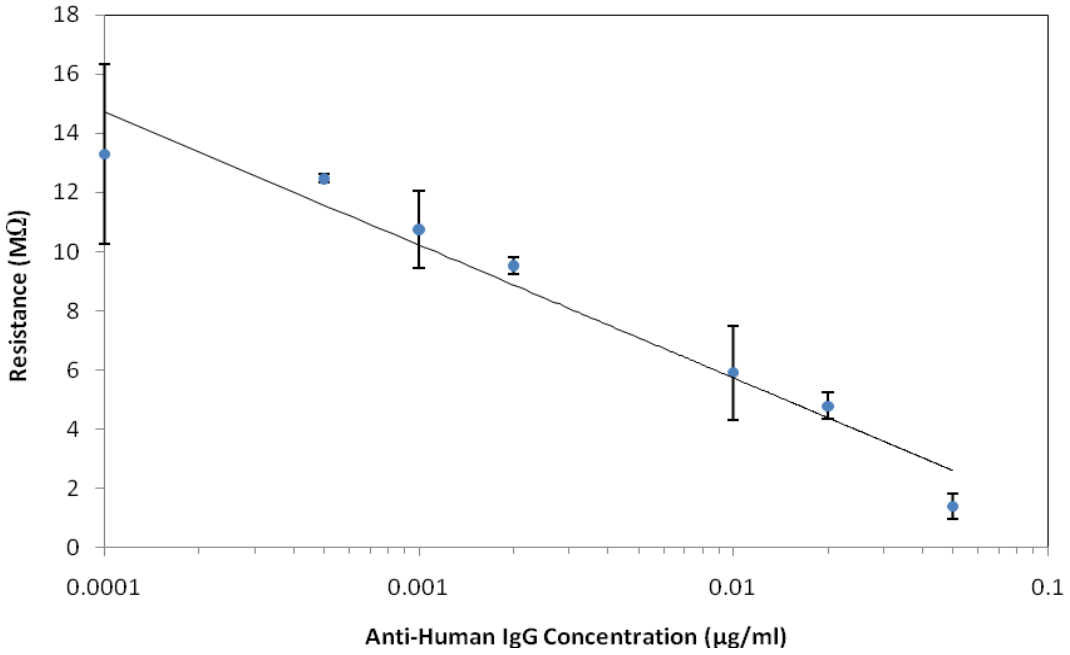

Figure 4.11 Calibration curve for anti-human IgG detection using LF sandwich immunoassay.

Table 4.1 Summary of the measured resistance values for varying anti-IgG concentrations for LF sandwich immunoassay.

Concentration (ng/ml)	Resistance (MΩ)	Standard Deviation
50	1.40	0.435
20	4.79	0.444
10	5.91	1.588
5	9.52	0.294
1	10.75	1.312
0.5	12.47	0.145
0.1	13.30	3.020
0	14.61	2.480

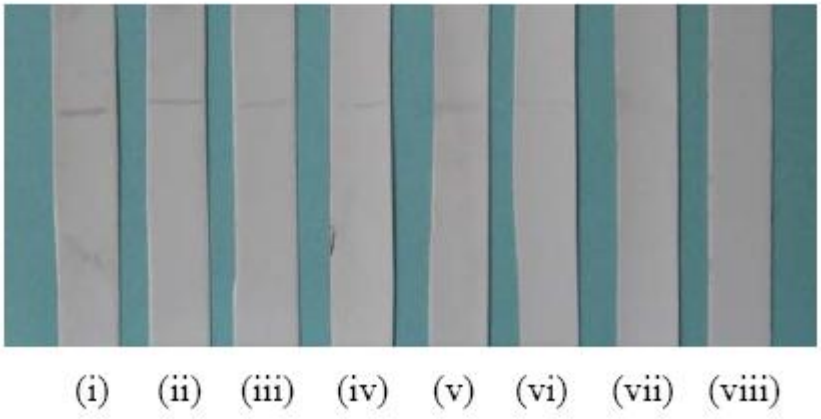

Figure 4.12 Lateral flow immunostrips demonstrating colorimetric detection capability in sandwich format for target concentrations in ng/ml (i) 50, (ii) 20, (iii) 10, (iv) 5, (v) 1, (vi) 0.5, (vii) 0.1, and (viii) 0.

For the low analyte concentration (ng/ml) tested in this work, the colorimetric signals obtained were difficult to quantify visually. However, distinct electrical measurements were obtained detecting anti-human IgG concentration below 1 ng/ml. Results show that lower

detection limits are possible, even though signals may take longer to stabilize as analyte concentration decreases.

4.5 Summary

The utility of CNT labels for sensitive immunoassay based on electrical detection was successfully demonstrated on LF system. Resistance of the MWCNT matrix formed at the capture zone was directly measured for conductimetric signal corresponding to low analyte concentration that otherwise would have been difficult to quantify based on colorimetric signals. Significant change in electrical resistance was observed for varying antigen concentrations and anti-human IgG concentration below 1 ng/ml was measured. The detection signals were measured using a conventional multimeter that is portable and easy to operate. The developed cartridge with the integrated electrodes also provided convenient packaging and testing apparatus for the immunostrips. The demonstrated CNT-based detection is simple, reliable, and inexpensive, which is suitable for point-of-care immunoassay devices.

One limitation of LF systems is precise flow control through the porous membranes. In this work, it was important to maintain the flow rate within a narrow range in order to fix detection time between the immunosensors. The flow rate was mainly determined by the capillary action of the porous (nitrocellulose) membrane. The results also suggest that obtaining higher sensitivity and lower detection limit (less than 1 ng/ml) is possible with the developed detection technique. However, further optimization of the immunosensor could be useful in increasing the efficiency of the devices. Automation of part of the LF system could be helpful in achieving these goals. For example, the manual formation of capture zone could be replaced by using methods such as inkjet printer, spraying, or liquid spotting.

CHAPTER 5

MICROFLUIDIC IMMUNOASSAY USING CARBON NANOTUBES

5.1 Introduction

This chapter reports the development of a microfluidic immunoassay using interdigitated array (IDA) microelectrode as the binding surface. Even though CNTs and IDA microelectrodes have independently been used for immunosensing applications, the concurrent utilization of CNT matrix and IDA microelectrodes have not been demonstrated prior to this work. The CNTs are used as a label, similar to the detection principle demonstrated in Chapter 4. However, microfluidic immunoassay using PDMS microchannel is developed in order to improve the flow control and influence the detection limit and time. Once sample is dispensed through the inlet, it is delivered to the reaction surface by passive control of capillary action. The capture antibodies are immobilized directly on top of the interdigitated array (IDA) microelectrode that is integrated within a PDMS microfluidic channel. As a result of binding, the CNTs form a conducting matrix across the IDA microelectrode for sensitive and continuous signal measurement. In addition, sample volume required to carry out the immunoassay detection is reduced due to the size of the microchannel. The fabrication technique and the detection principle of the on-chip immunoassay system in this chapter (as in the case for LF immunoassay) is simple, low-concentration, and disposable detection mechanism with a potential for a wide spread use of point-of-care tests. Dispersion and conjugation of MWCNTs was conducted using the developed methods descried in Chapter 3.

5.2 Microfluidic Immunoassay

The microfluidic technology has presented a new frontier in bioassay realm by integrating multiple functions. The miniaturization of fluidic channels and chambers into microscale allows the use of smaller sample volume, faster analysis time, and automation [128]. As a result of the improved parameters, sensitive, low cost, and reliable immunoassay devices with minimal human interference and errors have been developed [129]. In addition, the integration of analytical procedures within microchannels and microchambers has enabled the development of miniaturized analysis systems such as lab-on-a-chip (LOC) or micro total analysis systems (μTAS) [130]. These miniaturized systems have been studied extensively for applications such as protein detection, drug discovery, and clinical diagnosis. Immunoassays could benefit a great deal from advances in/of microfluidic systems for improved sensitivity and efficiency.

Advances in fabrication of microfluidic devices and components such as pumps, valves, and mixers have made immunoassay analysis faster with high detection capability [131]. Sample volume and flow rate can be precisely controlled in microfluidic system resulting in sensitive and accurate detection of antibody reactions [132]. Another important factor for immunoassay is cost. Sample and reagents for immunoassay are found in scarce amount and often come with high price. The reduction in size of devices cuts the overall cost, enabling high throughput immunoassay tests. In addition, small sample volume and integration of multiple functions decreases analysis time.

One major challenge for microfluidic system is to make it simple to use with minimized active component for reagent handling [129]. External flow control and incorporation of active component such as valves and pumps make the microfluidic device difficult to fabricate, complex to operate, and fragile. Especially, efficient immunoassay systems for point-of-care applications have to be simple to use, easy to fabricate from low-cost materials, and provide passive flow control [133].

5.3 Fabrication of Microfluidic Immunosensor

The mask fabrication for the microelectrodes was assisted by Edward Song, a collaborator and a PhD candidate. After the mask fabrication, conventional lithography and wet etching technique was used to pattern the IDA microelectrodes. The fabrication process is schematically illustrated in Figure 5.1. For patterning the electrodes a 2'' x 3'' glass substrates were used. Prior to metal deposition, cleaning of the glass substrates was carried out by soaking the glasses in trichloroethene (TCA) solution for 2 hours followed by a rinse using acetone, IPA, and DI water. After the cleaning and drying process, the substrates were placed in the oven overnight at ~ 200 ºC. Then, Cr/Au (50 nm/ 100 nm) layers were electron-beam deposited on the glass substrate at the Center for Advanced Microstructure and Devices, (CAMD) (Baton Rouge, LA). For the fabrication of the IDA microelectrodes, positive photoresist, S1805 (Shipley Co., Marlborough, MA) was first poured on the glass substrate. The PR was first spin coated at 3200 rpm for 30 seconds, and then the speed was ramped up to 4000 rpm for 30 more seconds resulting in a thin layer of PR with ~ 1 µm thickness. The substrate was transferred to a hot plate that was preheated to 105 ºC and stayed on the hot plate for 1 minute. After the pre-bake, the substrates were cooled down to room temperature before loading into the Quintel UL7000-OBS

Aligner and DUV Exposure Station (Quintel Corp., Morgan Hill, CA) located at CAMD clean room. The substrate was then exposed to UV light at an intensity of 32.8 mJ/cm^2 for 3.3 seconds. The PR was then developed by immersing the substrates in developer, MF 351 (Shipley Co., Marlborough, MA) that was diluted to 1:5 with water for ~ 3 minutes. The progress of the PR development was continuously monitored while in the solution with the application of gentle agitation and use of optical microscope. The substrate was then rinsed with acetone, IPA and DI water, and dried using nitrogen gas before proceeding to metal etching. The Au etching process was carried out for ~ 5 minutes in a gold etching solution, GE-8148 (Transene Comp., INC., Danvers, MA) that was diluted 10:1 with water. Following gold etching, Cr was etched using Cr etching solution. The inspection, rinsing, and drying process were repeated after each etching process. The final step of the fabrication was to strip the PR using acetone, IPA and DI water. Nitrogen gas was used at the last stage to dry the IDA electrodes.

Figure 5.2 shows low-magnification optical image of the fabricated electrode layout for 20 μm electrode spacing. The electrode array had a fixed area of 1.2 mm^2 at the center of the layout and the number of electrode fingers varied for each device depending on the electrode spacing. The length of the electrodes was 1 mm, leaving 200 μm spacing between the tip of the fingers and the electrode contact. For electrical contacts to the electrodes, wires were attached to the contact pads using conductive silver epoxy. Insulation of the contacts was carried out using uncured PDMS after fully curing the conductive epoxy. The IDA design with 20 μm electrode spacing was chosen for further development. Optimization of the fabrication process resulted in consistent electrode dimensions and avoided over etching problem.

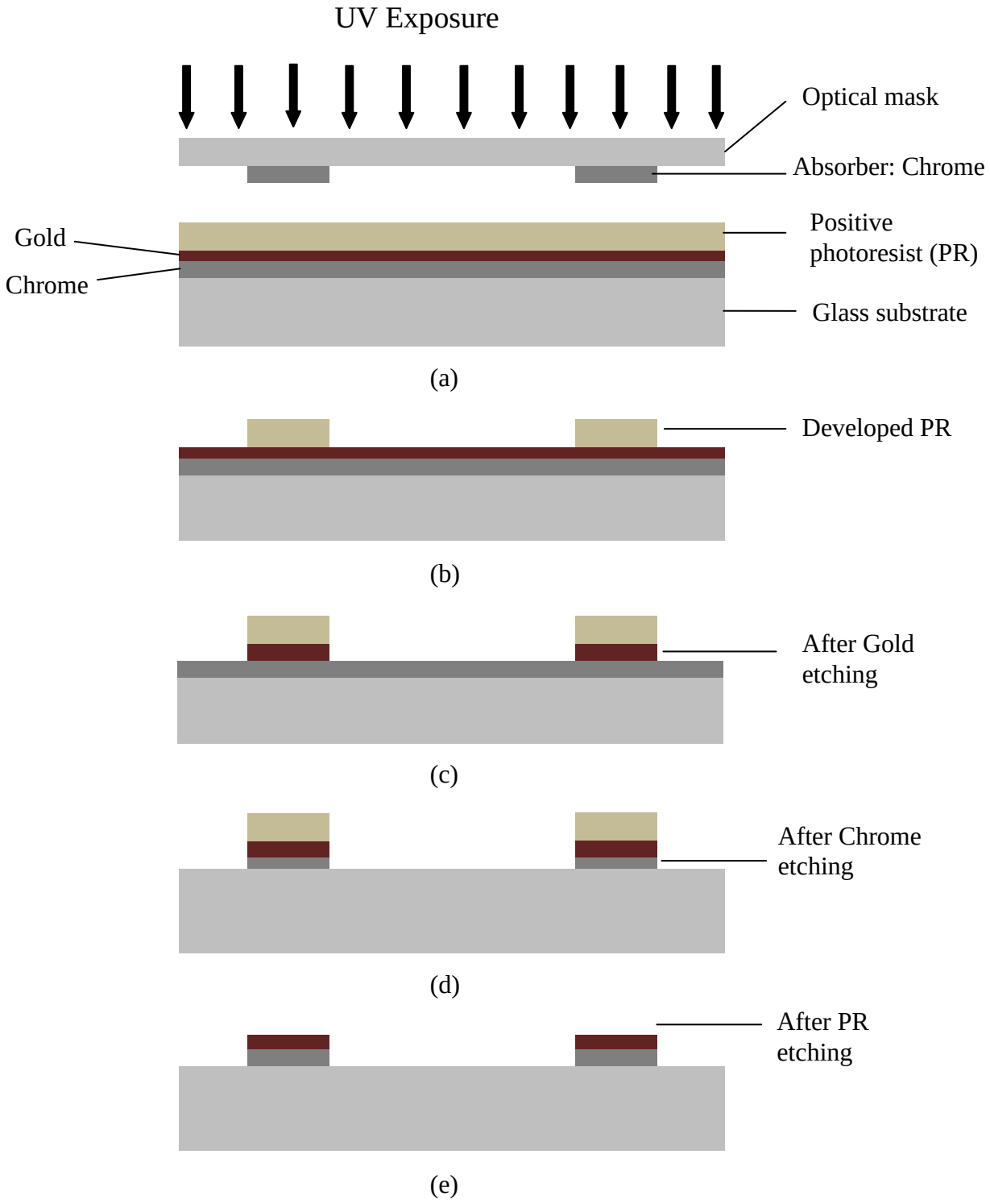

Figure 5.1 Fabrication steps of the IDA microelectrodes on glass substrate (a) UV exposure of positive photoresist on Cr/Au deposited glass substrate (b) development of positive PR in UV expose area (c) Au etching (d) Cr etching, and (e) PR etching.

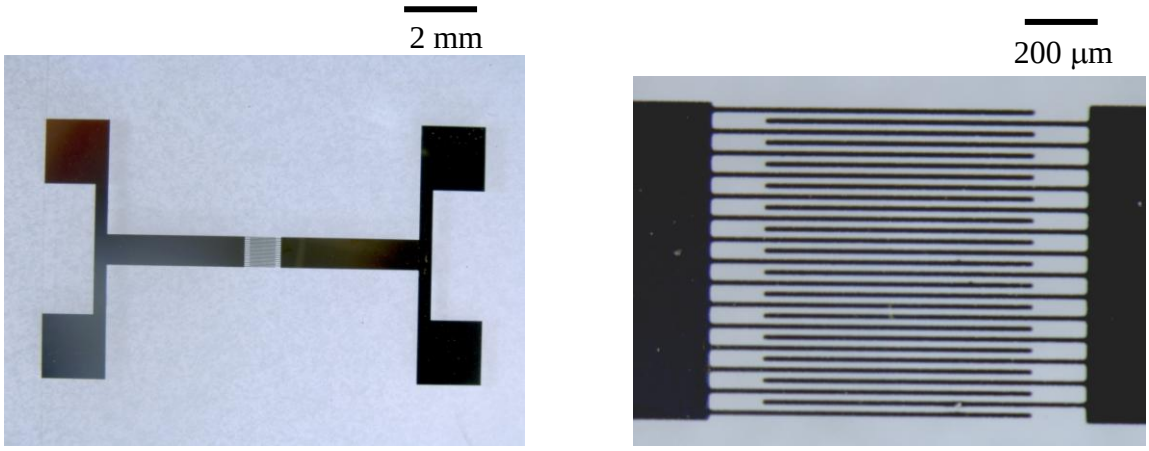

(a) (b)

Figure 5.2 Optical microscope images of the modified IDA microelectrodes (a) with 20 μm electrode width and spacing (b) closer view of the electrode fingers.

5.4 PDMS Microfluidic Device Fabrication

5.4.1 Fabricating PDMS SU-8 Mold Master

The mold master for the PDMS microfluidic structure was fabricated based on a negative photoresist process using SU-8 50 (MicroChem Corp., Boston, MA). The PDMS structures with 1 mm and 2 mm channel width were designed. The patterns for the mask were generated using AutoCAD for UV exposure. Figure 5.3(a) shows the detail design parameters for the PDMS microfluidic channel with 2 mm width. The UV lithography and fabrication process was conducted in clean room facility at CAMD. After fabricating the mask, the mold master was fabricated according to the procedures listed below and the fabricated mold is shown in Figure 5.3(b).

The steps in the procedures are:

1. Spin coat photoresist on 4" silicon wafer for 100 μm thickness:
    a. Spread at 500 rpm (20 s)
    b. Spin at 1250 rpm (30 s)

2. Pre-bake:
    a. Pre-heat hot plate to 25ºC and hold at 25ºC (30 min)
    b. Ramp from 25ºC to 65ºC, (30 min), hold at 65ºC (10 min)
    c. Ramp from 65ºC to 95ºC (30 min), hold at 95ºC (30 min)
    d. Cool down from 95ºC to 25ºC (2 hrs)

3. Measure the thickness of the SU-8 resist using digital caliber

4. Expose using 32.8 mJ/cm^2 exposure energy for 45 seconds

5. Post bake:
    a. Pre-heat hot plate to 25ºC and hold at 25ºC (30 min)
    b. Ramp from 25ºC to 65ºC, (30 min), hold at 65ºC (1 min)
    c. Ramp from 65ºC to 95ºC (30 min), hold at 95ºC (10 min)
    d. Cool down from 95ºC to 25ºC (2 hrs)

6. Patterns were developed using SU-8 Developer with continuous agitation inspection for ~ 10 minutes.

7. The mold master was cleaned using IPA, DI water, and blow dried with N_2 gas.

5.4.2 PDMS Casting

The PDMS was then prepared by mixing the base and curing agent 10:1 ratio. The PDMS was stirred well for ~ 2 minutes to ensure proper mixing. The mixture was left to degas at room temperature to remove the bubbles for ~ 20 minutes. Proper mixing and degassing are important steps in order obtain well cured PDMS structures. The PDMS mixture was then poured onto the SU-8 master that was placed on top of an aluminum foil cover. The PDMS was left to cure at room temperature for 12 hours. After curing, each PDMS structure was removed from the master by cutting the mold using a razor.

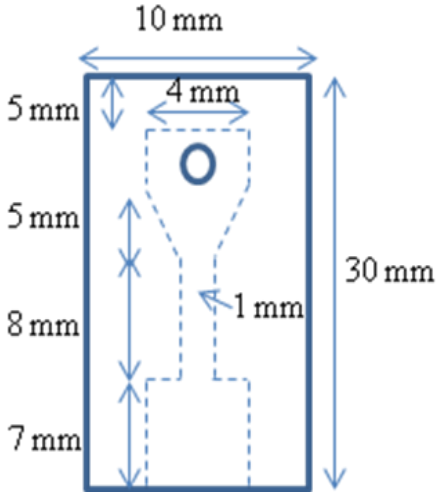

(a)

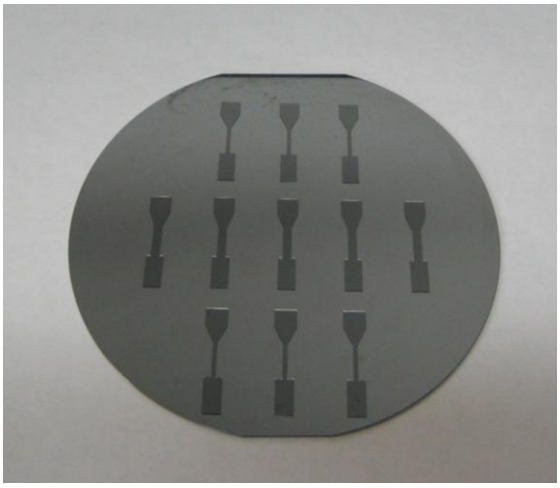

(b)

Figure 5.3 Fabricated PDMS microfluidic structure (a) dimensions of the microchannel with 1 mm (b) SU-8 mold master with 1 mm (top and bottom row) and 2 mm channel width (middle row).

5.4.3 PDMS Surface Treatment and Bonding

Surface treatment of the PDMS was investigated in regards to proper sealing of the channel structure with glass substrate and capillary action. The hydrophobic surface property of a cured PDMS slab was investigated before and after treatment with corona discharge. The corona discharge modifies the PDMS surface making it less hydrophobic similar to treatment with O_2 plasma. This effect could lead to improved sealing of the PDMS surface with a glass substrate and wetting properties when used in aqueous environment. In order to test the effect of the surface treatment, small droplet of DI water was dispensed at different spots on the PDMS slab and the contact angle was measured.

5.4.4 On-Chip Immunoassay Detection Mechanism

Diagram of the microfluidic immunoassay chip is shown in Figure 5.4. The glass substrate with IDA microlectrode is placed at the bottom of the device. The PDMS is placed on top of the glass substrate enclosing the IDA within the channel structure. Sample and reagents are applied through the inlet of the PDMS microfluidic structure using a pipette. The sample fills the channel, flows over the IDA microelectrode, and reaches the absorbent pad. The absorbent pad (a nitrocellulose membrane) with dimensions of 4 mm width x 20 mm length draws excess reagents flowing through the microfluidic channel. The flow rate of the sample and the total volume was mainly determined by the capillary action of the absorbent pad. Portion of the pad was inserted towards the end of the channel, squeezed between the PDMS and glass substrates. The remaining portion of the membrane was outside of the PDMS cover and it was exposed to air. Prior to actual immunoassay, preliminary tests were conducted with fluid samples to study the flow property through microfluidic chip. Sufficient sealing between the

PDMS and glass substrate is important in order to have proper flow through the channel. After sample application, the filling behavior and the flow speed within the channel based on the capillary force was investigated. The feasibility of immunoassay using CNT labels was also tested based on specific and non-specific binding on the IDA microelectrodes.

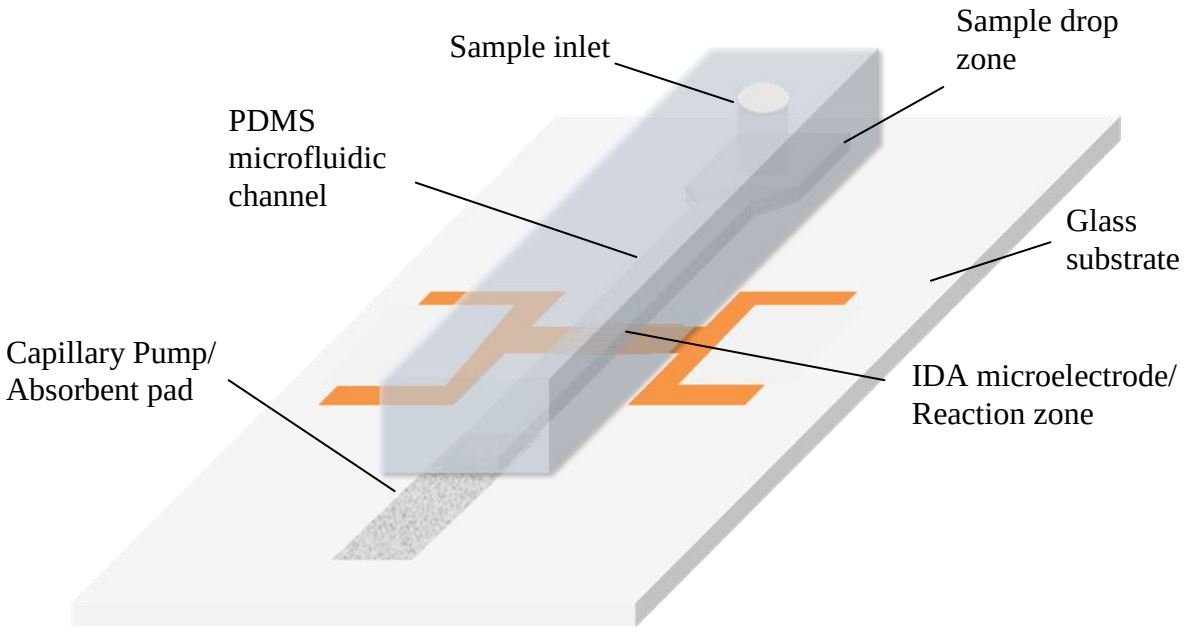

Figure 5.4 Design of the capillary-driven microfluidic chip.

5.5 Binding Test on IDA Microelectrodes

5.5.1 Specific and Non-specific Binding

Specific and nonspecific binding test was conducted based on sandwich immunoassay by applying sample and reagents directly onto the IDA microelectrode. The detection principle using CNT matrix as a label on the IDA microelectrodes can be seen in Figure 5.5. First, a small droplet containing capture molecules was dispensed on the IDA to cover most of the electrode area (Figure 5.5(a)). After immobilization of the capture molecules, a droplet of antigen was applied. Conjugate solution containing the antibody labeled CNTs was then dispensed onto the IDA (Figure 5.5(b)). Incubation time was allowed for interaction between capture molecules and conjugate solution. Finally, washing step was implemented to remove the unbound CNTs, where

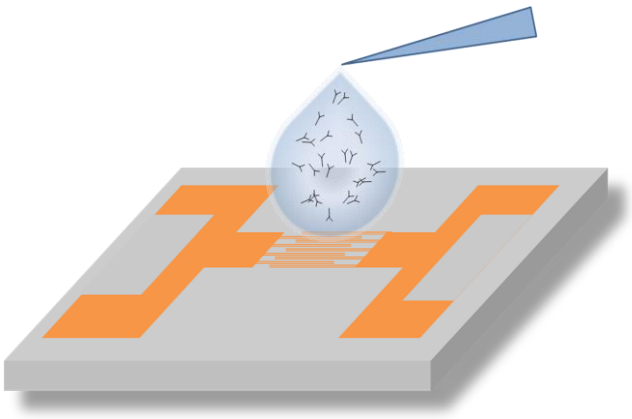

(a)

Figure 5.5 Illustrations of the detection principle using CNT labels on IDA microelectrodes (a) immobilization of capture molecule on gold IDA microelectrode (b) a cross-section of the IDA microelectrode during the application of conjugate solution, and (c) a cross-section of the IDA microelectrode showing the MWCNT network as a result of specific binding (Figure 5.5 con'd).

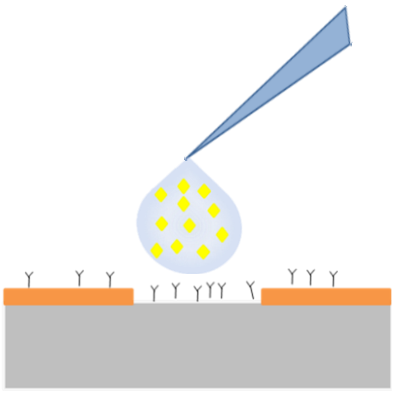

(b)

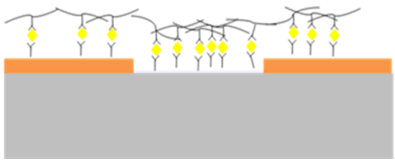

(c)

the bound CNTs formed a network bridging the electrodes (Figure 5.5(c)). The electrical signal was monitored during the binding reaction using the CNT labels through electrodes.

5.5.2 Materials and Reagents

Human IgG and anti-human IgG was used for the specific binding test on the IDA microelectrodes. MWCNT-human IgG conjugate solution was prepared using protocols discussed in Chapter 3. The concentration of the human IgG for conjugation was maintained at 200 µg/ml. Human IgG solution in 1 mg/ml concentration was used as a capture molecule and it was immobilized on the IDA electrode. For binding reaction, anti-human IgG in 200 µg/ml concentration was applied onto the capture molecule, followed by the MWCNT-human IgG conjugate. IDA microelectrode with 10, 20, and 40 µm spacing was tested. BSA in buffer solution was used as a control analyte for non-specific binding test with the human IgG on separate electrodes under similar experimental conditions.

5.5.3 Results of Binding Test

Results of the specific and non-specific test on the IDA microelectrode with 20 µm spacing is shown in Figure 5.6. The electrode with 20 µm spacing was chosen for the binding test because fabrication of the electrode with 10 µm spacing was not consistent and the 40 µm spacing was considered large for the application. The real-time dynamic current response flowing through the IDA electrodes were monitored, where the amount of antibody binding was indicated by the MWCNT labels. There was a significant increase in the electrical current response with the specific anti-human IgG binding compared to the non-specific binding of BSA. The variation in measured current signal was due to the difference in the amount of MWCNTs labels on the IDA microelectrodes as shown in Figure 5.7. The SEM images for the IDA microelectrode show that the resulting MWCNT network for specific binding test was denser compared to the non-specific binding.

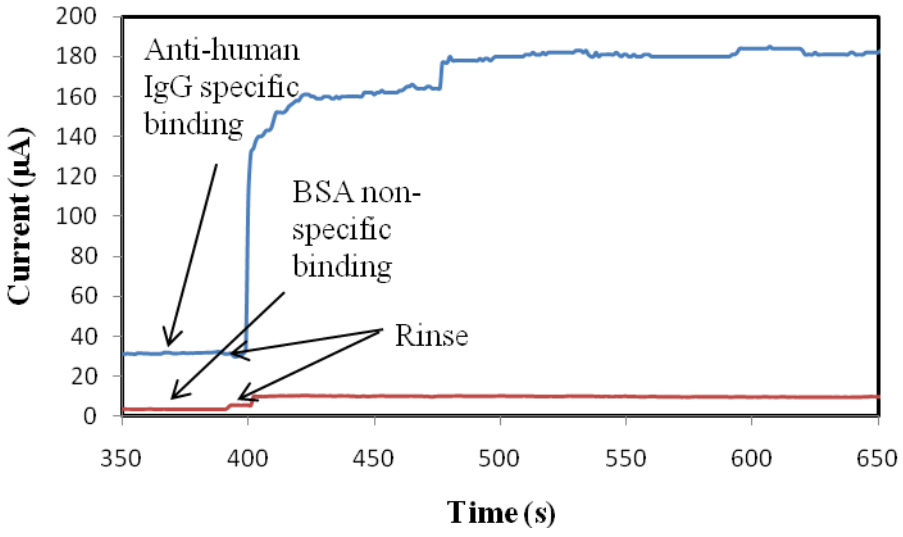

Figure 5.6 Dynamic electrical measurements as a result of specific binding with anti-human IgG and non-specific binding with BSA using MWCNT labels on IDA microelectrode.

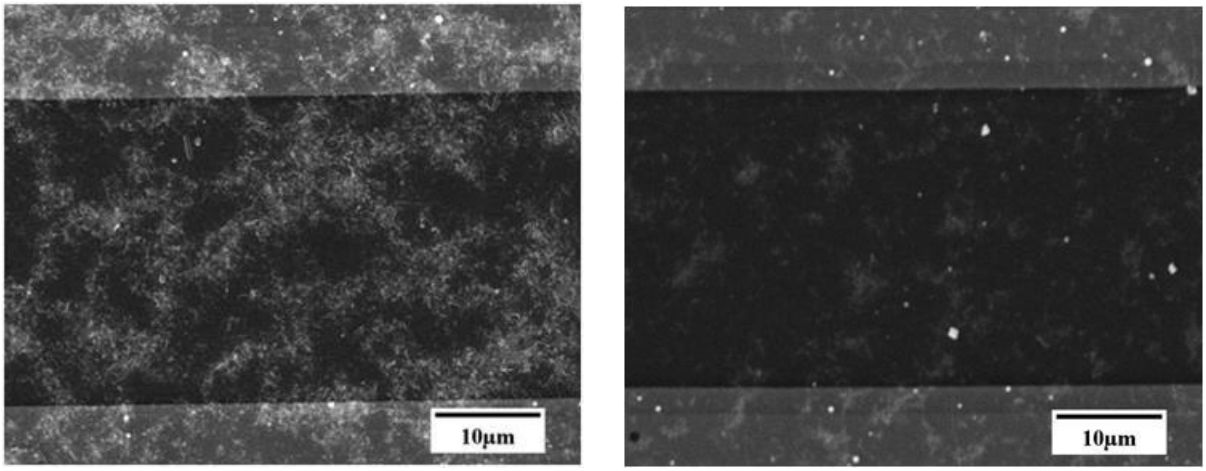

(a) (b)

Figure 5.7 SEM images showing the conducting network formed across the IDA microelectrode by the MWCNT labels (a) specific binding of anti-human IgG and (b) non-specific binding of BSA.

The specific and non-specific binding results demonstrated the feasibility of immunoassay using MWCNT labels on the IDA microelectrode for electrical measurements. The IDA microelectrode with 20 µm spacing was found to be the most suitable based on the results and other optimization protocols. Characterization of the sample delivery and rinsing step was difficult in this test, since they were conducted directly on top the IDA electrode. However, these problems are expected to be alleviated when implementing the microfluidic device for sample delivery.

5.5.4 Sealing and Alignment of PDMS Microfluidic Channel

The contact angle measurement for a PDMS slab with surface modification using corona discharge is shown in Figure 5.8(a). Results show that the PDMS surface is inherently hydrophobic with average contact angle of 96.98º prior to treatment. Drastic decrease in the hydrophilicity of the surface was observed immediately after treatment. However, the aging effective of the surface modification was observed 2 hours after treatment and continued to increase linearly over 96 hours. At day four, the contact angle was 93.35º, which is a close value to the contact angel before treatment. Droplets with low and high contact angles indicating different times of the surface treatments (after .5 hours and after 96 hours) are shown in Figure 5.8(b). The results show that PDMS surface treatment provides sufficient but temporary modifications.

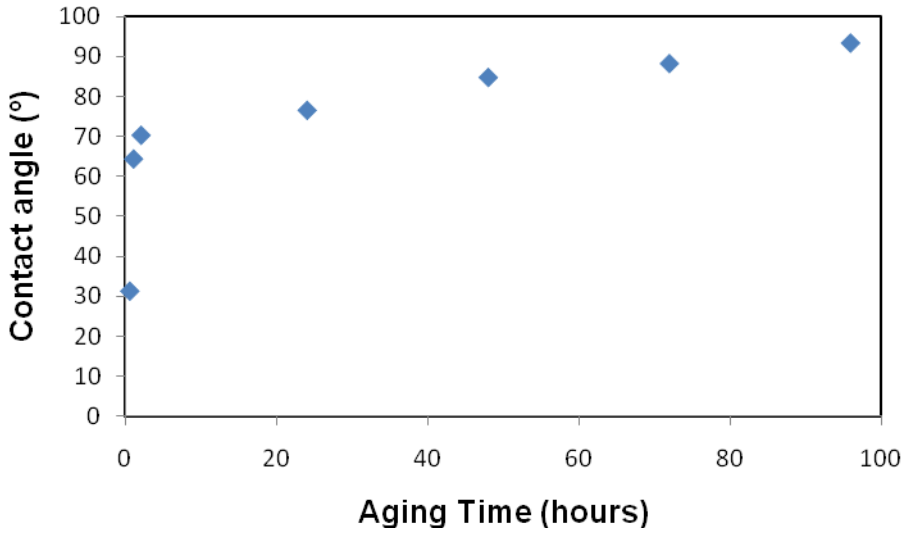

(a)

Figure 5.8 Results for PDMS surface modification with corona discharge (a) plot of the contact angle measurements as a function of aging time (b) images of water droplets with low and high contact angles (Figure 5.8 con'd).

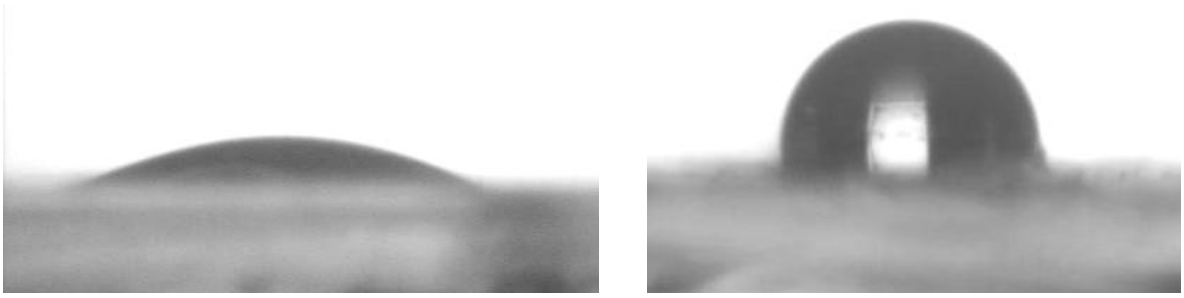

(b)

For the proposed microfluidic chip, permanent bonding between the PDMS and glass substrates was not necessary. Rather, good sealing of the microchannel is more critical in order to provide proper flow and detection capability. However, there are several parameters that have to be considered in order to achieve good sealing based on the proposed chip design. The IDA metal patterns on the glass substrate could introduce a gap that may not be easy to seal. Treatment of the microchannel with BSA for blocking purpose could also prevent successful sealing. In addition, the immobilization of capture molecules on the IDA limits further surface treatments to influence surface properties. For these reasons, the PDMS microchannel with and without corona discharge treatment was tested for sealing. It was observed that both PDMS surfaces provide good sealing and no leakage of the flow was observe. Alignment of the PDMS microfluidic structure could be performed using a stereo microscope or with the bare eye using alignment marks. Figure 5.9 shows the aligned PDMS channel on top of the glass substrate enclosing the IDA microelectrode.

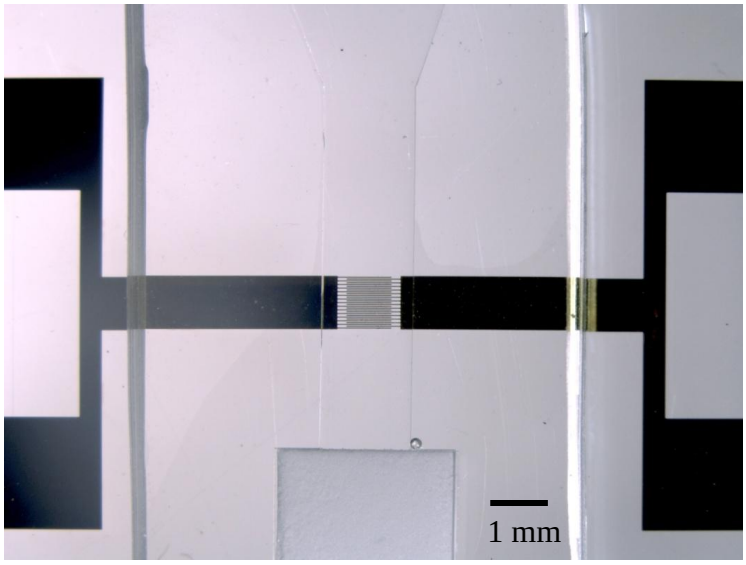

Figure 5.9 Microscopic image of the PDMS microfluidic structure placed on top of the IDA microelectrode on glass substrate.

5.6 CNT-Based Immunoassay Using PDMS Microfluidic Chip

5.6.1 Detection Protocol

The on-chip immunoassay using CNT labels for quantitative detection in sandwich format was conducted. IDA microelectrodes were used as a sensing surface and the detection protocol was similar to the detection protocols discussed in Section 5.5. However in this case, a PDMS microfluidic chip is used to transport sample and conjugate solution to the detection zone. The immunoassay was based on selective binding between human serum albumin (HSA) and anti-human serum albumin (anti-HSA). HSA is a predominant protein in the human blood plasma and the detection of HSA is used to indicate various complications including renal, liver, and kidney diseases. MWCNT labels that were covalently attached to HSA were used for signal detection. Capture HSA was immobilized on the IDA microelectrode, where the binding

reaction took place. After immobilization of capture HSA, blocking scheme was carried out on both the glass and the PDMS substrates by flowing through the microfluidic channel in order to minimize non-specific binding. Following the blocking treatment, both substrates were rinsed with DI water and blown using N_2 gas. After fully dried, the two substrates were sealed together. Sample and conjugate solutions were then applied through the sample inlet, where the sample was driven by capillary action once the front meniscus reaches the absorbent pad. The flow rate was determined by the capillary pump at the end of the PDMS channel that absorbed the excess reagents. As the sample flow over the IDA microelectrode, anti-HSA was captured by the immobilized HSA. MWCNT-HSA conjugate was also captured by the anti-HSA. The amount of binding was indicated by the MWCNT labels forming network/matrix across the IDA microelectrode. Electrical current response through the MWCNTs was monitored using the IDA microelectrode.

5.6.2 Materials and Reagents

Human serum albumin (HSA) and anti-human serum albumin (anti-HSA) were obtained from Sigma-Aldrich (St. Louis, MO). Carboxylated MWCNTs (Purity > 95 wt%) were obtained from Cheaptubes, Inc., (Brattleboro, VT). Hi-flow Plus nitrocellulose membranes (HF13502) were obtained from Millipore (Bedford, MA). PDMS Sylgard 184 was obtained from (Dow Corning, Midland, MI). Polyvinylpyrrolidone (PVP, MW 10,000), bovine serum albumin (BSA), Tween-20, glutaraldehyde, and 2-(*N*-morpholino)ethanesulfonic acid (MES) were from Sigma-Aldrich. 1-(3-(dimethylamino)-propyl)-3-ethylcarbodiimide hydrochloride (EDC) and N-hydroxysulfosuccinimide (Sulfo-NHS) were obtained from Thermo Fisher Scientific, Inc.

(Rockford, IL). 1X PBS buffer was prepared by diluting PBS powder concentrate (Fisher Scientific, Inc., Pittsburg, PA) in DI water and adjusting the pH to 7.4.

5.6.3 Experimental Procedure

Each PDMS microfluidic structure was cut out from the mold and an inlet with ~ 1 mm in diameter was punched through. The PDMS structure was then washed with DI water and dried using N_2 gas. 2 µl of the HSA solution with 10% (v/v) concentration was used for immobilization on the IDA electrode. The PDMS substrate was placed on the IDA electrode and 5 µl of blocking solution was applied through the inlet. The blocking solution was prepared using 2 % BSA in PBS buffer with 0.05 % Tween-20 (v/v). After 10 minutes of incubation, the blocking solution was rinsed by applying PBS buffer through the inlet. The PDMS and glass substrates were separated and completely dried before sealing again. The MWCNT-HSA conjugate solution was prepared following similar procedures discussed in Chapters 3 and 4. HSA solution, 0.3 % (v/v) in PBS buffer was used for conjugation. The electrical current readings for 1V applied voltage were obtained using Keithley 6485 Picoammeter (Keithley Instruments Inc.,) with RS232 interface for data recording.

5.7 Results and Discussion

5.7.1 On-Chip Immunoassay

The developed PDMS microfluidic device for CNT-based immunoassay is shown in Figure 5.10. Continuous flow of the applied sample solution in the microchannel was obtained by the capillary pump of the absorbent pad. Initial investigation of the flow behavior revealed that the flow could be too fast in order to realize efficient binding and detection capability. Optimization of the flow was thus conducted to obtain slower speed based the absorbent pad

property and the selected dimensions. The speed of the flow was reduced by keeping the absorbent pad moist prior to sample application. For analyte detection, anti-HSA solution was prepared in varying concentrations. Sample solution containing each concentration of the anti-HSA solution and conjugate solution were prepared 1:4 ratio, respectively. Prior to sample application, the current through each chip was measured to ensure the viability and consistency of the devices. 5 µl of sample solution was then applied to each chip. Anti-HSA and conjugates were captured as the solution moved across the IDA, where the MWCNT labels formed a network/matrix corresponding to the amount of binding. Detection of 0, 0.5, 1, 5, 10, 20 ng/ml of anti-HSA was made successfully. The flow was fast immediately after sample application and it slowed down as the flow front reached the absorbent pad at the end of the channel. The flow was continuously driven by the capillary action. The current response for the binding reaction was monitored starting from sample application and long after the sample was removed from the channel as shown in Figure 5.11. Signal fluctuation was observed when the flow front first reached the IDA. The signal increased instantly, but dropped back and continued to stabilize for the remaining measurements. The current drop observed overtime could be explained by the binding reaction that mostly occurred at early stage of the flow. Figure 5.12 shows the measured stabilized current as a function of time for varying anti-HSA concentrations. The current values during the last 60 seconds after the flow completely crossed the IDA electrode (~ t = 200 seconds) were used to plot the calibration curve with the relative standard deviation as shown in Figure 5.13 and Table 5.1.

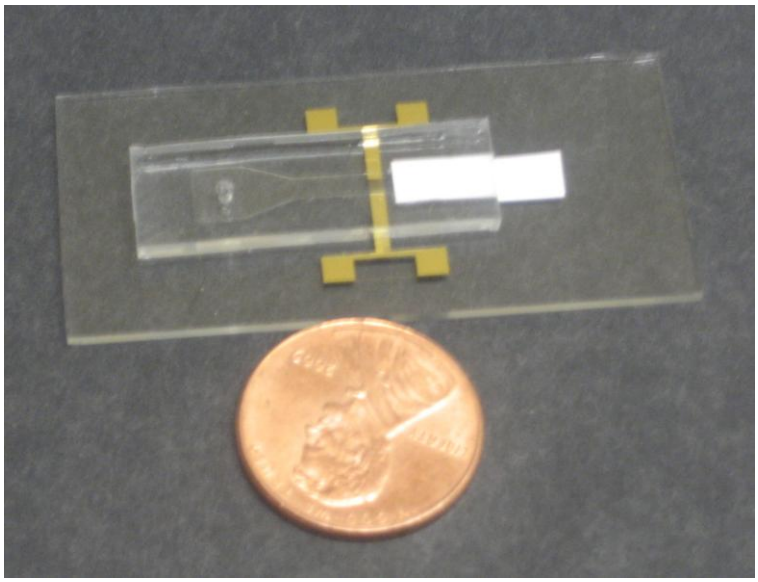

Figure 5.10 Developed PDMS microfluidic chip with integrated IDA microelectrode for immunoassay.

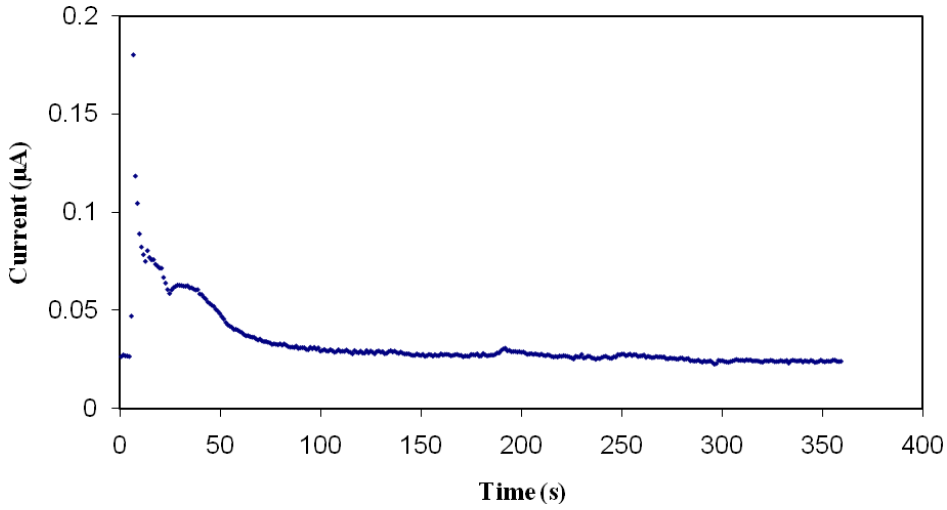

Figure 5.11 Plot of the full current reading starting at sample application until signal saturation was reached.

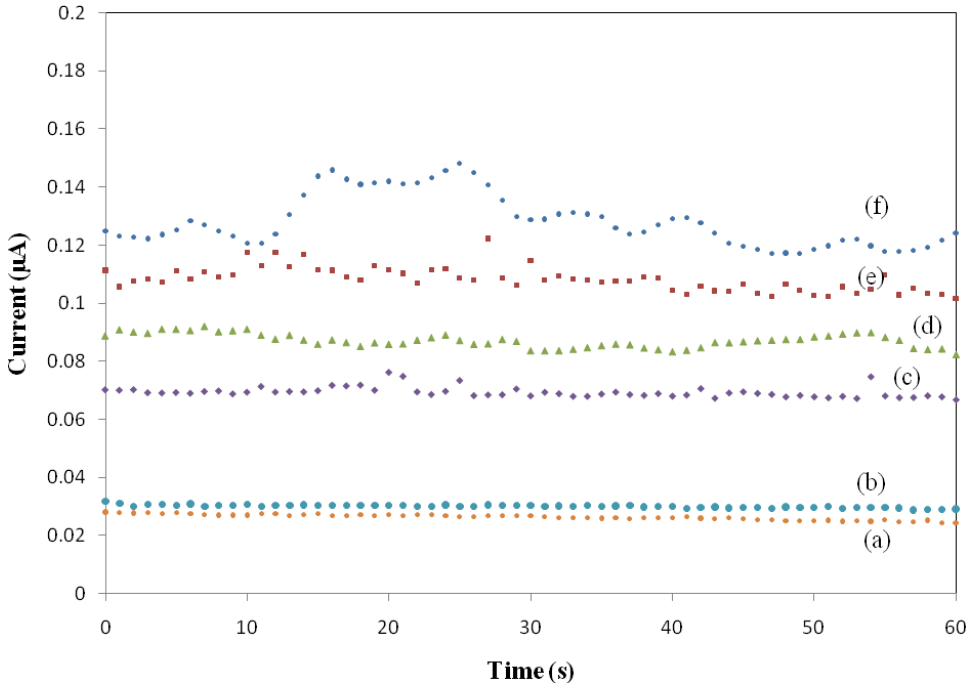

Figure 5.12 Plot of the current measurements as a function of time obtained for on-chip immunoassay with varying anti-HSA concentrations in ng/ml (a) 0, (b) 0.5, (c) 1, (d) 5, (e) 10, and (f) 20.

Table 5.1 Summary of the measured current for varying anti-HSA concentrations for on-chip immunoassay.

Concentration (ng/ml)	Current (µA)	Standard Deviation
0	0.025	0.0007
0.5	0.028	0.0016
1	0.077	0.0082
5	0.083	0.0109
10	0.108	0.0110
20	0.136	0.0086

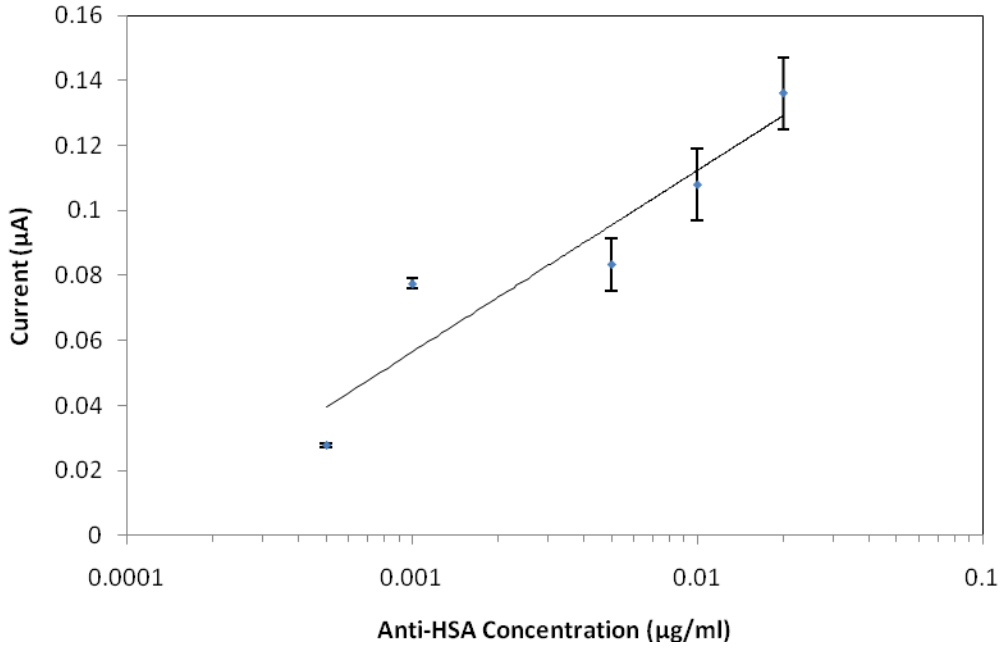

Figure 5.13 Calibration curve for anti-HSA detection using PDMS microfluidic chip.

The measured current values increased with increasing antigen concentration. Results show that the on-chip immunoassay provides a sensitive detection mechanism with concentration below 1 ng/ml. In addition, the PDMS microfluidic chip provides convenient sample delivery with autonomous flow control.

The formation of the MWCNT network on the IDA was characterized using SEM as shown in Figure 5.14. The images show the MWCNT network formation connecting the fingers of the IDA electrode. Higher density of MWCNT labels corresponding to larger amount of captured target analyte (concentration) is shown in Figure 5.14(a). A lower coverage of the MWCNT labels is shown for lower amount of captured analyte in Figure 5.14(b).

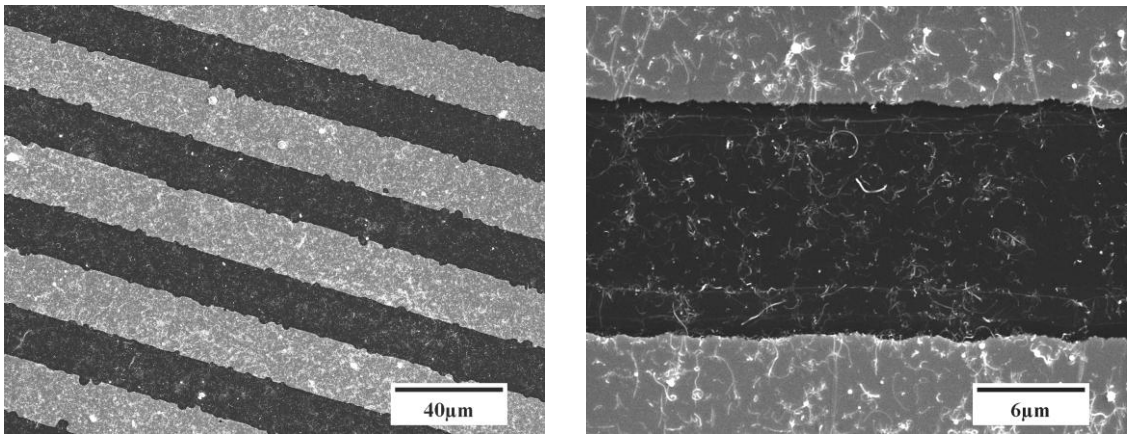

(a)

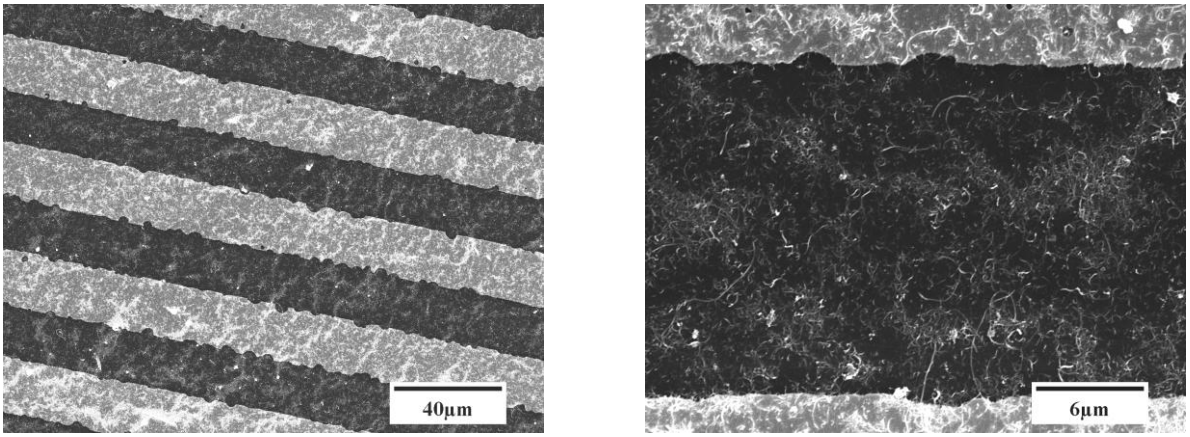

(b)

Figure 5.14 SEM characterization of MWCNT matrix formation across the IDA microelectrodes as a result of HSA and anti-HSA binding (a) lower density of the MWCNT labels for low anti-HSA concentration and (b) higher density of the MWCNT matrix for larger anti-HSA concentration (Figure 5.14 con'd).

5.7.2 Flow Characterization

Figure 5.15 represents the sequence of images that occurred within the first three seconds after sample application. The time prior to sample application is indicated by t = 0 seconds, where no solution was present within the microchannel or in sample drop zone. The point of sample application was set as t = 1 second. At t = 2 seconds, the figure demonstrates that the solution had just crossed the electrodes, but did not reach the absorbent pad yet. This stage is equivalent to the spike in current reading as shown in Figure 5.11. At t = 3 seconds, the solution has reached the absorbent pad and the electrode was fully covered with the sample solution. As demonstrated in the pictures, the initial flow of the solution is extremely fast, where the flow front moved at average speed of ~ 5.5 mm/s. However, the average flow speed of the solution was much slower than the initial speed. This average speed was determined by optimizing the pumping rate of the absorbent pad. In order to achieve the experimental flow speed, the absorbing capacity of the pad without causing back flow into the microchannel was first determined. Accordingly, 10 µl of buffer solution was applied to each absorbent pad prior to the sample application into the microchannel. The applied buffer reduced the pumping capacity of the absorbent pad. The modified rate of the absorbent pad determined the flow rate and total volume of the applied sample solution. The flow speed of the solution was optimized to give an average velocity of 153 µm/s.

Most of the binding reaction occurred when the sample solution first covered the IDA microelectrode. The average time for the flow to finish crossing the IDA was 180 $\pm$ 10 seconds. Figure 5.16 shows before and after the sample flow end crossed the IDA electrode. The anti-HSA and HSA binding took place on the IDA microelectrode surface followed by the MWCNT-

HSA conjugate. Then the MWCNTs formed a conducting network on the IDA electrode corresponding to the amount of binding. The current measurement taken for one minute duration after 200 seconds was used to plot the calibration curve and quantify the amount of binding.

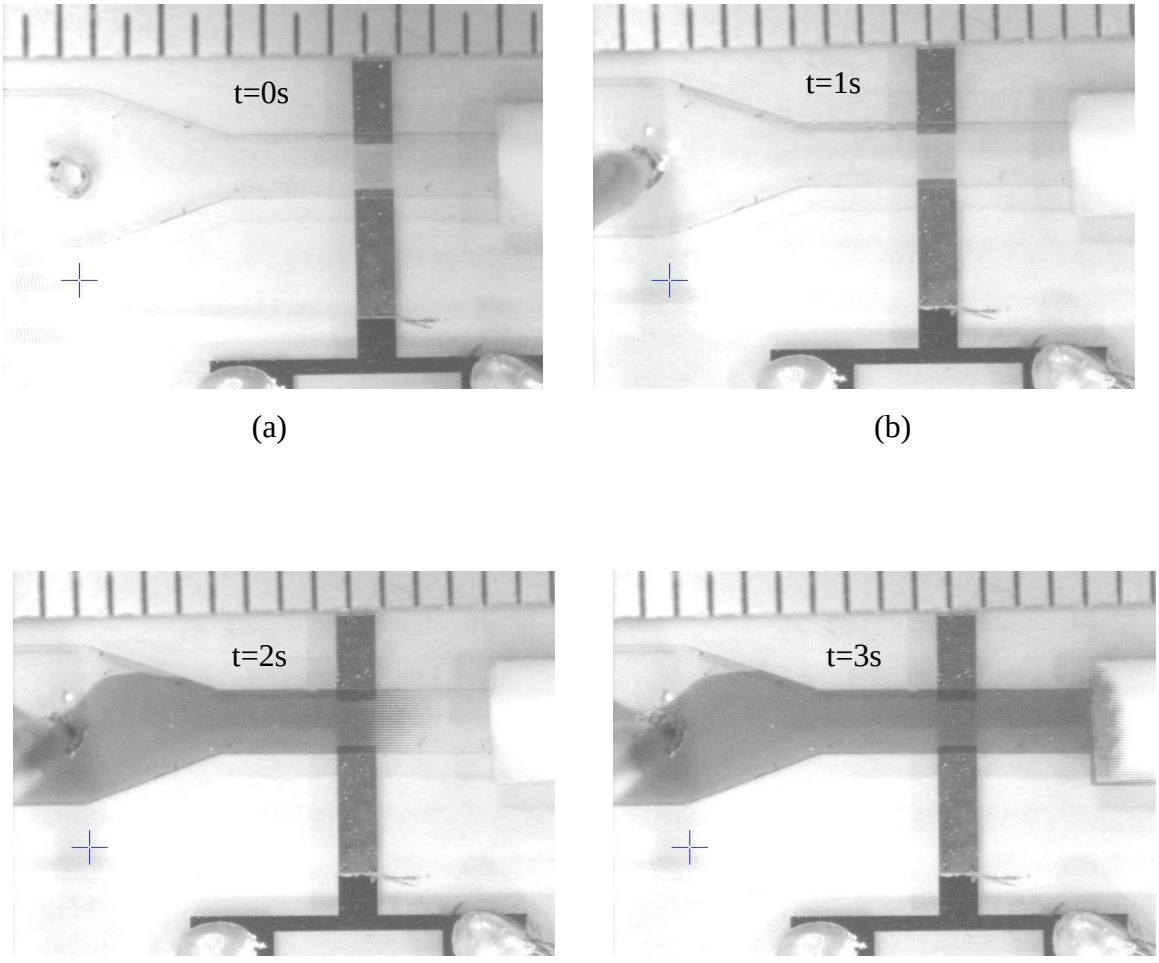

Figure 5.15 Characterization of the flow of the sample solution in the PDMS microfluidic channel in the first three seconds of sample application at (a) t = 0 s, (b) t = 1 s, (c) t = 2 s, and (d) t = 3 s.

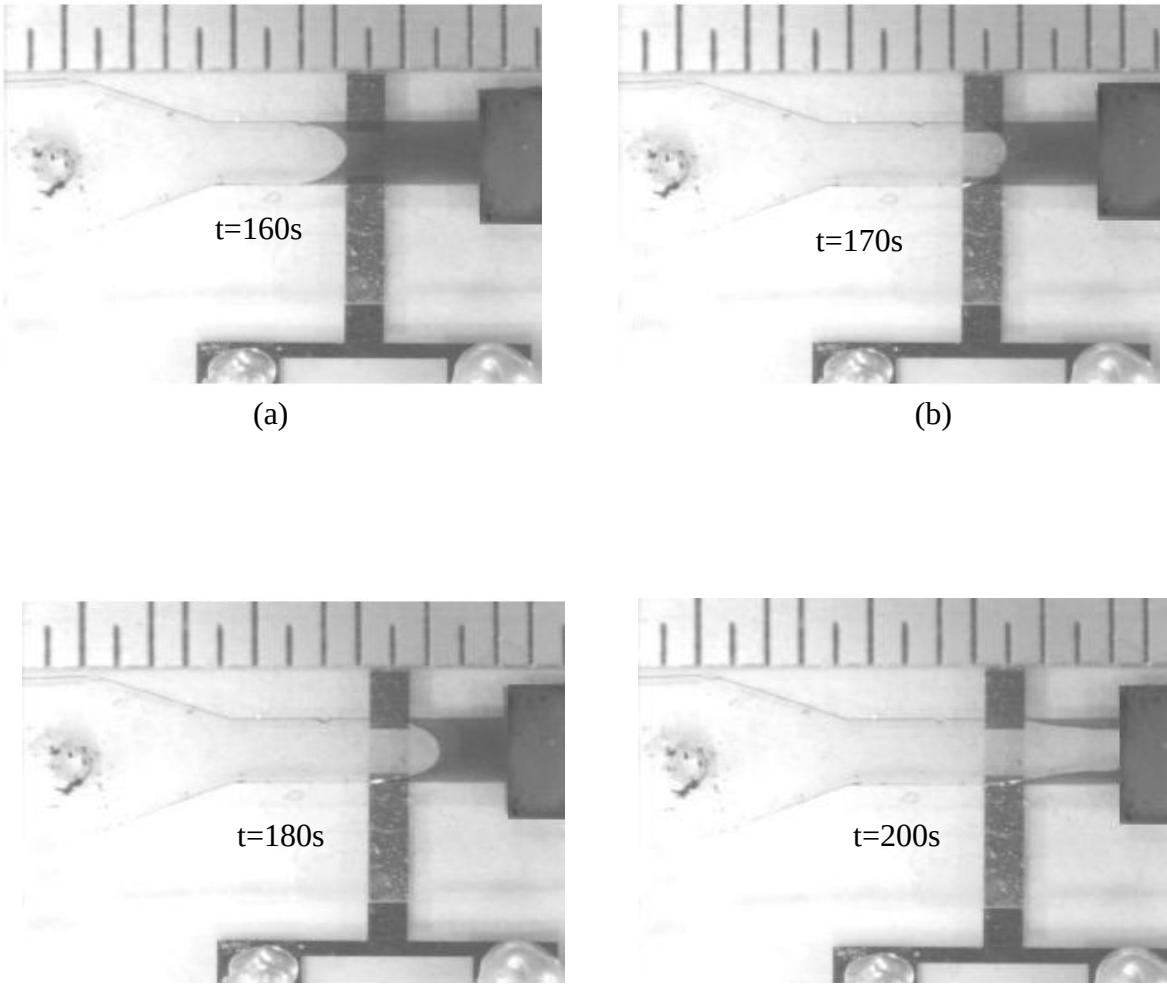

Figure 5.16 Characterization of the flow in the PDMS microfluidic channel before and after the sample solution crossed over the IDA at (a) t = 160 s, (b) t = 170 s, (c) t = 180 s, (d) t = 200 s, and (e) t = 230 s (Figure 5.16 con'd).

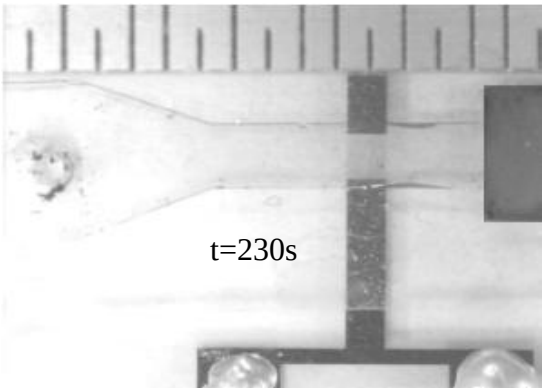

(e)

5. 8 Simulation

5.8.1 Fundamental Equations in Microfluidics

The basic equation governing incompressible fluid dynamics is the Navier-Stokes equation

$$\rho\left[\frac{\partial \boldsymbol{u}}{\partial t} + (\boldsymbol{u}\cdot\nabla)\boldsymbol{u}\right] = -\nabla P + \eta\nabla^2\boldsymbol{u} + \boldsymbol{f} \qquad (5.1)$$

where ρ is the density, $\boldsymbol{u}$ is the fluid velocity, P is the pressure, η is the fluid viscosity, and $\boldsymbol{f}$ is body forces. The Navier-Stokes equation comes from conservation of mass and momentum equations assuming that density and viscosity is constant for a given fluid. The terms on the left side are for the inertial acceleration of the fluid and the terms on the right are for forces acting on the fluid including body forces. Scaling flow equations and dimensions of the microfluidic

geometry provides a reasonable method in analyzing the different forces acting on the flow and characterizing the flow in the microchannels.

Another important parameter often expressed in dimensionless number is the Reynolds number. The Reynolds number provides the ratio of the inertial force to the viscous forces

$$Re = \frac{\rho u_o l}{\eta} \tag{5.2}$$

where u_o is the average flow velocity and l is the characteristic length. At low Reynolds numbers, the fluid dynamics is dominated by the viscous drag rather than by inertia. For fluid flow in microstructures having characteristic length of 10 ~ 200 μm, the Reynolds number ranges between 10^{-3} and 10. In such cases of low Reynolds number, fluid flow has a laminar pattern. The governing Navies-Stokes equation also simplifies, since the left-hand side of Equation 5.1 dealing with inertial terms can be ignored. The simplified Navies-Stokes equation becomes linear eliminating the time derivatives

$$\eta \nabla^2 \boldsymbol{u} = \nabla P. \tag{5.3}$$

In this case, the fluid flow is dominated by the pressure distribution, the incompressibility constraint, and the boundary condition at the walls.

5.8.2 Microfluidics Simulation

In this research, simulations were performed in order to analyze the different parameters involved in the developed microfluidic immunoassay system. Simulation can provide an in-depth understanding of the kinetics of microfluidic immunoassay system. In addition, numerical

analysis is essential to the efficient design of the microchannel with optimized parameters. These parameters include analyte concentration, flow velocity, and height of microfluidic channel. Similarly, bulk analyte transport and binding ability are important factors in the reaction kinetics between analytes and immobilized capture molecules such as anti-IgG and IgG. The specific binding kinetics of anti-IgG and immobilized IgG occurs at the solid-liquid interface/binding surface of the immunosensor. In this work, a microelectrode was used as the reaction surface where the binding occurred. The detected immunoassay signal was dependent on the reaction kinetics of association and dissociation, and diffusion based analyte transport within the microchannel [134]. Several numerical studies have been conducted in regards to binding kinetics of antibody-antigen related to microfluidic immunoassay [135-138].

The reaction kinetics can be expressed as a two-step process [139]. The first is a mass-transport process, where the IgG is transported by diffusion from the bulk solution toward the microelectrode surface.

$$C_{bulk} \leftrightarrow C_{surface}$$

The second is a chemical reaction process where the binding of the antigen-antibody takes place,

$$C_{surface} + B \leftrightarrow CB$$

where C_{bulk} is the concentration of the anti-IgG in the bulk, C_{surface} is the anti-IgG concentration at the binding surface, B is the immobilized IgG concentration at the surface of the microelectrode, and CB is the anti-IgG and IgG complex concentration.

Analyte concentration gradient is often formed when the analyte/anti-IgG takes a longer time to travel to the reaction surface than the binding reaction [140]. The thickness of the gradient layer depends on the influence of the reaction and diffusion rates as well as the flow velocity [141]. The diffusion velocity of many biomolecules is relatively slow compared to the reaction rate in a fluid environment, as measured by the Damkoehler number [141]. Therefore, analyte concentration gradient layer was formed on the reaction surface of the microelectrode (with the assumption of no-slip condition at the walls).

COMSOL Multiphysics, a finite element analysis software package, was used to simulate the reaction of immobilized IgG and anti-IgG biomolecules on a microelectrode and understand the influence of the microfluidics and flow parameters. A 2-D sketch is drawn in Figure 5.17 representing the model used in the simulation. The conjugate solution flows from left to right in the positive y-axis direction. The microelectrode is assumed to be fully covered by the immobilized IgG with a concentration of *B*.

The fluid is incompressible and obeys the Navier-Stokes equations of fluid motion. Fick's second law also governs the diffusion of the anti-IgG, with the equation described as,

$$\frac{\partial C}{\partial t} + s\frac{\partial C}{\partial x} + q\frac{\partial C}{\partial y} = D\left(\frac{\partial^2 C}{\partial x^2} + \frac{\partial^2 C}{\partial y^2}\right) \tag{5.4}$$

where C is the same as C_{bulk}, s is the component of the velocity in the x direction, q is the component of the velocity in the y direction, and D is the coefficient of diffusion of IgG equal to 5×10^{-11} m^2/s [142]. The concentration of the anti-IgG and IgG complex obviously increases with time, and follows the Langmuir model as [143],

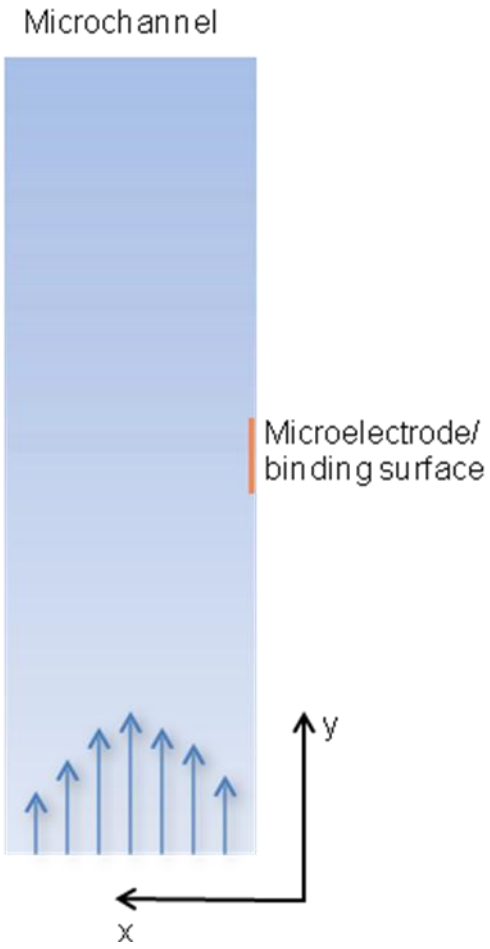

Figure 5.17 2D model of the sample flow in a microchannel with microelectrode as a binding surface for immunoassay.

$$\frac{\partial(CB)}{\partial t} = k_a C_{surface}(B_0 - CB) - k_d (CB) \tag{5.5}$$

where B_0 is the initial concentration of the immobilized IgG, and k_a and k_d are the association and dissociation rate constants of the reaction, respectively.

At the microelectrode, which represents the entire reaction surface, the diffusion is set equal to the reaction rate,

$$-D(\frac{\partial C}{\partial x})_{surface} = k_a C_{surface}(B_0 - CB) - k_d(CB) \tag{5.6}$$

The association and disassociation rate constants, k_a and k_d, used in this simulation were 2.5 x 10^5 $m^3/(mole \cdot s)$ and 3 x 10^{-4} (1/s), respectively [134, 142].

5.8.3 Flow Conditions

Prior to discussing the results of the simulation, the initial flow and boundary conditions as well as the fixed microfluidic parameters are stated. The flow was considered as a neutral buffer solution with similar properties as water. The flow in the microfluidic channel was laminar with low Reynolds number. The velocity of the flow was taken as 1 mm/s unless stated otherwise. The microchannel had a length of 500 μm and height of 150 μm. The microelectrode had a length of 50 μm and height of 1 μm. The height of the microchannel and length of the microelectrode varied for computation to observe their influence on the binding reaction. The left end point of the microelectrode was located at the middle distance of the channel, 250 μm. The boundary conditions were set as P = 0 for the pressure at the outlet and no-slip conditions at the walls. Initial concentration of the anti-IgG in the solution and therefore on the surface of the microelectrode was the same as the analyte concentration in the solution. The anti-IgG and IgG complex concentration on the surface of the microelectrode at t = 0 was also equal to zero. The initial concentration of the immobilized IgG, B_0, was taken to be 2 x 10^{-8} $mole/m^2$.

5.8.4 Simulation Results

One of the most important parameters in the simulation was the anti-IgG concentration in the solution. As in the case of the experimental work conducted using anti-HSA, the resulting binding reaction or detection signal varied based on the amount of anti-IgG. Anti-IgG concentrations used in the simulation were 0.5×10^{-9}, 1×10^{-9}, 10×10^{-9}, 40×10^{-9}, and 80×10^{-9} mole/m^3. Figure 5.18 demonstrates the simulation results of the surface concentration of the anti-IgG and IgG complex with varying concentration of the anti-IgG solution. The saturation concentration for the complex was lower with decreasing anti-IgG concentrations. Similarly, the rate of reaction decreased when the anti-IgG concentration was reduced. The time to reach complex saturation concentration increased dramatically for the low anti-IgG concentrations, as shown in Table 5.2. The other parameters such as flow velocity, immobilized IgG concentration, length of the microchannel and height of the microelectrode were kept constant in this simulation. The results signify the importance of optimization of these experimental parameters in order to increase the binding reaction time for low analyte concentrations. The influence of some of these experimental parameters will be discussed later.

The saturation concentrations of the anti-IgG and IgG complex are also shown in Figure 5.19, where the saturation values for the IgG and anti-IgG complex concentrations were larger for higher anti-IgG concentrations. The saturation concentration represents the maximum limit of the complex value that can be obtained from a set of experimental parameters. Figure 5.19 demonstrates the relationship between one of these parameters, the anti-IgG concentration, *C*, and the saturated complex concentration, *CB*. The relationship is obtained from simulation and setting Equation (5.5) to zero

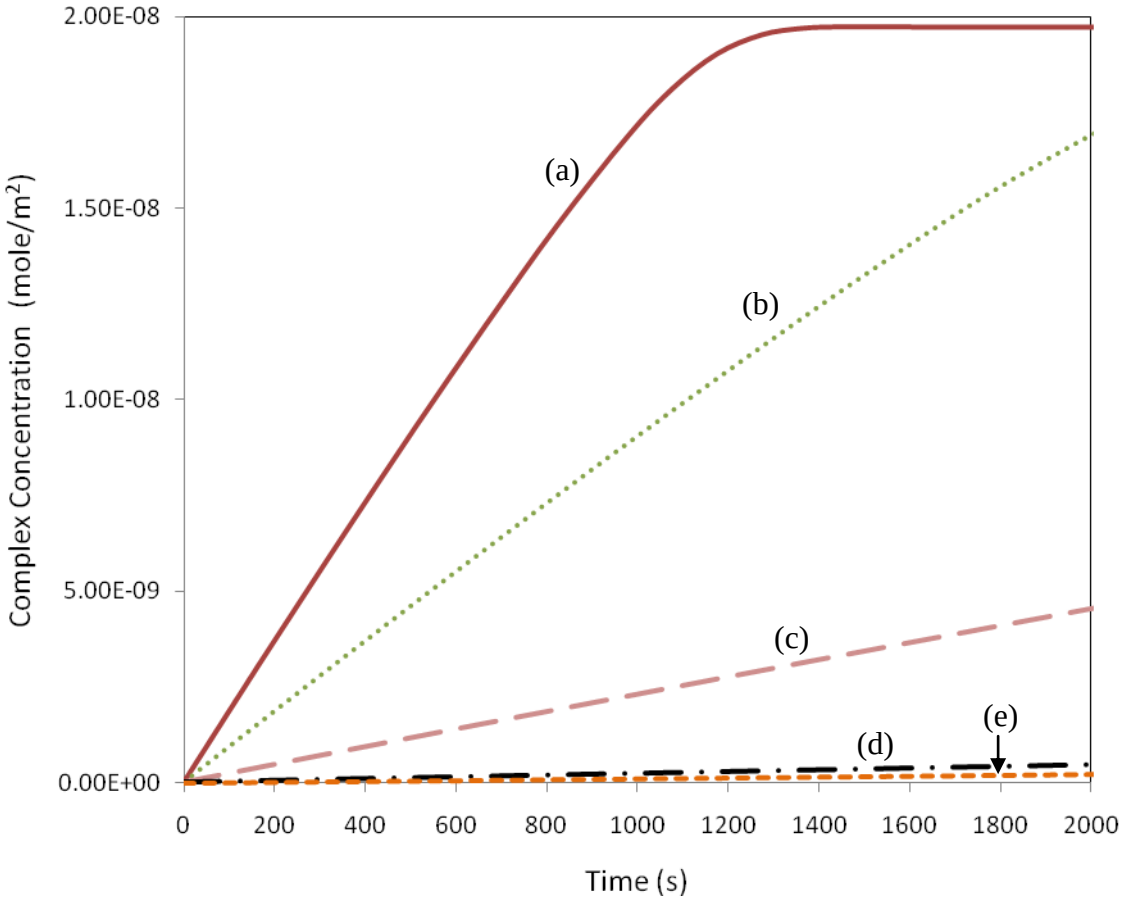

Figure 5.18 The anti-IgG and IgG complex concentration at the microelectrode surface as a function of time for anti-IgG concentrations in mole/m^3 (a) 80 x 10^{-9}, (b) 40 x 10^{-9}, (c) 10 x 10^{-9}, (d) 1 x 10^{-9}, and (e) 0.5 x 10^{-9}.

Table 5.2 Saturation concentration and time for the anti-IgG and IgG complex at the surface of the microelectrode.

Anti-IgG Concentration (10^{-9} mole/m^3)	Complex Concentration (mole/m^2) from Equation 5.7	Complex Concentration (mole/m^2) from Simulation	Saturation Time (s)
80	1.970 x 10^{-8}	1.974 x 10^{-8}	1513
40	1.942 x 10^{-8}	1.949 x 10^{-8}	2862
10	1.786 x 10^{-8}	1.801 x 10^{-8}	13967
1	9.091x10^{-9}	9.373x10^{-9}	207300
0.5	5.882 x 10^{-9}	6.097 x 10^{-9}	414000

$$\frac{\partial(CB)}{\partial t} = 0$$

and resulted in parameters,

$$C = C_{surface} = \frac{k_d / k_a}{(B/CB)-1} \cdot \tag{5.7}$$

There was no significant difference between the complex concentration values obtained from simulation and theory (Equation 5.7).

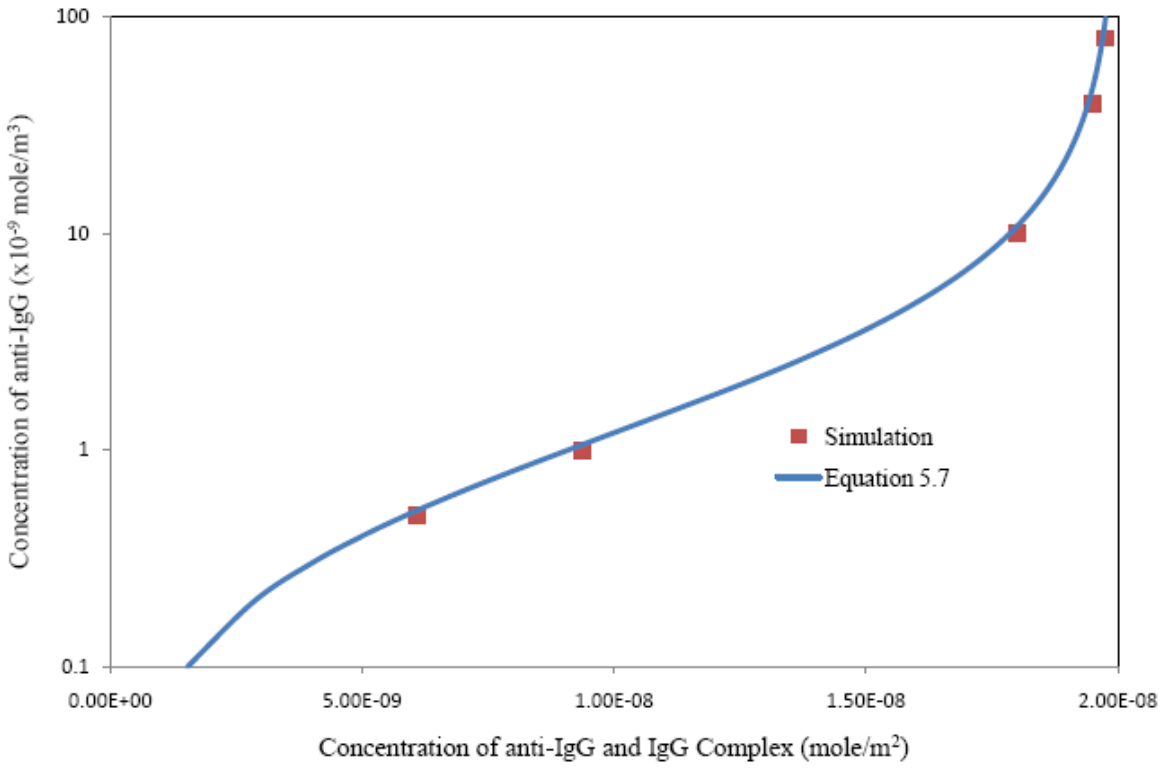

Figure 5.19 The relationship of anti-IgG concentration and the saturation concentration for the anti-IgG and IgG complex.

The analyte concentration gradient that was formed near the microelectrode surface had lower anti-IgG concentration due to the higher rate of binding reaction than the diffusion mass transport of the anti-IgG. Reducing the gradient layer thickness can be assumed to be similar to increasing the anti-IgG concentration in the original gradient layer. Figure 5.20 shows the analyte concentration gradient of the reaction after 0 (initial), 100, 500, and 1600 (saturation) seconds. The gradient slowly diminished during this association phase as the supply of the anti-IgG continues [143].

Another important parameter for the microfluidic-based immunoassay was the flow velocity in the microchannel. Figure 5.21 clearly demonstrates the influence of velocity, where the rate of reaction increased with increasing velocity. However, the saturation values of the complex remained the same with varying flow velocity. Therefore, faster speed could be advantageous if the solution was expected to be abundant. For the same flow duration, more anti-IgG molecules would cross over the microelectrode for flows with higher velocity. Therefore, faster flows would have higher potential for the formation of anti-IgG and IgG complex than slower flows. However, if the available sample solution would be expected to be small in quantity, as in the case of microfluidic immunoassay, lower velocity would provide similar results.

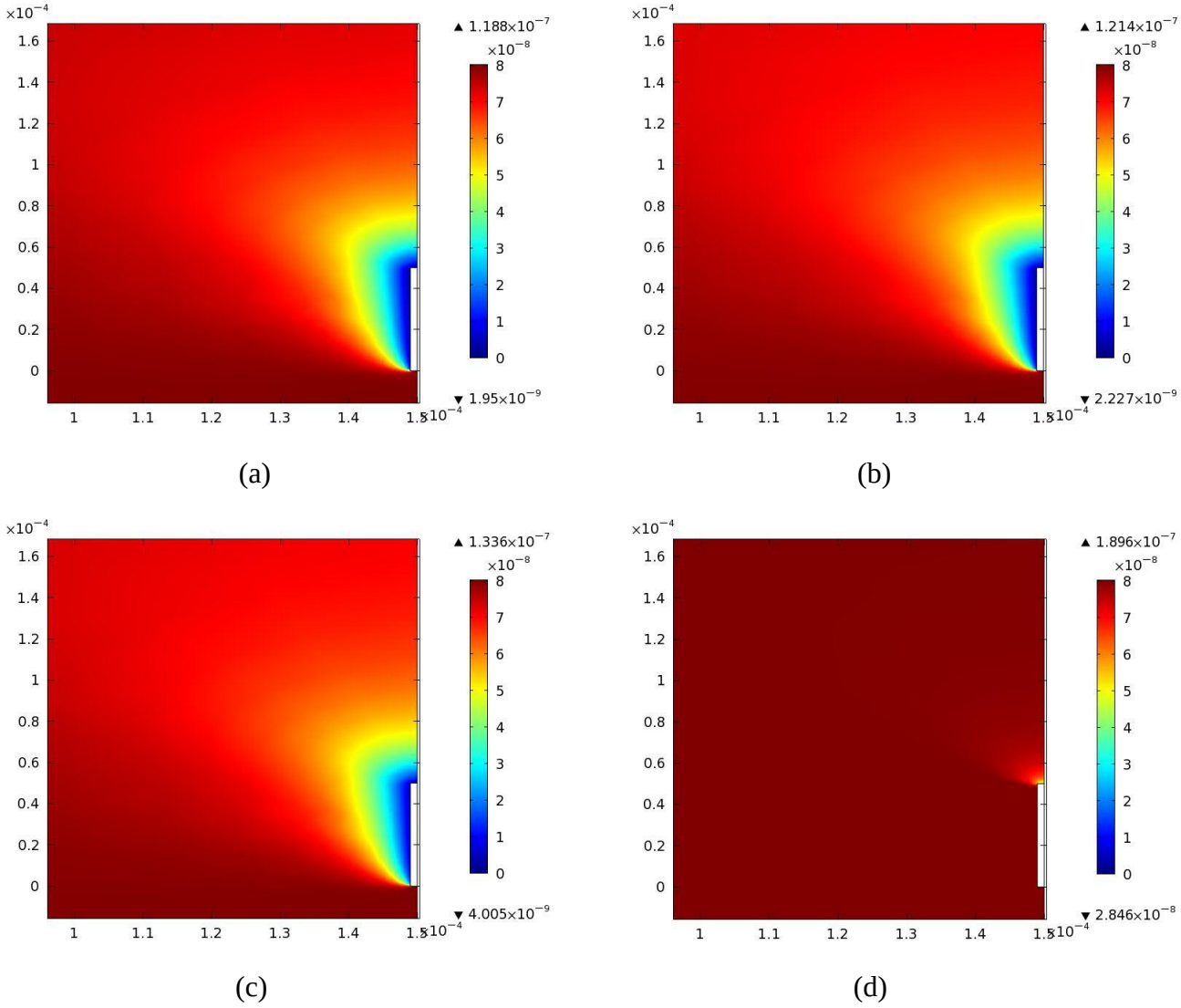

Figure 5.20 Analyte concentration gradient at the microelectrode for 80 x 10^{-9} mole/m^3 anti-IgG concentration after (a) 0 (initial), (b) 100, (c) 500, and (d) 1600 (saturation) seconds. The graphs are plotted with the x and y axes reversed.

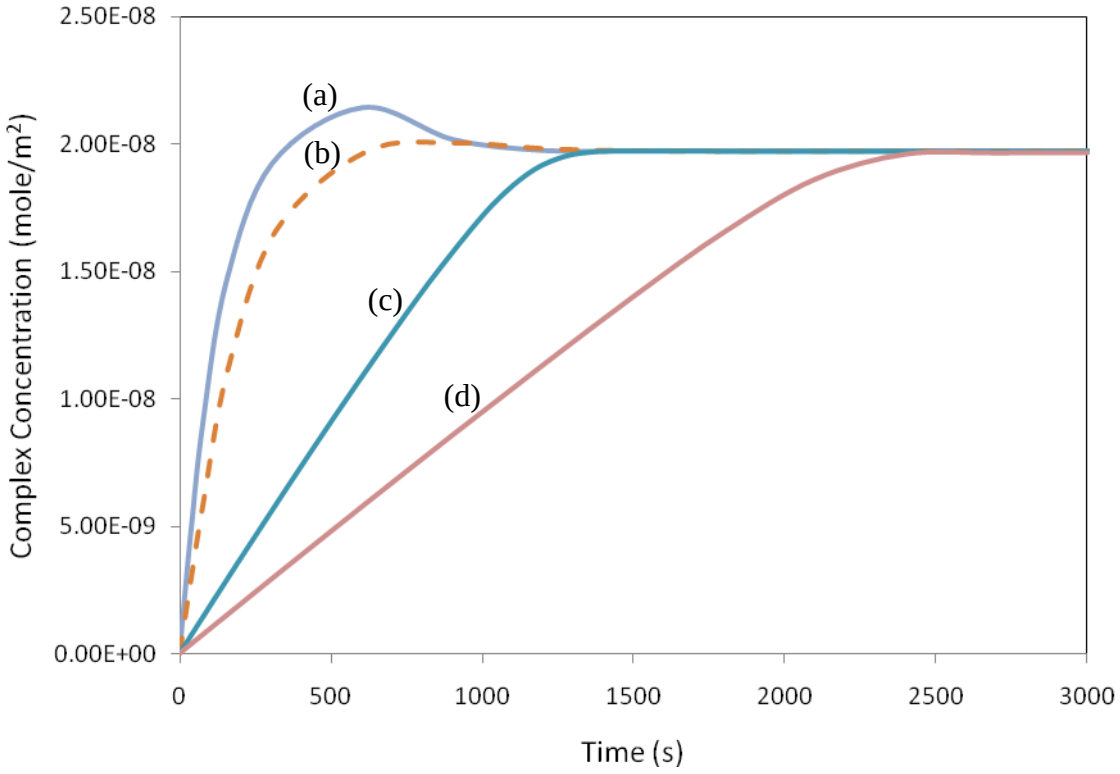

Figure 5.21 Influence of flow velocity on the rate of reaction or surface concentration of anti-IgG and IgG complex in mm/s are (a) 10, (b) 5, (c) 1, and (d) 0.5.

Other parameters that could influence the binding reaction were height of the microchannel and length of the microelectrode. Figure 5.22 shows the reaction rate for varying height of the microchannel. The simulation results have not shown any significant difference in binding reaction rate for the range of 18.5 - 300 μm microchannel height. However, the rate of reaction has decreased in the case of 4.6875 and 9.375 μm channel height. The similarity in the reaction rate in the 18.5 - 300 μm height range could be explained by the fact that the analyte concentration gradient layer was not affected significantly. Therefore, the change in

microchannel height did not influence the ratio of the anti-IgG diffusion rate to the binding reaction rate. The observed binding rate reduction for the 4.6875 and 9.375 μm could be explained by the significant reduction of the amount of anti-IgG in the gradient layer. Therefore, the analyte reaching the microelectrode was considerably lowered for the same time duration. The sample flow velocity was kept the same for the different heights in this simulation while the flow rate varied due to change in dimensions. Therefore, it could be concluded that the channel height would influence the binding reaction based on the range of dimensions considered.

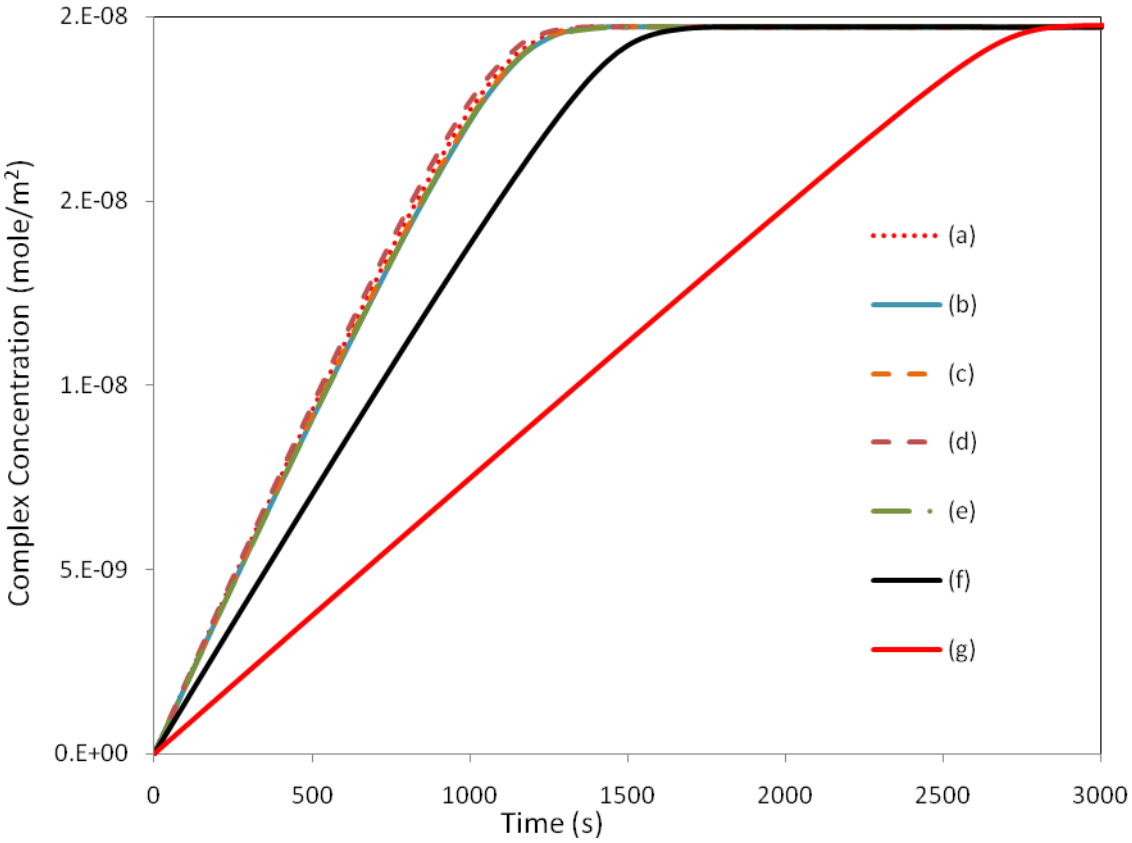

Figure 5.22 Influence of microchannel height on the rate of reaction. The heights used are (a) 300, (b) 150, (c) 75, (d) 37.5, (e) 18.75, (f) 9.375, and (g) 4.6875 μm.

Final parameter considered was the flow velocity by modifying the microchannel geometry around the microelectrode. The modification was based on varying the protrusion from the opposite side of the microelectrode. Figure 5.23 shows the 2D model used for the modified geometry and the corresponding rate of reaction for varying height of the microchannel. The simulation results show that the reaction time decreased as the flow gap between the microelectrode and protruded geometry reduced. In the case of microchannel geometry modification, the initial flow velocity was fixed and therefore constant flow rate was maintained. Constant flow rate provides control of the sample volume necessary to carry out immunoassay tests. In the previous case where the flow velocity was varied based on different flow rates, faster reaction time was achieved using a constant flow rate. This was achieved by varying the velocity at the microelectrode due to the change in the microchannel geometry. This also provides a reasonable comparison to the developed microfluidic immunoassay where the flow rate was determined by the capillary action of the absorbent material.

5. 9 Summary

On-chip immunoassay capability was successfully demonstrated using MWCNT labels for antibody reaction on IDA microelectrode. The detection was based on selective binding between HSA and anti-HSA, a protein with relevance in clinical diagnosis of liver, kidney, and renal complications. MWCNTs were conjugated with HSA, providing dynamic current response for real-time monitoring of the binding reaction. The fabricated PDMS microfluidic system provided passive sample flow control by capillary action. Active/external flow control mechanism was not needed and detection signal was obtained once the sample was dispensed in

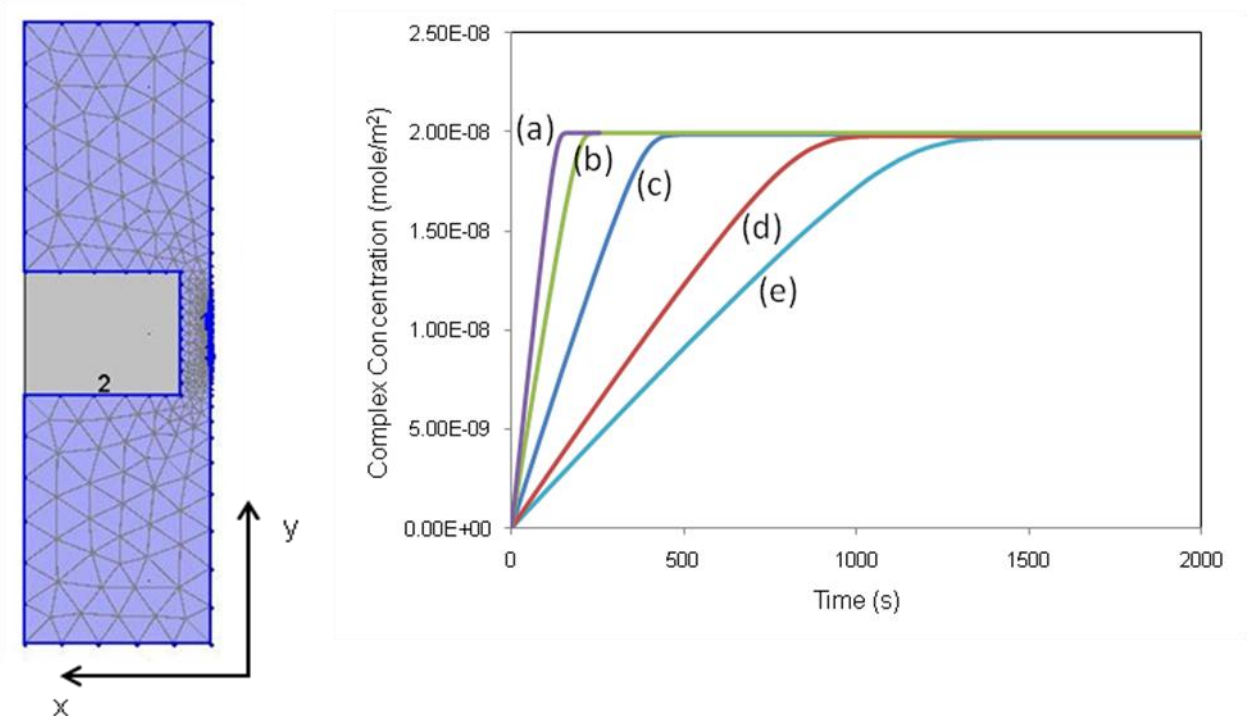

Figure 5.23 Influence of microchannel geometry on the rate of reaction. The heights used are (a) 15, (b) 25, (c) 50, (d) 100, and (e) 150 µm from the microelectrode surface.

the inlet using a pipette. This immunoassay mechanism was simple and sensitive, with detection capability of anti-HSA below 1 ng/ml concentration. The detection capability obtained could be attributed to the MWCNT matrix maintaining high conductivity on the IDA microelectrode. The MWCNTs provided a stable and highly conductive labeling technique that was easily integrated within a microfluidic chip. Signal measurement could be conducted with multimeters or current measuring tools found in most laboratories with micro/nano ampere measuring capability. Overall, the fabrication materials and techniques of the immunoassay chip were simple and sensitive for high throughput point-of-care testing.

Simulation of the flow in a microfluidic immunoassay system was demonstrated in this research. Simulation shows that the anti-IgG and IgG complex concentration is directly related to the analyte concentration. Varying the channel height influences the binding reaction only if the analyte concentration gradient layer is affected reducing the amount of analyte transported to the binding surface. The reaction rates are faster for higher velocities and the complex saturation values remain the same. Modifying the channel geometry close to the reaction surface provides constant flow rate and reduces the overall reaction rates. Therefore, simulation can lead to an optimized microfluidic immunoassay that uses small volume and short detection time. In addition, simulation can facilitate the experimental design and tests.

CHAPTER 6

CONCLUSIONS AND FUTURE WORK

6.1 Conclusions

6.1.1 Functionalization of Carbon Nanotubes

Functionalization protocol was successfully developed for chemically modifying the surface of MWCNTs for immunosensing based on electrical detection. The modification of MWCNTs was carried out in covalent and non-covalent methods with multiple functional groups for uniform dispersion and antibody conjugation in aqueous solution. Dispersion is essential in exposing the surface of the nanotubes for robust antibody conjugation on the MWCNT through stable and irreversible amide linkage. A comparative work was conducted for surfactant assisted dispersion of the MWCNTs suitable for immunoassay process. The nanotube suspension was studied using PEG, PVP, and DI water, separately. Summary of the dispersion and the conjugation results are summarized below:

- PVP treatment was the most effective in the initial dispersion of the MWCNTs and maintenance of the solubility over a period of time,
- PEG also provided reasonable MWCNT dispersion and solubility,
- DI water without surfactant had the least solubility and experienced phase separations in the solution when interacting with coupling agents, confirming the importance of CNT modification with surfactants,

- Surfactants have also provided efficient blockage mechanism in order to avoid non-specific interaction of the CNTs with antibodies and therefore reduced false signaling,
- Antibody, specifically human-IgG, was effectively conjugated on MWCNT using EDC/Sulfo-NHSS coupling method, and
- The number of antibody conjugated on the MWCNTs was limited by the available (surfactant free) nanotube surface area. However, the amount was sufficient to provide immunoassay test.

Optimization of the conjugation process was conducted in order to increase the number of antibodies per CNT. Enhancing the amount of conjugated antibodies could lead to better detection capability. Two parameters were identified for optimization: reducing the amount of surfactant coverage and increasing the concentration of antibody for conjugation. Reducing the amount of PVP used to disperse the MWCNTs resulted in increased number of conjugated antibodies. The reduction of the PVP was able to provide more binding sites for the antibodies. However, reducing the amount of PVP too low was also shown to have a reverse effect on conjugation by compromising the uniform dispersion of the CNTs. On the other hand, increasing the concentration of the antibody used for conjugation also resulted in increased amount of antibodies attached on the CNTs. However, an increase in antibodies not bound to the CNTs was also observed. This observation could require different conjugation protocol in order to achieve better detection capability.

6.1.2 Carbon Nanotube Labels for LF Immunoassay

Immunoassay for antigen detection using MWCNTs as a sensing label on lateral flow system was developed. Competitive and sandwich immunoassay formats were demonstrated, where the MWCNTs provided electrical conductimetric and colorimetric detection for quantitative and qualitative measurements. Integrated electrode system was also developed in order to measure the electrical signals across the capture zone on the immunosensors. The developed functionalization methods were implemented to disperse the MWCNTs and attach the antibodies. Summary of the LF immunoassay detection results are provided below:

- The high conductivity of carbon nanotube network on LF immunosensor coupled with highly specific biorecognition capabilities of antibodies provided enhanced signal detection for simple and rapid detection mechanism suitable for point-of-care diagnostics,
- The LF competitive immunoassay clearly showed the feasibility of electrical conductimetric and colorimetric measurements for concentrations of target human IgG varying from 25 to 200 μg/ml,
- The LF sandwich immunoassay provided sensitive and quantitative electrical measurements, detecting antigen concentration below 1 ng/ml. Visual evaluation of the test strips also corroborated the conductance results demonstrating varying color intensity for different concentrations,
- Improved LF cartridge was developed with integrated electrodes for simple and direct electrical measurements. The cartridge also was used to house the immunostrips for portable and easily disposable POC tests, and
- Results showed the feasibility of obtaining lower detection limit.

6.1.3 Microfluidic Immunoassay Using Carbon Nanotube on IDA Microelectrodes

Microfluidic immunosensing based on conductimetric detection using CNT matrix was demonstrated using HSA protein in sandwich format. PDMS microfluidic system was developed for passive sample transport to the detection surface by capillary action. The binding reaction occurred on IDA microelectrode that was fabricated on a glass substrate and incorporated within the microfluidic channel. CNTs conjugated with antibody formed a conducting matrix across the IDA providing electrical signal corresponding to the amount of captured antigen. The developed functionalization methods were implemented to disperse the MWCNTs and attach the antibodies. Simulation is used in order to understand the influence of the different parameters involved in the microfluidic system. Summary of the on-chip immunoassay detection results are provided below:

- The PDMS microfluidic system enabled the manipulation of small sample volume with passive control. In addition, replication of the PDMS structure was carried out under normal laboratory condition, once the mold master was fabricated using lithography process,
- The IDA microelectrode provided large sensor area for real-time monitoring of the antibody reaction through the formation of CNT matrix between the electrodes,
- The microfluidic immunoassay system provided sensitive and low-concentration detection of anti-HSA in sandwich format with detection capability below 1 ng/ml and
- The simple fabrication technique, passive flow control, CNT-based electrical detection provided immunosensing chip with a potential for high throughput screening of proteins and disease markers in a POC setup.

6.2 Future Work

6.2.1 Carbon Nanotube-Antibody Conjugation and Quantification

Increasing the number antibodies on the CNTs could lead to improved detection capability. One of the methods to accomplish this is by using higher antibody concentration for conjugation. However, in doing so, it is important to modify some of the conjugation parameter such as incubation time and washing step in order to minimize unbound antibodies. Depending on the increase, longer incubation time could be used in order to increase the chance of conjugation. The washing step also could be increased to ensure that all unbound antibodies are removed. In this case, it is important not to wash away the CNTs. Another possibility for optimizing the antibody and CNT conjugation would be to implement a quantification protocol to identify the amount of unbound antibodies. Efficient quantification would provide the flexibility in choosing the antibody concentration for conjugation that could lead to sensitive detection.

6.2.2 Pathogen Detection on Lateral Flow System

The developed methodology for functionalization of CNTs allows the detection of various analytes in different configurations. Some of the interesting follow up work could be to use the LF immunoassay system for clinical application of viral detection. Accurate and rapid diagnostic tools for viral detection such as dengue and malaria have a global need. This work is underway by Fang Liu, a PhD student in the BioMEMS and Bioelectronics lab under Dr. Choi. This work will be conducted in collaboration with Department of Tropical Medicine at Tulane University, who will be supplying the samples and certified testing facility. Automation of the sub-system of the LF immunosensing could be useful in achieving lower detection limits. For

example, the immobilization of capture antibodies could be conducted using systems such as inkjet printer, spraying, or sputtering. In addition, reagent storage of the MWCNT-antibody conjugate solution pre-dried on porous membrane and incorporated within the LF system would minimize the sample application steps enabling one-step immunoassay.

6.2.3 Microfluidic Parameters for On-Chip Immunoassay

For the developed PDMS microfluidic immunoassay, the flow rate and total volume was determined based on the optimization of the capillary pump. An absorbent pad inserted within the fluidic structure continuously drove the sample by capillary action. These parameters could be manipulated further by changing the dimensions of the capillary pump for better detection capability without changing the chip design. In addition, reducing the channel dimensions could reduce the sample volume and influence the sensitivity of the immunoassay tests further. The CNT-antibody conjugate solution could be embedded within the microfluidic system in order to eliminate the application of multiple reagents. Simulation of the microfluidic system could be an efficient method of characterizing the different parameters rather than continuous experimental based testing.

REFERENCES

[1] L. C. Clark and C. Lyons, "Electrode systems for continuous monitoring in cardiovascular surgery," Ann N Y Acad Sci, vol. 102, pp. 29-45, Oct 31 1962.

[2] C. Yi, Q. Zhang, C.-W. Li, J. Yang, J. Zhao, and M. Yang, "Optical and electrochemical detection techniques for cell-based microfluidic systems," Analytical and Bioanalytical Chemistry, vol. 384, pp. 1259-68, 2006.

[3] X. Song and M. Knotts, "Time-resolved luminescent lateral flow assay technology," Analytica Chimica Acta, vol. 626, pp. 186-92, 2008.

[4] S. Iijima, "Helical microtubules of graphitic carbon," nature, vol. 354, pp. 56-58, 1991.

[5] P. M. Ajayan, "Nanotubes from Carbon," in Chem Rev vol. 99, pp. 1787-1800, 1999.

[6] P. Avouris, "Molecular electronics with carbon nanotubes," Acc Chem Res, vol. 35, pp. 1026-34, Dec 2002.

[7] M.-F. Yu, O. Lourie, M. J. Dyer, K. Moloni, T. F. Kelly, and R. S. Ruoff, "Strength and Breaking Mechanism of Multiwalled Carbon Nanotubes Under Tensile Load," Science vol. 287, pp. 637-40, 2000.

[8] L. X. Li, R. P. Liu, Z. W. Chen, Q. Wang, M. Z. Ma, Q. Jing, G. Li, and Y. Tian, "Tearing, folding and deformation of a carbon-carbon sp2-bonded network," Carbon, vol. 44, pp. 1544-47, 2006.

[9] R. Saito, M. Fujita, G. Dresselhaus, and M. S. Dresselhaus, "Electronic structure of graphene tubules based on C60," Physical Review B, vol. 46, pp. 1804-11, 1992.

[10] N. Hamada, S.-i. Sawada, and A. Oshiyama, "New one-dimensional conductors: Graphitic microtubules," Physical Review Letters, vol. 68, pp. 1579-81, 1992.

[11] T. W. Ebbesen, "Nanotubes, nanoparticles, and aspects of fullerene related carbons," Journal of Physics and Chemistry of Solids, vol. 58, pp. 1979-82, 1997.

[12] T. W. Odom, J.-L. Huang, P. Kim, and C. M. Lieber, "Atomic structure and electronic properties of single-walled carbon nanotubes," nature, vol. 391, pp. 62-64, 1998.

[13] W. Liang, M. Bockrath, and H. Park, "Shell Filling and Exchange Coupling in Metallic Single-Walled Carbon Nanotubes," Physical Review Letters, vol. 88, pp. 126801-04, 2002.

[14] R. A. Jishi, M. S. Dresselhaus, and G. Dresselhaus, "Symmetry properties of chiral carbon nanotubes," Physical Review B, vol. 47, pp. 16671-74, 1993.

[15] D. H. Robertson, D. W. Brenner, and J. W. Mintmire, "Energetics of nanoscale graphitic tubules," Physical Review B, vol. 45, pp. 12592-95, 1992.

[16] S. C. Tsang, J. J. Davis, M. L. H. Green, H. A. O. Hill, Y. C. Leung, and P. J. Sadler, "Immobilization of Small Proteins in Carbon Nanotubes: High-resolution Transmission Electron Microscopy Study and Catalytic Activity," Chem. Soc., Chem. Commun., pp. 1803-04, 1995.

[17] S. N. Kim, J. F. Rusling, and F. Papadimitrakopoulos, "Carbon Nanotubes for Electronic and Electrochemical Detection of Biomolecules," Advanced Materials, vol. 19, pp. 3214-28, 2007.

[18] K. Bradley, M. Briman, A. Star, and G. Gruner, "Charge transfer from adsorbed proteins," Nano Letters, vol. 4, pp. 253-56, Feb 2004.

[19] G. Sanchez-Pomales, L. Santiago-Rodriguez, and C. R. Cabrera, "DNA-functionalized carbon nanotubes for biosensing applications," J Nanosci Nanotechnol, vol. 9, pp. 2175-88, Apr 2009.

[20] J. Kong, N. R. Franklin, C. Zhou, M. G. Chapline, S. Peng, K. Cho, and H. Dai, "Nanotube molecular wires as chemical sensors," Science, vol. 287, pp. 622-25, Jan 28 2000.

[21] J. Okuno, K. Maehashi, K. Kerman, Y. Takamura, K. Matsumoto, and E. Tamiya, "Label-free immunosensor for prostate-specific antigen based on single-walled carbon nanotube array-modified microelectrodes," Biosens Bioelectron, vol. 22, pp. 2377-81, Apr 15 2007.

[22] V. Kunduru, M. Bothara, J. Grosch, S. Sengupta, P. K. Patra, and S. Prasad, "Nanostructured surfaces for enhanced protein detection toward clinical diagnostics," Nanomedicine, Mar 27 2010.

[23] M. S. Dresselhaus, G. Dresselhaus, and P. C. Eklund, Science of Fullerenes and Carbon Nanotubes, New York: Academic Press, 1996.

[24] H. Kataura, Y. Kumazawa, Y. Maniwa, I. Umezu, S. Suzuki, Y. Ohtsuka, and Y. Achiba, "Optical properties of single-wall carbon nanotubes," Synthetic Metals, vol. 103, pp. 2555-58, 1999.

[25] H. J. Li, W. G. Lu, J. J. Li, X. D. Bai, and C. Z. Gu, "Multichannel ballistic transport in multiwall carbon nanotubes," Phys Rev Lett, vol. 95, pp. 086601-05, Aug 19 2005.

[26] J. J. Ge, D. Zhang, Q. Li, H. Hou, M. J. Graham, L. Dai, F. W. Harris, and S. Z. D. Cheng, "Multiwalled Carbon Nanotubes with Chemically Grafted Polyetherimides," Journal of the American Chemical Society, vol. 127, pp. 9984-9985, 2005.

[27] H. Ago, T. Kugler, F. Cacialli, W. R. Salaneck, M. S. P. Shaffer, A. H. Windle, and R. H. Friend, "Work Functions and Surface Functional Groups of Multiwall Carbon Nanotubes," The Journal of Physical Chemistry B, vol. 103, pp. 8116-21, 1999.

[28] H. Kong, C. Gao, and D. Yan, "Functionalization of Multiwalled Carbon Nanotubes by Atom Transfer Radical Polymerization and Defunctionalization of the Products," Macromolecules, vol. 37, pp. 4022-30, 2004.

[29] R. S. Ruoff, J. Tersoff, D. C. Lorents, S. Subramoney, and B. Chan, "Radial Deformation of Carbon Nanotubes by Van-Der-Waals Forces," nature, vol. 364, pp. 514-16, Aug 5 1993.

[30] C. A. Dyke and J. M. Tour, "Overcoming the insolubility of carbon nanotubes through high degrees of sidewall functionalization," Chemistry-a European Journal, vol. 10, pp. 813-17, Feb 20 2004.

[31] T. Ramanathan, F. T. Fisher, R. S. Ruoff, and L. C. Brinson, "Amino-functionalized carbon nanotubes for binding to polymers and biological systems," Chemistry of Materials, vol. 17, pp. 1290-95, Mar 22 2005.

[32] K. A. Worsley, I. Kalinina, E. Bekyarova, and R. C. Haddon, "Functionalization and Dissolution of Nitric Acid Treated Single-Walled Carbon Nanotubes," Journal of the American Chemical Society, vol. 131, pp. 18153-58, Dec 23 2009.

[33] H. Peng, L. B. Alemany, J. L. Margrave, and V. N. Khabashesku, "Sidewall Carboxylic Acid Functionalization of Single-Walled Carbon Nanotubes," Journal of the American Chemical Society, vol. 125, pp. 15174-82, 2003.

[34] P. K. Rai, A. N. Parra-Vasquez, J. Chattopadhyay, R. A. Pinnick, F. Liang, A. K. Sadana, R. H. Hauge, W. E. Billups, and M. Pasquali, "Dispersions of functionalized single-walled carbon nanotubes in strong acids: solubility and rheology," J Nanosci Nanotechnol, vol. 7, pp. 3378-85, Oct 2007.

[35] R. E. Anderson and A. R. Barron, "Solubilization of single-wall carbon nanotubes in Organic solvents without sidewall functionalization," J Nanosci Nanotechnol, vol. 7, pp. 3436-40, Oct 2007.

[36] K. D. Ausman, R. Piner, O. Lourie, R. S. Ruoff, and M. Korobov, "Organic Solvent Dispersions of Single-Walled Carbon Nanotubes: Toward Solutions of Pristine Nanotubes," The Journal of Physical Chemistry B, vol. 104, pp. 8911-15, 2000.

[37] P. M. Ajayan and J. M. Tour, "Materials science: nanotube composites," nature, vol. 447, pp. 1066-68, Jun 28 2007.

[38] S. T. Y. Lin, H. Li, K. A. S. Fernando, L. Qu, W. Wang, and B. Z. a. Y.-P. S. L. Gu, "Advances toward bioapplications of carbon nanotubes," J Mater chem., vol. 14, pp. 527-41, 2004.

[39] N. Nakashima, "Solubilization of single-walled carbon nanotubes with condensed aromatic compounds," Science and Technology of Advanced Materials, vol. 7, pp. 609-16, 2006.

[40] J.-Y. Shin, T. Premkumar, and Kurt E. Geckeler, "Dispersion of Single-Walled Carbon Nanotubes by Using Surfactants: Are the Type and Concentration Important?," Chemistry - A European Journal, vol. 14, pp. 6044-48, 2008.

[41] M. F. Islam, E. Rojas, D. M. Bergey, A. T. Johnson, and A. G. Yodh, "High Weight Fraction Surfactant Solubilization of Single-Wall Carbon Nanotubes in Water," Nano Letters, vol. 3, pp. 269-73, 2003.

[42] A. Star, J. F. Stoddart, D. Steuerman, M. Diehl, A. Boukai, E. W. Wong, X. Yang, S. W. Chung, H. Choi, and J. R. Heath, "Preparation and Properties of Polymer-Wrapped Single-Walled Carbon Nanotubes," Angew Chem Int Ed Engl, vol. 40, pp. 1721-25, May 4 2001.

[43] M. J. O'Connell, P. Boul, L. M. Ericson, C. Huffman, Y. Wang, E. Haroz, C. Kuper, J. Tour, K. D. Ausman, and R. E. Smalley, "Reversible water-solubilization of single-walled carbon nanotubes by polymer wrapping," Chem. Phys. lett., vol. 342, pp. 265-71, 2001.

[44] M. J. O'Connell, S. M. Bachilo, C. B. Huffman, V. C. Moore, M. S. Strano, E. H. Haroz, K. L. Rialon, P. J. Boul, W. H. Noon, C. Kittrell, J. Ma, R. H. Hauge, R. B. Weisman, and R. E. Smalley, "Band Gap Fluorescence from Individual Single-Walled Carbon Nanotubes," Science, vol. 297, pp. 593-96, July 26, 2002.

[45] V. C. Moore, M. S. Strano, E. H. Haroz, R. H. Hauge, R. E. Smalley, J. Schmidt, and Y. Talmon, "Individually Suspended Single-Walled Carbon Nanotubes in Various Surfactants," Nano Letters, vol. 3, pp. 1379-82, 2003.

[46] K. A. Fernando, Y. Lin, and Y. P. Sun, "High aqueous solubility of functionalized single-walled carbon nanotubes," Langmuir, vol. 20, pp. 4777-78, May 25 2004.

[47] J. U. Lee, J. Huh, K. H. Kim, C. Park, and W. H. Jo, "Aqueous suspension of carbon nanotubes via non-covalent functionalization with oligothiophene-terminated poly(ethylene glycol)," Carbon, vol. 45, pp. 1051-57, 2007.

[48] Y. Lin, L. F. Allard, and Y.-P. Sun, "Protein-Affinity of Single-Walled Carbon Nanotubes in Water," The Journal of Physical Chemistry B, vol. 108, pp. 3760-64, 2004.

[49] K. Besteman, J. O. Lee, F. G. M. Wiertz, H. A. Heering, and C. Dekker, "Enzyme-Coated Carbon Nanotubes asSingle-Molecule Biosensors," Nano Lett, vol. 3, pp. 727-30, 2003.

[50] F. Balavoine, P. Schultz, C. Richard, V. Mallouh, T. W. Ebbesen, and C. Mioskowski, "Helical Crystallization of Proteins on Carbon Nanotubes: A First Step towards the Development of New Biosensors," Angewandte Chemie International Edition, vol. 38, pp. 1912-15, 1999.

[51] J. J. Davis, M. L. H. Green, H. Allen O. Hill, Y. C. Leung, P. J. Sadler, J. Sloan, A. V. Xavier, and S. Chi Tsang, "The immobilisation of proteins in carbon nanotubes," Inorganica Chimica Acta, vol. 272, pp. 261-66, 1998.

[52] M. Shim, N. W. S. Kam, R. J. Chen, Y. M. Li, and H. J. Dai, "Functionalization of carbon nanotubes for biocompatibility and biomolecular recognition," Nano Letters, vol. 2, pp. 285-88, Apr 2002.

[53] T. Waterboer, P. Sehr, and M. Pawlita, "Suppression of non-specific binding in serological Luminex assays," Journal of Immunological Methods, vol. 309, pp. 200-204, 2006.

[54] E. Ostuni, R. G. Chapman, M. N. Liang, G. Meluleni, G. Pier, D. E. Ingber, and G. M. Whitesides, "Self-Assembled Monolayers That Resist the Adsorption of Proteins and the Adhesion of Bacterial and Mammalian Cells," Langmuir, vol. 17, pp. 6336-43, 2001.

[55] R. J. Chen, S. Bangsaruntip, K. A. Drouvalakis, N. W. Kam, M. Shim, Y. Li, W. Kim, P. J. Utz, and H. Dai, "Noncovalent functionalization of carbon nanotubes for highly specific electronic biosensors," Proc Natl Acad Sci USA, vol. 100, pp. 4984-89, Apr 29 2003.

[56] D. Pantarotto, C. D. Partidos, R. Graff, J. Hoebeke, J.-P. Briand, M. Prato, and A. Bianco, "Synthesis, Structural Characterization, and Immunological Properties of Carbon Nanotubes Functionalized with Peptides," Journal of the American Chemical Society, vol. 125, pp. 6160-64, 2003.

[57] N. Nakajima and Y. Ikada, "Mechanism of amide formation by carbodiimide for bioconjugation in aqueous media," Bioconjug Chem, vol. 6, pp. 123-30, Jan-Feb 1995.

[58] D. Sehgal and I. K. Vijay, "A Method for the High Efficiency of Water-Soluble Carbodiimide-Mediated Amidation," Analytical Biochemistry, vol. 218, pp. 87-91, 1994.

[59] Y. Gao and I. Kyratzis, "Covalent Immobilization of Proteins on Carbon Nanotubes Using the Cross-Linker 1-Ethyl-3-(3-dimethylaminopropyl)carbodiimide-a Critical Assessment," Bioconjugate Chemistry, vol. 19, pp. 1945-50, 2008.

[60] C. Fernandez-Sanchez, E. Pellicer, J. Orozco, C. Jimenez-Jorquera, L. M. Lechuga, and E. Mendoza, "Plasma-activated multi-walled carbon nanotube-polystyrene composite substrates for biosensing," Nanotechnology, vol. 20, pp. 1-7, Aug 19 2009.

[61] Y. Lin, T. Elkin, S. Taylor, L. Gu, B. Chen, L. M. Veca, B. Zhou, H. Yang, J. Brown, R. Joseph, E. Jones, X. Jiang, and Y.-P. Sun, "Preparation, Characterization, and Evaluation of Immuno Carbon Nanotubes," Microchimica Acta, vol. 152, pp. 249-54, 2006.

[62] J. J. Zhao, H. K. Park, J. Han, and J. P. Lu, "Electronic properties of carbon nanotubes with covalent sidewall functionalization," Journal of Physical Chemistry B, vol. 108, pp. 4227-30, Apr 8 2004.

[63] P. W. Chiu, G. S. Duesberg, U. Dettlaff-Weglikowska, and S. Roth, "Interconnection of carbon nanotubes by chemical functionalization," Applied Physics Letters, vol. 80, pp. 3811-13, May 20 2002.

[64] E. T. Mickelson, C. B. Huffman, A. G. Rinzler, R. E. Smalley, R. H. Hauge, and J. L. Margrave, "Fluorination of single-wall carbon nanotubes," Chemical Physics Letters, vol. 296, pp. 188-194, Oct 30 1998.

[65] K. H. An, J. G. Heo, K. G. Jeon, D. Bae, C. S. Jo, C. W. Yang, C. Y. Park, Y. H. Lee, Y. S. Lee, and Y. S. Chung, "X-ray photoemission spectroscopy study of fluorinated single-walled carbon nanotubes," Applied Physics Letters, vol. 80, pp. 4235-37, Jun 3 2002.

[66] M. Stadermann, S. J. Papadakis, M. R. Falvo, J. Novak, E. Snow, Q. Fu, J. Liu, Y. Fridman, J. J. Boland, R. Superfine, and S. Washburn, "Nanoscale study of conduction through carbon nanotube networks," Physical Review B, vol. 69, pp. 201402-3, 2004.

[67] R. Martel, T. Schmidt, H. R. Shea, T. Hertel, and P. Avouris, "Single- and multi-wall carbon nanotube field-effect transistors," Applied Physics Letters, vol. 73, pp. 2447-49, 1998.

[68] S. J. Tans, M. H. Devoret, H. Dai, A. Thess, R. E. Smalley, L. J. Geerligs, and C. Dekker, "Individual single-wall carbon nanotubes as quantum wires," nature, vol. 386, pp. 474-77, 1997.

[69] H. Dai, E. W. Wong, and C. M. Lieber, "Probing Electrical Transport in Nanomaterials: Conductivity of Individual Carbon Nanotubes," Science, vol. 272, pp. 523-26, April 26, 1996.

[70] S. J. Tans, A. R. M. Verschueren, and C. Dekker, "Room-temperature transistor based on a single carbon nanotube," nature, vol. 393, pp. 49-52, 1998.

[71] A. Bezryadin, A. R. M. Verschueren, S. J. Tans, and C. Dekker, "Multiprobe Transport Experiments on Individual Single-Wall Carbon Nanotubes," Physical Review Letters, vol. 80, p. 4036-39, 1998.

[72] J. Wang, "Carbon-Nanotube Based Electrochemical Biosensors: A Review," Electroanalysis, vol. 17, pp. 7-14, 2005.

[73] Y. Yun, Z. Dong, V. Shanov, W. R. Heineman, H. B. Halsall, A. Bhattacharya, L. Conforti, R. K. Narayan, W. S. Ball, and M. J. Schulz, "Nanotube electrodes and biosensors," Nano Today, vol. 2, pp. 30-37, 2007.

[74] X. Yu, D. Chattopadhyay, I. Galeska, F. Papadimitrakopoulos, and J. F. Rusling, "Peroxidase activity of enzymes bound to the ends of single-wall carbon nanotube forest electrodes," Electrochemistry Communications, vol. 5, pp. 408-411, 2003.

[75] J. Liu, A. Chou, W. Rahmat, Michael N. Paddon-Row, and J. J. Gooding, "Achieving Direct Electrical Connection to Glucose Oxidase Using Aligned Single Walled Carbon Nanotube Arrays," Electroanalysis, vol. 17, pp. 38-46, 2005.

[76] A. Star, J.-C. P. Gabriel, K. Bradley, and G. Gruner, "Electronic Detection of Specific Protein Binding Using Nanotube FET Devices," Nano Letters, vol. 3, pp. 459-463, 2003.

[77] J. Marulanda, "Current Transport Modeling of Carbon Nanotube Field Effect Transistors for Analysis and Design of Integrated Circuits," PhD Dissertation, Electrical and Computer Engineering, Louisiana State University, Baton Rouge, 2008.

[78] K. Maehashi, T. Katsura, K. Kerman, Y. Takamura, K. Matsumoto, and E. Tamiya, "Label-Free Protein Biosensor Based on Aptamer-Modified Carbon Nanotube Field-Effect Transistors," Analytical Chemistry, vol. 79, pp. 782-87, 2006.

[79] E. Bakker, "Electrochemical Sensors," Analytical Chemistry, vol. 76, pp. 3285-98, 2004.

[80] G. Gruner, "Carbon nanotube transistors for biosensing applications," Anal Bioanal Chem, vol. 384, pp. 322-35, Jan 2006.

[81] G. Zheng, F. Patolsky, Y. Cui, W. U. Wang, and C. M. Lieber, "Multiplexed electrical detection of cancer markers with nanowire sensor arrays," Nat Biotechnol, vol. 23, pp. 1294-301, Oct 2005.

[82] J. Koehne, J. Li, A. M. Cassell, H. Chen, Q. Ye, H. T. Ng, J. Han, and M. Meyyappan, "The fabrication and electrochemical characterization of carbon nanotube nanoelectrode arrays," Mater. Chem., vol. 14, pp. 676-684, 2004.

[83] H. Cai, X. Cao, Y. Jiang, P. He, and Y. Fang, "Carbon nanotube-enhanced electrochemical DNA biosensor for DNA hybridization detection," Analytical and Bioanalytical Chemistry, vol. 375, pp. 287-293, 2003.

[84] X. Tang, S. Bansaruntip, N. Nakayama, E. Yenilmez, Y. L. Chang, and Q. Wang, "Carbon nanotube DNA sensor and sensing mechanism," Nano Lett, vol. 6, pp. 1632-36, Aug 2006.

[85] X. Yu, B. Munge, V. Patel, G. Jensen, A. Bhirde, J. D. Gong, S. N. Kim, J. Gillespie, J. S. Gutkind, F. Papadimitrakopoulos, and J. F. Rusling, "Carbon Nanotube Amplification Strategies for Highly Sensitive Immunodetection of Cancer Biomarkers," Journal of the American Chemical Society, vol. 128, pp. 11199-205, 2006.

[86] N. Shao, S. Lu, E. Wickstrom, and B. Panchapakesan, "Integrated molecular targeting of IGF1R and HER2 surface receptors and destruction of breast cancer cells using single wall carbon nanotubes," Nanotechnology vol. 18, pp. 1-9, 2007.

[87] Z. Liu, X. Sun, N. Nakayama-Ratchford, and H. Dai, "Supramolecular Chemistry on Water-Soluble Carbon Nanotubes for Drug Loading and Delivery," ACS Nano, vol. 1, pp. 50-56, 2007.

[88] R. J. Chen, H. C. Choi, S. Bangsaruntip, E. Yenilmez, X. Tang, Q. Wang, Y.-L. Chang, and H. Dai, "An Investigation of the Mechanisms of Electronic Sensing of Protein Adsorption on Carbon Nanotube Devices," Journal of the American Chemical Society, vol. 126, pp. 1563-68, 2004.

[89] C. Li, M. Curreli, H. Lin, B. Lei, F. N. Ishikawa, R. Datar, R. J. Cote, M. E. Thompson, and C. Zhou, "Complementary Detection of Prostate-Specific Antigen Using In2O3 Nanowires and Carbon Nanotubes," Journal of the American Chemical Society, vol. 127, pp. 12484-85, 2005.

[90] B. Panchapakesan, G. Cesarone, S. Liu, K. Teker, and E. Wickstrom, "Single-wall carbon nanotubes with adsorbed antibodies detect live breast cancer cells," NanoBiotechnology, vol. 1, pp. 353-60, 2005.

[91] A. H. Peruski and L. F. Peruski, "Immunological methods for detection and identification of infectious disease and biological warfare agents," Clinical and Diagnostic Laboratory Immunology, vol. 10, pp. 506-513, Jul 2003.

[92] P. E. Andreotti, G. V. Ludwig, A. H. Peruski, J. J. Tuite, S. S. Morse, and L. F. Peruski, "Immunoassay of infectious agents," Biotechniques, vol. 35, pp. 850-59, Oct 2003.

[93] R. F. Schall and H. J. Tenoso, "Alternatives to Radioimmunoassay - Labels and Methods," Clinical Chemistry, vol. 27, pp. 1157-64, 1981.

[94] L. J. Kricka, "Strategies for immunoassay," Pure and Applied Chemistry, vol. 68, pp. 1825-30, Oct 1996.

[95] S. Ray, G. Mehta, and S. Srivastava, "Label-free detection techniques for protein microarrays: Prospects, merits and challenges," Proteomics, vol. 10, pp. 731-748, Feb 2010.

[96] C. L. Morgan, D. J. Newman, and C. P. Price, "Immunosensors: Technology and opportunities in laboratory medicine," Clinical Chemistry, vol. 42, pp. 193-209, Feb 1996.

[97] J. S. Daniels and N. Pourmand, "Label-free impedance biosensors: Opportunities and challenges," Electroanalysis, vol. 19, pp. 1239-57, Jun 2007.

[98] A. Bange, J. Tu, X. Zhu, C. Ahn, H. B. Halsall, and William R. Heineman, "Electrochemical Detection of MS2 Phage Using a Bead-based Immunoassay and a NanoIDA," Electroanalysis, vol. 19, pp. 2202-07, 2007.

[99] K. W. O. J.-W. Choi, J. H. Thomas, W. R. Heineman, H. B. Halsall, J. H. Nevin, A. J. Helmicki, H. T. H. and Chong H. Ahn, "An integrated microfluidic biochemical detection system for protein analysis with magnetic bead-based sampling capabilities," Lab Chip, vol. 2, pp. 27-30, 2002.

[100] D. Erickson and D. Q. Li, "Integrated microfluidic devices," Analytica Chimica Acta, vol. 507, pp. 11-26, Apr 1 2004.

[101] S. Takeda, A. Sbagyo, Y. Sakoda, A. Ishii, M. Sawamura, K. Sueoka, H. Kida, K. Mukasa, and K. Matsumoto, "Application of carbon nanotubes for detecting anti-hemagglutinins based on antigen-antibody interaction," Biosens Bioelectron, vol. 21, pp. 201-5, Jul 15 2005.

[102] J. Wang, G. Liu, and M. R. Jan, "Ultrasensitive Electrical Biosensing of Proteins and DNA: Carbon-Nanotube Derived Amplification of the Recognition and Transduction Events," Journal of the American Chemical Society, vol. 126, pp. 3010-11, 2004.

[103] M. Moniruzzaman and K. I. Winey, "Polymer Nanocomposites Containing Carbon Nanotubes," Macromolecules, vol. 39, pp. 5194-5205, 2006.

[104] A. Hirsch, "Functionalization of single-walled carbon nanotubes," Angew Chem Int Ed Engl, vol. 41, pp. 1853-59, Jun 3 2002.

[105] D. Wang, W.-X. Ji, Z.-C. Li, and L. Chen, "A Biomimetic “Polysoap” for Single-Walled Carbon Nanotube Dispersion," Journal of the American Chemical Society, vol. 128, pp. 6556-57, 2006.

[106] H.-i. Shin, B. G. Min, W. Jeong, and C. Park, "Amphiphilic Block Copolymer Micelles: New Dispersant for Single Wall Carbon Nanotubes," Macromolecular Rapid Communications, vol. 26, pp. 1451-57, 2005.

[107] D. A. Britz and A. N. Khlobystov, "Noncovalent Interactions of Molecules with Single Walled Carbon Nanotubes," Chem. Soc. Rev., vol. 35, pp. 637-659, 2006.

[108] F. Tournus, S. Latil, M. I. Heggie, and J. C. Charlier, "pi -stacking interaction between carbon nanotubes and organic molecules," Physical Review B, vol. 72, pp. 075431-35, 2005.

[109] J. L. Bahr and J. M. Tour, "Covalent chemistry of single-wall carbon nanotubes," Journal of Materials Chemistry, vol. 12, pp. 1952-58, 2002.

[110] A. H. Liu, I. Honma, M. Ichihara, and H. S. Zhou, "Poly(acrylic acid)-wrapped multi-walled carbon nanotubes composite solubilization in water: definitive spectroscopic properties," Nanotechnology, vol. 17, pp. 2845-49, Jun 28 2006.

[111] J. U. Lee, J. Huh, K. H. Kim, C. Park, and W. H. Jo, "Aqueous suspension of carbon nanotubes via non-covalent functionalization with oligothiophene-terminated poly(ethylene glycol)," Carbon, vol. 45, pp. 1051-1057, 2007.

[112] M. S. Strano, V. C. Moore, M. K. Miller, M. J. Allen, E. H. Haroz, C. Kittrell, R. H. Hauge, and R. E. Smalley, "The role of surfactant adsorption during ultrasonication in the dispersion of single-walled carbon nanotubes," J Nanosci Nanotechnol, vol. 3, pp. 81-6, 2003.

[113] G. Guo, J. Guo, D. Tao, W. C. H. Choy, L. Zhao, W. Qian, Z. Wang, "A Simple method to prepare multi-walled carbon nanotube/ZnO nanoparticle composites." Appl. Phys. A, Vol. 89, pp. 525-528, 2007.

[114] H. Peng, L. B. Alemany, J. L. Margrave, and V. N. Khabashesku, "Sidewall carboxylic acid functionalization of single-walled carbon nanotubes," J Am Chem Soc, vol. 125, pp. 15174-82, Dec 10 2003.

[115] K. Nam, T. Kimura, and A. Kishida, "Controlling Coupling Reaction of EDC and NHS for Preparation of Collagen Gels Using Ethanol/Water Co-Solvents," Macromolecular Bioscience, vol. 8, pp. 32-37, 2008.

[116] C. Richard, F. Balavoine, P. Schultz, T. W. Ebbesen, and C. Mioskowski, "Supramolecular Self-Assembly of Lipid Derivatives on Carbon Nanotubes," Science, vol. 300, pp. 775-8, May 2, 2003.

[117] R. E. Biagini, D. L. Sammons, J. P. Smith, B. A. MacKenzie, C. A. Striley, J. E. Snawder, S. A. Robertson, and C. P. Quinn, "Rapid, sensitive, and specific lateral-flow immunochromatographic device to measure anti-anthrax protective antigen immunoglobulin g in serum and whole blood," Clin Vaccine Immunol, vol. 13, pp. 541-6, May 2006.

[118] S. Buhrer-Sekula, H. L. Smits, G. C. Gussenhoven, J. van Leeuwen, S. Amador, T. Fujiwara, P. R. Klatser, and L. Oskam, "Simple and fast lateral flow test for classification of leprosy patients and identification of contacts with high risk of developing leprosy," J Clin Microbiol, vol. 41, pp. 1991-5, May 2003.

[119] T. J. Clark, P. H. McPherson, and K. F. Buechler, "The Triage Cardiac Panel: Cardiac Markers for the Triage System," Point of Care, vol. 1, pp. 42-46, 2002.

[120] P. Corstjens, M. Zuiderwijk, A. Brink, S. Li, H. Feindt, R. S. Niedbala, and H. Tanke, "Use of up-converting phosphor reporters in lateral-flow assays to detect specific nucleic acid sequences: a rapid, sensitive DNA test to identify human papillomavirus type 16 infection," Clin Chem, vol. 47, pp. 1885-93, Oct 2001.

[121] C. Fernandez-Sanchez, C. J. McNeil, K. Rawson, and O. Nilsson, "Disposable Noncompetitive Immunosensor for Free and Total Prostate-Specific Antigen Based on Capacitance Measurement," Analytical Chemistry, vol. 76, pp. 5649-5656, 2004.

[122] J. Ryan, K. Dave, E. Emmerich, B. Fernandez, M. Turell, J. Johnson, K. Gottfried, K. Burkhalter, A. Kerst, A. Hunt, R. Wirtz, and R. Nasci, "Wicking assays for the rapid detection of West Nile and St. Louis encephalitis viral antigens in mosquitoes (Diptera: Culicidae)," J Med Entomol, vol. 40, pp. 95-9, Jan 2003.

[123] C. Fernandez-Sanchez, C. J. McNeil, K. Rawson, and O. Nilsson, "Disposable noncompetitive immunosensor for free and total prostate-specific antigen based on capacitance measurement," Anal Chem, vol. 76, pp. 5649-56, Oct 1 2004.

[124] C. Jonsson, M. Aronsson, G. Rundstrom, C. Pettersson, I. Mendel-Hartvig, J. Bakker, E. Martinsson, B. Liedberg, B. MacCraith, O. Ohman, and J. Melin, "Silane-dextran chemistry on lateral flow polymer chips for immunoassays," Lab Chip, vol. 8, pp. 1191-7, Jul 2008.

[125] X. Song and M. Knotts, "Time-resolved luminescent lateral flow assay technology," Anal Chim Acta, vol. 626, pp. 186-92, Sep 26 2008.

[126] S. Pal, E. C. Alocilja, and F. P. Downes, "Nanowire labeled direct-charge transfer biosensor for detecting Bacillus species," Biosens Bioelectron, vol. 22, pp. 2329-36, Apr 15 2007.

[127] J. H. Kim, J. H. Cho, G. S. Cha, C. W. Lee, H. B. Kim, and S. H. Paek, "Conductimetric membrane strip immunosensor with polyaniline-bound gold colloids as signal generator," Biosens Bioelectron, vol. 14, pp. 907-15, Feb 2000.

[128] E. Delamarche, D. Juncker, and H. Schmid, "Microfluidics for processing surfaces and miniaturizing biological assays," Advanced Materials, vol. 17, pp. 2911-2933, 2005.

[129] V. Linder, S. K. Sia, and G. M. Whitesides, "Reagent-loaded cartridges for valveless and automated fluid delivery in microfluidic devices," Anal Chem, vol. 77, pp. 64-71, Jan 1 2005.

[130] P. S. Dittrich, K. Tachikawa, and A. Manz, "Micro total analysis systems. Latest advancements and trends," Anal Chem, vol. 78, pp. 3887-908, Jun 15 2006.

[131] D. J. Beebe, G. A. Mensing, and G. M. Walker, "Physics and applications of microfluidics in biology," Annual Review of Biomedical Engineering, vol. 4, pp. 261-286, 2002.

[132] A. Bange, H. B. Halsall, and W. R. Heineman, "Microfluidic immunosensor systems," Biosens Bioelectron, vol. 20, pp. 2488-503, Jun 15 2005.

[133] P. Yager, T. Edwards, E. Fu, K. Helton, K. Nelson, M. R. Tam, and B. H. Weigl, "Microfluidic diagnostic technologies for global public health," nature, vol. 442, pp. 412-8, Jul 27 2006.

[134] G. Hu, Y. Gao, and D. Li, "Modeling micropatterned antigen-antibody binding kinetics in a microfluidic chip," Biosens Bioelectron, vol. 22, pp. 1403-9, Feb 15 2007.

[135] R. A. Vijayendran, F. S. Ligler, and D. E. Leckband, "A computational reaction−diffusion model for the analysis of transport-limited kinetics," Analytical Chemistry, vol. 71, pp. 5405-5412, 1999.

[136] D. B. Holt, A. W. Kusterbeck, and F. S. Ligler, "Continuous flow displacement immunosensors: a computational study," Anal Biochem, vol. 287, pp. 234-42, Dec 15 2000.

[137] O. D. Hendrickson, A. V. Zherdev, A. P. Kaplun, and B. B. Dzantiev, "Experimental study and mathematical modeling of the interaction between antibodies and antigens on the surface of liposomes," Mol Immunol, vol. 39, pp. 413-22, Nov 2002.

[138] M. Zimmermann, E. Delamarche, M. Wolf, and P. Hunziker, "Modeling and optimization of high-sensitivity, low-volume microfluidic-based surface immunoassays," Biomedical Microdevices, vol. 7, pp. 99-110, Jun 2005.

[139] N. Camillone, "Diffusion-Limited Thiol Adsorption on the Gold(111) Surface," Langmuir, vol. 20, pp. 1199-1206, 2004.

[140] C.-K. Yang, J.-S. Chang, S. D. Chao, and K.-C. Wu, "Two dimensional simulation on immunoassay for a biosensor with applying electrothermal effect," Applied Physics Letters, vol. 91, pp. 113904-3, 2007.

[141] W. M. Deen, Analysis of Transport Phenomena, New York: Oxford University Press, 1998.

[142] C. Chou, H.-Y. Hsu, H.-T. Wu, K.-Y. Tseng, A. Chiou, C.-J. Yu, Z.-Y. Lee, and T.-S. Chan, "Fiber optic biosensor for the detection of C-reactive protein and the study of protein binding kinetics," Journal of Biomedical Optics, vol. 12, pp. 024025-9, 2007.

[143] D. B. Hibbert, J. J. Gooding, and P. Erokhin, "Kinetics of Irreversible Adsorption with Diffusion: Application to Biomolecule Immobilization," Langmuir, vol. 18, pp. 1770-76, 2002.

VITA

Adeyabeba Abera was born in Addis Ababa, Ethiopia. She received her Bachelor of Science degree in electrical engineering from Virginia Polytechnic Institute and State University in Blacksburg, Virginia in 2004. She worked at DLP™ Texas Instruments from 2004 to 2005 as a hardware engineer. She entered the doctoral program in the Department of Electrical and Computer Engineering at Louisiana State University in 2005. She obtained her Master of Science degree in electrical engineering in 2007. Her research interests include micro/nano technology, nanoelectronics using carbon nanotubes, biological detection, microfluidics, and computational fluid dynamics. She is expected to earn the degree of Doctor of Philosophy in December 2010.